Biological Uranium (VI) Reduction in Fixed-Media and Suspended Culture Systems

by

Phalazane Johanna Mtimunye

A thesis submitted in partial fulfilment
of the requirements for the degree

Philosophiae Doctor (Chemical Technology)

in the

Department of Chemical Engineering
Faculty of Engineering, the Built Environment and Information Technology

University of Pretoria
Pretoria

April 2015

ABSTRACT

Biological Uranium (VI) Reduction in Fixed-Media and Suspended Culture Systems

By

Phalazane Johanna Mtimunye

Supervisor: Professor EMN Chirwa
Department: Chemical Engineering
Degree: Philosophiae Doctor (Chemical Technology)

Tailing dumps and process waste stockpiles at uranium mining sites and nuclear power processing facilities contain significant levels of uranium. Uranium in the tailing dumps can exist either as U(VI) or U(IV) depending on the pH and redox conditions within the dump. However, it is desirable to keep uranium in the dump sites in its tetravalent form, U(IV), since the hexavalent form, U(VI), is highly mobile and very toxic to aquatic life forms and humans. Natural attenuation processes such as bacterial reductive/precipitation and immobilization of soluble uranium emerge as viable method for remediating U(VI) contaminated sites. For example, dissimilatory metal-reducing bacteria (DMRB) have been investigated for their capability to remove uranium from aqueous solutions. These bacteria were able to use U(VI) as an electron acceptor thereby reducing U(VI) to U(IV) which is easier to remove from solution by precipitation.

In this study, the efficiency of indigenous culture of bacteria from the local contaminated site in reducing U(VI) was evaluated using both batch and continuous flow bioreactor systems. Because the stability of uranium in the tailing dumps and stockpiles of uranium concentrate at uranium mining fields is affected by the pH, redox potential, the presence of complexing anions in the waste rocks, toxic metals, organics, inhibitors, and chelators, the effect of these factors in U(VI) bioremediation process was also evaluated in this study. Batch kinetics

studies showed near complete U(VI) removal of up to 400 mg/L. Experiments on suspended culture bioreactor system conducted in 10 L Erlenmeyer's flask under shock loading conditions also showed U(VI) removal of up 400 mg/L. Higher U(VI) removal rates achieved in a suspended culture system operated without re-inoculation were associated with continuous addition of nutrients and glucose in a bioreactor over time. This demonstrate the effectiveness of carbon source and nutrients in enhancing U(VI) reduction process in bioreactor systems.

Further experiments were conducted in a fixed-film, continuous flow bioreactor system to evaluate the capacity of the indigenous mixed culture in reducing U(VI) under oxygen stressed and nutrient deficient conditions. The experiments in the fixed-film bioreactor system were conducted using columns with four equally spaced intermediate sampling ports along the length to facilitate finite difference modelling of the U(VI) concentration profile within the column. Near complete U(VI) removal of up to 85 mg/L was achieved in the fixed-film bioreactor operated without organic carbon source. At higher U(VI) feed concentration of 100 mg/L the bioreactor system was able to achieve the removal efficiency of 60%. A sterile control column on the other hand showed insignificant U(VI) removal over time, indicating U(VI) removal by biochemical processes. The shift in microbial culture was monitored in the fixed-film bioreactor after 99 days of exposure to U(VI) using the 16S rRNA genotype fingerprinting method.

The fate of U(VI) within a complex biofilm structure was predicted and evaluated using mathematical modelling. The mathematical model developed in this study for describing the biofilm system incorporated both the mass transport kinetics, microbial growth kinetics, and reduction kinetics, thus the diffusion-reduction equation. The model successfully captured the trends of U(VI) removal within the biofilm for different loading conditions. The validity of the model in predicting U(VI) reduction within the bench-scale biofilm reactor at various U(VI) concentrations demonstrated the feasibility of the model in predicting field scale system and improving design and operation of site for clean-up.

Declaration

I, **Phalazane Johanna Mtimunye**, hereby declare that the work provided in this dissertation is to the best of my knowledge original (except where cited) and that this work has never been submitted for another degree at this or any other tertiary education institution.

Signature of candidate…… Date ……..

Dedication

This dissertation is dedicated to

My family

My late father Klaas Mtimunye who has always believed in me and encouraged me to pursue with my studies; I will forever be grateful for all his teachings and love

My one and only wonderful mother Lena Mtimunye for her ongoing support, endless love, understanding, for believing in me always and encouraging me to always pray and ask God for guidance. I really thank God for her because she is special.

My brothers and sisters who were always there for me every step of the way, I will forever be grateful for their support and I really thank God for them

My friends who were always supportive and there when I needed to talk. I would never trade them for anything in this world, because they really mean a lot to me and I love them beyond measures.

Acknowledgements

First and foremost, I thank God the Almighty and my Saviour Jesus Christ for the many blessings that he has bestowed upon me since birth. Without him I cannot achieve anything. I thank God for the favour and for his sufficient grace in my life and I will forever praise him for being God in my life and going with me through all my tribulations.

Regarding my doctoral studies at the University of Pretoria, I am thankful to several individuals that contributed directly through guidance and help during my entire time of study. I especially would like to express my gratitude to the following persons without whom this dissertation would not be possible:

Professor Evans Chirwa my study leader who has always been doing his best to assist me and inspired me through his supervision and motivation. I will forever be grateful for all the efforts he took to assist in this study. May the good Lord bless him.

Professor Fanus Venter at the Department of Microbiology for assistance with the characterization of bacterial isolates.

Microscopy Units at the University of Pretoria and NECSA, Phelindaba (South Africa) for allowing me to use their equipment for the analysis of my samples.

I would also like to express my appreciation to the following organizations that made this dissertation possible: SASOL Bursary Programme and National Research Foundation (NRF) for financial support.

My sincere gratitude also goes to Christopher Mahlathi, Jonathan Shock, for their invaluable advice which contributed effectively to this study.

I would also like to thank all my colleagues and Laboratory Technician for their friendship and support. I have learned so much from all of you.

I would also like to thank the Pastor and all members of Charisma Community church in Pretoria for his teachings. They really kept me going, positive, strong, and hopeful that all the things work out for good for those who trust in the Lord. May the good Lord bless him.

Table of Contents

List of Figures

List of Tables

Abbreviations

APHA	American public health agency
BLAST	Basic Logical Alignment Search Tool
U	Uranium
U(VI)	Hexavalent uranium
U(IV)	Tetravalent uranium
URB	U(VI) reducing bacteria
CFU	Colony forming units
DMRB	Dissimilatory metal reducing bacteria
DNA	Deoxyribonucleic acid
ETC	Electron transport chain
BMM	Basal mineral medium
NADH	Nicotinamide adenine dinucleotide
NADPH	Nicotinamide adenine dinucleotide phosphate
ORP	Oxidation-Reduction Potential
pH	Potential hydrogen
ppm	Parts per million
PVC	Polyvinyl chloride
PRB	Permeable reactive barrier
RT-PCR	Reverse transcriptase- Polymerase chain reaction
rDNA	Ribosomal deoxyribonucleic acid
rRNA	Ribosomal Ribonucleic acid
rpm	Rotation per minute
SEM	Scanning electron microscopy
SRB	Sulphate reducing bacteria
TEM	Transmission electron microscopy
US EPA	United States Environmental Protection Agency
WHO	World Health Organization

Symbol Nomenclature

A_f	biofilm surface area [L^2]
$A(t)$	effective cross-sectional area of a reactor [L^2]
b_x	cell death rate [T^{-1}]
D_{xw}	diffusion coefficient of particulate matter [L^2T^{-1}]
D_{uw}	dissolved species diffusion coefficient [L^2T^{-1}]
d_p	particle size [L]
ID	internal diameter [L]
j_u	dissolved species flux rate [$ML^{-2}T^{-1}$]
j_x	flux rate of particulate matter [$ML^{-2}T^{-1}$]
k_u	reaction rate coefficient [$L^3M^{-1}T^{-1}$]
K_u	half velocity U(VI) concentration [ML^{-3}]
k_{ad}	adsorption rate coefficient [T^{-1}]
k_d	cell detachment rate [$TM^{-1}L^{-1}$]
k_{LU}	mass transport coefficient[LT^{-1}]
μ_{max}	maximum specific cell growth rate [T^{-1}]
L_f	biofilm thickness [L]
L_w	stagnant film thickness [L]
L	length of the reactor [L]
ρ_f	cell density [ML^{-3}]
Q	inflow rate [$L^{-3}T^{-1}$]
q_c	adsorption rate [$ML^{-3}T^{-1}$]
r_u	U(VI) reduction rate [$ML^{-3}T^{-1}$]
r_x	cell production rate [$ML^{-3}T^{-1}$]
T_u	U(VI) reduction capacity coefficient [MM^{-1}]
t	time [T]
U	U(VI) concentration at time, t [ML^{-3}]
U_s	U(VI) concentration at the surface [ML^{-3}]
U_B	U(VI) concentration in the bulk liquid phase [ML^{-3}]
U_f	U(VI) concentration in the biofilm phase [ML^{-3}]
U_r	U(VI) toxicity threshold concentration [ML^{-3}]
U_{eq}	Equilibrium concentration at surface area [ML^{-3}]
v	flow velocity [LT^{-1}]
V	volume of the reactor [L^3]
X	biomass concentration at time, t [ML^{-3}]

Subscripts

U	uranium
B	in the bulk liquid phase
f	in biofilm
w	in water
o	initial
s	surface

CHAPTER 1

INTRODUCTION

1.1 Background

Energy affects every aspect of our lives. In the recent years, the demand for electricity in many developed or developing countries around the world such as South africa has escalated. The consumption of electricity in South Africa has been steadily increasing since the 1980s and it is predicted that, by the year 2025, the electricity demand will exceed supply (Musango *et al*., 2009). The unprecedented increase of energy demand due to population growth, urbanisation, and industrialization puts a stress on the current non-renewable energy source – fossil fuel. Generation of electricity using fossil fuel, notably coal and natural gas, contributes significantly to greenhouse gases in the atmosphere. Concerns over energy resource availability, global warming, and energy security have led to the future use of what was once considered as a death market, nuclear power, to sustain economic growth. It has been reported by Mourogov and co-workers (2002) that nuclear power can assist to reduce the current output of CO_2 emissions associated with the burning of fossil fuel in the atmosphere by approximately 8% (Mourogov *et al*., 2002; Ngwenya, 2011). Among all the proposed alternative energy sources such as wind, solar, and geothermal energy, nuclear energy offers the most feasible altenative to fossil fuels as a base-load generation capacity. The other alternatives such as solar and wind power can only be used as peak load capacity substitues using the currently available technologies.

Although nuclear power holds promise of cleaner production in terms of carbon emission, the technology introduces the problem of short-term and long-term radiotoxicity from waste generated in the reactors and in processes for producing and reprocessing nuclear fuel. The waste from nuclear fuel reactors contains approximately 95% U-238, 3% fission products plus transuranic isotopes, 1% plutonium, and 1% U-235 (Soudek *et al*, 2006; WNA, 2008; Chabalala, 2011). The waste component originating from nuclear energy generation accounts for over 95% of the total volume of the radioactive waste and is classified as high level waste (HLW). Large quantities of low-level waste are also created due to the leakage of uranium fission products [cesium ($^{70}Cs^{+}$), strontium ($^{90}Sr^{2+}$), and cobalt ($^{60}Co^{2+}$)] into the spent fuel pools from cracks in the fuel cladding (Singh *et al*., 2008). Fission products comprise of

lighter elements than uranium and transuranic elements. Among the above listed fission elements, strontium ($^{90}Sr^{2+}$) causes the most environmental concern due to its relatively long half-live of radioactive decay. Upon reaching the environment, radiostrontium-90 ($^{90}Sr^{2+}$) may easily be taken up by plants and other animal life forms (Ajlouni, 2007). Moreover, because its chemical properties resemble that of Ca^{2+} which is a critical component of the mammalian bone structure, $^{90}Sr^{2+}$ may be easily incorporated into bone tissue. When incorporated in the organism in such manner, $^{90}Sr^{2+}$ may continuously irradiate localized tissues with eventual development of bone sacroma and leukaemia (Chen, 1997). Therefore as a result of their radiotoxicity to living organisms in the environment uranium and its fission products are considered as the most hazardous elements in the nuclear fuel waste stream that requires special attention.

In the past, radioactive waste from the nuclear reactors was stored underground for decades using engineered systems with the primary objective of permanently isolating the disposed waste from the biosphere (Merroun *et al.*, 2008). The main concern about this method of disposal is associated to the possibility of radioactive waste escaping and migrating from the radioactive waste repository site into groundwater systems rendering groundwater unsuitable for use as portable water supply. Cleanup of sites already contaminated with uranium and other radionuclides involves application of abiotic processes with pump-and-treat or dig- and-treat methods that require follow up precipitation or immobilization steps using chemicals (Gavirelsceu, 2009; Mtimunye and Chirwa, 2013). These methods are not suitable for treatment of contamination at large scale since they are cost intensive. Additionally, chemical products used for treatment generate harmful residuals and by-products that are also difficult to treat. Microbial reduction of highly mobile U(VI) to relatively insoluble U(IV) as a normal function of their metabolism offers promise as a technology that could play an important role in the remediation of U(VI) polluted sites.

In situ immobilization of uranium has been suggested as a potential alternative strategy for containing or attenuating the spread of U(VI) in groundwater systems. Recently, a more detailed and long term investigation on *in situ* bioremediation of uranium was carried out at the field site in Rifle, Colorado (Anderson *et al.*, 2003; Wu *et al.*, 2006; Chirwa, 2011) using pure culture of *Geobacter* species. *In situ* bioremediation of uranium at the site was facilitated by addition of external electron donor to stimulate the growth of *Geobacter* species.

Although, the later study was effective for fundamental understanding of interaction taking place between the cells and the metals, results from the previous study does not provide a robust understanding between the field and laboratory studies. This is because in nature microorganisms rarely exist as separate pure cultures. Moreover, the addition of external carbon source does not give a clear indication of the cells potential in reducing metals in actual groundwater systems characterized by low nutrient concentration.

The present study evaluates the potential of indigenous mixed-culture of bacteria in reducing U(VI) in the environment under nutrient deficient conditions without the addition of any external organic carbon source. The remidaiation technology proposed in this study has the potential of minimizing cost and negative impacts associated with addition of foreign materials into the actual system. Fundamental knowledge and understanding of kinetic processes taking place within a bioreactor system will be valuable in developing appropriate remediation and waste management strategies as well as predicting the microbial impacts on the long-term stewardship of contaminated sites.

1.2 Objectives of the Study

The main objective of this study was to evaluate the prospect of uranium control in the environment and to achieve separation and recovery of radionuclides in waste using natural microbial processes. To achieve the primary objective, different experimental tasks were conducted on U(VI) reduction process:

- To investigate the kinetics of U(VI) reduction in indigenous U(VI) reducing bacteria under oxygen stressed conditions in batch reactors over a wide range of initial U(VI) concentrations.
- To characterize the electron flow pathway of U(VI) reduction in facultative anaerobic bacteria.
- To evaluate U(VI) reduction in continuous-flow bioreactor systems (suspended-growth and fixed-film bioreactor systems) over a range of U(VI) feed concentrations.
- To investigate change in the microbial culture diversity during U(VI) bioremediation in continuous-flow bioreactor systems.
- To develop a mathematical model that predicts the movement of the contaminant across the biofilm reactor at both transient and steady-state.

1.3 Outline of Thesis

The outline of this dissertation is subdivided into three main parts:

Literature Review – The initial step towards the methodology of this study was to collect as much information as possible related to the impacts of U(VI) contamination in the environment and current treatment practices from literature. This section contains the background information of the study and the records of recent developments on the U(VI) bioremediation process. The information is focused on the occurrence of uranium in the environment, impact of uranium on human health, animals, and microorganisms, remediation strategies, U(VI) reducing microorganisms, and biological U(VI) reduction pathways.

Materials and Methods – illustrate all the materials and methods used to conduct the research.

U(VI) Reduction Kinetic Studies – contains the performance evaluation of U(VI) reduction bacteria under various conditions, the kinetic modeling of the batch and continuous-flow bioreactor system.

1.4 Significance of Research and Main Findings

Nuclear energy is currenly receiving special attention as an alternative energy source in many countries around the world due to its ability of producing electricity with low carbon outputs. Although the perception of the public towards the nuclear power technology is steadily improving; however some of the leading problems associated with this technology still remain. Currently, no suitable alternative route of radioactive waste treatment has been yet formulated, while in the interim huge amount of nuclear spent fuel are discharged globally (Lior, 2008). Many tailings sites all over the world remain unremediated mainly due to cost and the ineffeciency related to the currently used conventional methods. In this study, experimental results on a packed-bed bioreactor system demonstrated the feasibility of biological treatment of U(VI) contaminated waste stream with a further possibility of recovery of the reduced uranium. Both processes could contribute in the protection of natural water resources from radiotoxic wastewater arising from uranium mineral processing faclities, medical and research facilities.

CHAPTER 2

LITERATURE REVIEW

2.1 Occurrence of Uranium in the Environment

Uranium in its elemental form is characterised by a silver-white colour. It is a ductile, malleable, and pyrophoric metal with an atomic number of 92. Uranium is slightly softer than steel and has a specific density of (19 g/cm^3) and it is 1.6 times more dense than lead (Blesie *et al.*, 2003). Uranium is ubiquitous in the environment. It is found in varying but small amounts in air, soil, rocks, ocean, and the seas. It is actually more abundant than metals such as gold, silver, cadmium, and more or less as common as tin, arsenic and cobalt (Todorov and Ilieva, 2006). Uranium can exist in the environment as complex ores, soluble oxyions, and hydroxide complexes. Examples of natural uranium compounds are pitchblende, uraninite, carnotite, autunite, uranophane, and tobernite. These compounds can be detected in monazite sands, phosphate rocks, and phosphate fertilizers. The concentration of natural uranium in the earth's crust is about 2.8 mg/kg. Vast amounts of uranium occur in the world's oceans, groundwater, plants, and animals. On average about 90 μg of uranium exist in human body from normal intakes of air, water, and plants. About 66% of uranium is found in the skeleton, 16% in liver, 8% in kidneys, and 10% in other tissues (WHO, 2001). Volcanic eruptions can intermittently increase the uranium concentration above the background level in the locale of the eruption. However, the main input of uranium to water bodies is determined to be from weathering of rocks, wet precipitation, dry fallouts from the atmosphere, and run-off from terrestrial systems.

2.2 Radiological Properties

In the earth crust, natural uranium exist mainly as three different radioactive isotopes, namely: U-238 (99.26%), U-235 (0.72%), and traces of U-234 (0.01%) (Bleise *et al.*, 2003; WNA, 2008). These isotopes have similar chemical properties, but different radiological properties. Uranium-238 (U-238) and uranium-235 (U-235) are the parent nuclides of two independent decay series, whereas U-234 is a decay product of the U-238 series. All uranium isotopes undergo the same chemical reactions in nature and possess almost identical physical characteristics such as melting point, boiling point and volatility. Radiological properties such as the decay rate, half-life, and specific activity are different for each isotope. Uranium-

238 has a specific radioactivity of 12.455 Bq/g (half-life of 4.47×10^{9} years), U-235 has a specific radioactivity of 80 Bq/g (half-life of 7×10^{8} years), and U-234 has a specific radioactivity 231×10^{6} Bq/g (half-life of 2.46×10^{5} years) (Bleise *et al*., 2003; WNA, 2008). The smaller amount of U-234 is more radioactive than any other uranium isotope. The low concentration of U-234 in nature is attributed to its fast decay rate as evidenced by its short half-life (2.46×10^{5} years).

2.3 Chemical Forms of Uranium

Uranium exists in the environment mainly as oxides, organic or inorganic complexes, and rarely as a free metal ion (Mtimunye and Chirwa, 2013). Free elemental uranium primarily exists in higher oxidation states typically bound to oxygen. The oxygen bound uranium exists mainly as triuranium octaoxide also known as pitchblende (U_3O_8), uraninite (UO_2), and uranium trioxide (UO_3) (Stefaniak *et al*., 2009). U_3O_8 is relatively insoluble in water and relatively stable over a wide range of environmental conditions. UO_2 on the other hand is not as stable as U_3O_8 in the environment as it may undergo alteration under various environmental conditions (Senanayake *et al*., 2005). Upon exposure to air, UO_2 is subjected to oxidation and as a result produces a secondary mineral (UO_2^{2+}) which complexes easily with phosphates, carbonates, silicates, and sulphates (Senanayake *et al*., 2005; Stefaniak *et al*., 2009).

The chemistry of uranium and other radionuclides in the environment is totally dependent on their oxidation states. The natural uranium exists in the four oxidation states, i.e., trivalent uranium [U(III)], tetravalent uranium [U(IV]), pentavalent uranium [U(V)], and hexavalent uranium [U(VI)]. U(IV) and U(VI) are the most stable oxidation states in the environment (Francis, 1998; Gavrilescu *et al*., 2009). Uranium (III) may easily oxidize to U(IV) while U(V) readily disproportionate to U(IV) under most reducing conditions found in nature. The highly soluble U(VI) ion mainly exist as UO_2^{2+} (uranyl) under oxidising conditions, while U(IV) exist as sparingly soluble UO_2 (uraninite) under reducing conditions. In soil of pH range 4-7.5, uranium typically exits in the hydrolysed form $UO_2(OH)_4^{2-}$ while in water uranium typically exists as hydroxyl carbonate complexes such as $(UO_2)_2CO_3(OH)_3^{-}$, $UO_2(CO_3)_2^{2-}$, $UO_2CO_3^{0}$, and $UO_2(CO_3)^{4-}$ (Roh *et al*., 2000).

2.4 Production of Uranium and Its Use

Although there are several uranium mining activities around the world, about 66% of all the uranium extracted comes from only ten mines. The rest of the sources are distributed among the low output mines and uranium recovered from waste streams of gold and copper mining. Uranium mining involves open cut mining (30%), underground mining (50%), and *in situ* leach (ISL) mining (20%). Open cut mining is applied where the ore bodies lie close to the surface (250 m deep), whereas underground mining is applied where the ore bodies lie deeper, and involves construction of access tunnels and shafts. In the case of ore bodies that lie in groundwater resources, *in situ* leaching mining is applied which involves oxygenating of groundwater and pumping it out to a treatment plant on the surface. In South Africa, uranium production has generally been a by-product of gold or copper mining. The concentration of uranium recovered as a by-product from the treatment of other ores is however relatively small as compared to that from the ore bodies mined primarily for their uranium content. Thus, it is about 10% of that from the ore bodies mined primarily for their uranium content. In South Africa only about 7% of the world's available uranium can be recovered from waste streams of gold and copper processing.

For many years (from as early as 79 AD) prior to the discovery of its radioactive properties, uranium was primarily used as a colorant in ceramic glazes, producing orange-red to lemon-yellow color. It was also used in early photographs for tinting and shading. Later in 1896, Henry Becquerel discovered its radioactive properties (Gavrilescu *et al.*, 2009). Soon after that, old uranium deposits were mined to obtain its decay product, radium (Ra) which was used in luminous paint, particularly for dials of watches, and aircraft instruments. From 1940 to 1970, almost all of the uranium that was mined was used in the production of nuclear weapons. For example, during the later stages of World War II, the entire Cold War, and to a lesser extent afterwards, uranium has been used as the fissile explosive material to produce nuclear bombs (1950-1980). In recent times, uranium is significantly used as a fuel in nuclear reactors to generate electricity. Smaller specially built reactors have been used with uranium as a fuel to produce isotopes for medical and industrial purposes around the world. Moreover, uranyl acetate and uranyl formate is still used to produce electron-dense stains in transmission electron microscopy to increase the contrast of biological specimens in ultrathin sections and in negative staining of viruses, isolated cell organelles, and macromolecules. In very small amounts uranium salts are still also used as mordents of silk or wool and in leather and wood industries for stains and dyes (ATSDR, 1999).

2.5 Uranium as a Fuel for Nuclear Power

Uranium is sourced from rich ores with concentrations up to 10%. However, ores with uranium oxide concentration as low as 0.2% are also mined and are the most common (Sovacool, 2008; Tudiver, 2009). Uranium producers have been able to utilise ores with uranium oxide concentration as low as 0.0004%. Uranium is recovered from ore by communition of the rocks followed by leaching using alternative solutions of acid and/or alkaline chemicals. The end product from ore milling and leaching results into a bright yellow powder called yellow cake (U_3O_8) which is about 75-90% uranium oxide (Sovacool, 2008). Before this uranium oxide concentrate can be used in a reactor for generating electricity, it must first be converted into uranium hexafluoride (UF_6), which is used in a gaseous diffusion enrichment process. During the uranium enrichment process, U^{235} concentration is increased to least 3.5% for atypical commercial light water reactor and up to 4-5% for other modern reactors while at the same time the U^{238} isotope is decreased notably. Suffice to say U^{235} is the only natural occurring isotope that can sustain a fission chain reaction by capturing neutrons and splitting into two parts yielding large amount of energy (Soudek *et al*., 2006; WNA, 2008). On average, the specific radioactivity of natural uranium is 25 kBq/g, double that of U^{238}. During its decay process uranium may generate 0.1 watts/tonne which is enough to warm the Earth's mantle (WNA, 2008).

After the enrichment process, about 85% of oxide comes out as waste in the form of depleted UF_6 and the remaining 15% emerges as enriched uranium and is converted into ceramic pellets of UO_2. Fresh UO_2 which contains up to 5% of U^{235} (hereafter presented as U-235) is then packaged in zirconium alloy tubes and bundled together to form fuel rod assembles for reactors. Thereafter, the used reactor fuel which contains up to 95% U^{238} (also presented as U-238), 3% fission products and transuranic isotopes, 1% plutonium, 1% U-235 is removed and stored to be reprocessed prior to disposal (Soudek *et al*., 2006; WNA, 2008). During the reprocessing stage, uranium (U-235) and plutonium (Pu-239) are separated from the spent fuel using the PUREX method and then reused as mixed oxide (MOX) fuel in the reactor. This process is referred to as the close fuel cycle (Figure 2-1).

As of the year 2010, there were approximately 438 nuclear power plants in operation in 31 countries around the world providing about 14% of the world's primary energy needs. The world's nuclear generating capacity currently stands at about 372 GWe, with the United States of America, and France being the leading producers of the world nuclear energy, at

27%, and 17%, respectively (IAEA, 2009; 2011). The slow progression towards wider application of nuclear energy technology in many countries of the world since 1986 has mainly been due to concerns over famous reactor accidents such as those which occurred in Three Mile Island, Chernobyl, and Fukushima; the possibility of proliferation of atomic bomb making materials to renegade regimes and terrorists; and long term radiation contamination (Mtimunye and Chirwa, 2013).

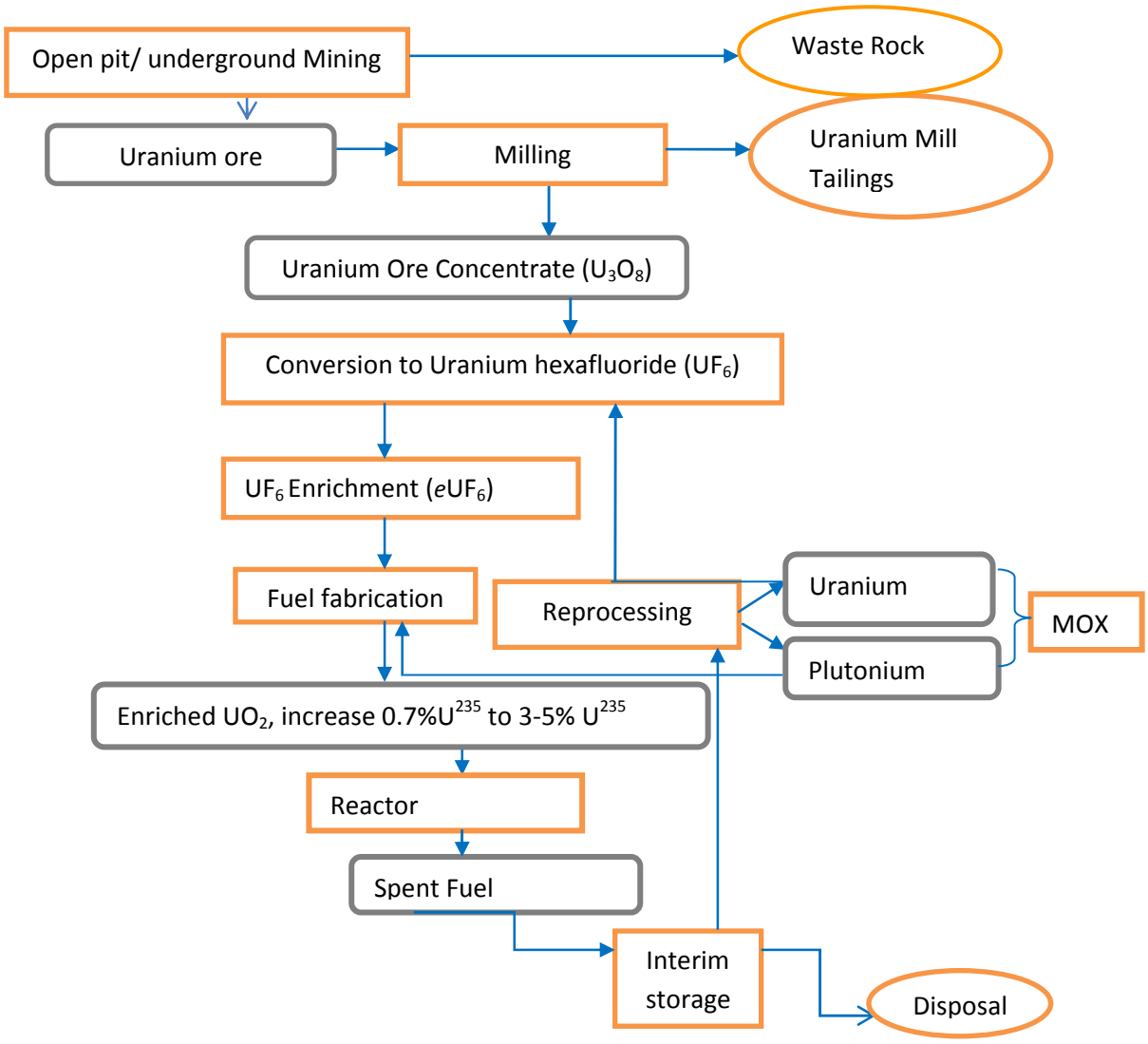

Figure 2-1: Nuclear fuel closed cycle

In the developed world, most nuclear power plants in operation today have reached or are nearing their design life. Most of these power plants were constructed in the 1960's and 1970's. These reactors include light water cool reactors (LWRs), pressurized water reactors (PWRs), and boiling water reactors (BWRs) all of which rely on enriched uranium oxide as a

fuel and water as a coolant. These reactors need to be decommissioned and dismantled and be replaced by new environmentally sustainable nuclear power reactors with improved safety features. Examples of these new power generation reactors include high temperature reactor (HTR) and the Pebble Bed Reactor (PBR) technology. This fourth generation (Generation IV) reactor technology utilizes graphite as the neutron moderator and inert gas such as helium instead of water in the reactor core as a coolant (Koster *et al*., 2003). Because these reactors can be allowed to operate at higher temperatures than the conventional water cooled reactors, the efficiency of the system is greatly enhanced. To avoid catastrophic events such as Chernobyl 1984 in Ukraine, new designs with inherent safety based on helium-cooled, self-regulating Bryton cycle have been researched (IAEA, 2002; Poullikkas, 2013). Systems such as the Pebble Bed Reactor prevent fuel elements from ever coming into contact with each other by encasing them in graphic and carbide protective layers. It is therefore said that a PBR cannot melt down under overloaded conditions (McConnell, 2012; Poullikkas, 2013).

2.6 Radioactive Waste

Uranium mining has always been a strategic issue for profit generation in countries involved in nuclear energy, quite often prioritized over the environment protection. Uranium ore mining and milling of lower grade uranium ore with uranium oxide concentration of (0.1%-0.2%) to produce the uranium concentrate (U_3O_8) yields large amount of radioactive waste. This is mainly because about 1000 tons of rocks are required to produce 1 ton of yellow cake of 75-90% purity. The waste rock generated from uranium ore mining contain minerals of interest such as radium (Ra) which has high commercial value and base metals. Extraction of Ra from the waste rocks also releases prodigious quantities of uranium waste which become an ever growing environmental legacy. The uranium waste resulting from uranium ore mining and milling to generate U_3O_8 concentrate and other minerals of commercial value ultimately yield a fine sandy tailing which contains a wide range of radioactive materials associated with mineral ore processing (WNA, 2008; Stefaniak, 2009). This waste is radioactive and, if not treated or managed properly, may cause long-term radiation pollution to air and water resources.

Uranium mining to extract Ra and U_3O_8 is not the only source of potential radioactive pollution in the environment. Other activities such as radioisotope manufacturing and biomedical research have also contributed significant amounts of radioactive waste into the environment (Tikilili and Chirwa, 2011). Moreover, the radioactive waste generated from

various industrial activities contains various radioactive materials such as irradiated organic compounds and fission products (Ngwenya, 2011; Tikilili and Chirwa, 2011).

2.7 Classification of Radioactive Waste

Several categories of radioactive waste are produced in the nuclear industry ranging from highly radioactive waste to low radiation level waste. A detailed categorization of the radioactive waste is provided by the United States Nuclear Regulatory Commission (*http://www.nrc.gov/waste*); the main categories are summarized below.

Low Level Waste (LLW): primarily generated from hospitals, radioisotope manufacturing industries, and nuclear fuel cycles. It comprises of lightly contaminated items like, papers, working tools and clothes from power plant operation. It accounts for about 1% of the total volume of the radioactive waste. It does not require shielding during handling and transportation and is suitable for shallow land burial.

Intermediate Level Waste (ILW): results from fuel processing, and nuclear reactor decommissioning. It comprises of used filters, steel components from within reactor. It accounts for about 4% of the total volume of the radioactive waste. Shielding of ILW generally depends on the source of the waste. For example, the waste from reactors such as filters does not require shielding and can be buried in a shallow repository as a result of its short-live radioactivity. Waste from fuel processing on the other hand requires shielding and should be buried deep underground taking into consideration longer half-lives.

High Level Waste (HLW): results from nuclear weapons processing and from the use of uranium fuel in nuclear reactors. The high level waste includes uranium and its fission products, and transuranic elements which accounts for over 95% of the total radioactivity of radioactive waste (IAEA, 2009). The lightweight fission products emanating from nuclear fuel processing plants includes caesium (Cs-137), strontium (Sr-90), and cobalt (Co-60). These elements are characterised by very high radiological decay rates and short half-lives. As a result of the long half-lives of these elements, the waste containing these elements may not be disposed off and handled as the LLW and ILW.

Transuranic Waste (TRU): As defined by United States of America's regulations, transuranic (TRU) waste is without regard to source or form, waste that is contaminated with alpha-emitting trans-uranium radionuclides with half-lives greater than 20 years, and activity

greater than 100 nCi/g of waste but not including HLW. Transuranic elements are elements with atomic number beyond that of uranium (92). These elements include plutonium, neptunium, americium, and others. Transuranic elements have been released in the environment (air, soil, and water) as consequence of nuclear weapon testing, and reactor accidents. It consists of clothing, tools, rags, residues, debris and other such items contaminated with small amounts of radioactive elements mostly plutonium. Because of the long half-lives of these elements, TRU waste may not be disposed off as either LLW or ILW. It does not have the very high radioactivity of HLW or its high heat generation. The United States currently permanently disposes off transuranic waste of military origin at the Waste Isolation Pilot Plant.

2.8 Waste from High Temperature Fast Reactors

High Temperature Gas-Cooled Reactors (HTGR), also known as Fast Reactors, mostly utilise graphite as the fission reaction moderator. Graphite in the fast reactors is used either as part of the structural materials for the reactor core vessel or as fuel containment elements in the form of pebbles (spheres). The graphite used from natural sources contains non-carbon impurities within the carbon matrix. Among these impurities are oxygen and nitrogen from entrapped air, cobalt, chromium, calcium, iron, and sulfur (Khripunov *et al*., 2006). Upon exposure to high neutron flux, most of the impregnated impurities are expected to transmute to unstable radioactive forms. Impurities such as transitional metals Cr^{6+} and Co^{2+} may also be found in the radioactive forms.

Improper disposal of radioactive wastes from nuclear power plants and various industrial activities as a result of cost related issues and other issues may pose a threat to living organisms including mammals as these elements may easily be taken up by plants and other animal life forms upon reaching the environment (Ajlouni, 2007).

2.9 Chemical and Radiological Toxicity: Risk to Human and Animal Health

Uranium compounds from the environment can enter the human body through three main routes of exposure thus, ingestion, inhalation, and dermal contact. Inhalation and ingestion is the most likely route of uranium exposure while dermal contact is relatively an unimportant type of exposure. Uranium has both chemical and radiological toxicity. The permissible body level for soluble compounds is based on chemical toxicity, while the permissible body level for insoluble compounds is based on radiological toxicity. The toxicity of uranium

compounds is closely related to its mobility. That is, the more soluble the uranium compound, the more toxic it is to organisms (Craig, 2001; Winde, 2010). The less soluble uranium compounds which include UO_2, U_3O_8, UO_3, UF_4, uranium hydrides, and carbides are less reactive in mammalian cells as they dissolve slowly in body fluids (weeks for UO_3 to years for U_3O_8 and UO_2) while the highly soluble uranium compounds such as UF_6, UCl_4, UO_2F_2, $UO_2(NO_3)_2$, UO_2Cl_2, uranyl acetate, uranyl sulphates, and uranyl carbonates, exhibit high toxicity to mammalian cells.

2.9.1 Chemical Toxicity

The major chemical toxicity associated with exposure to soluble uranium compounds through inhalation or digestion is kidney failure. The inhaled or digested uranium compounds enter the blood stream where they are filtered by the kidneys. At lower intake levels around 25 to 40 mg, damage can be detected by the presence of protein and dead cells in the urine. However, high uranium intake ranging from about 50 to 150 mg, may cause acute liver or kidney failure and even death (Choy *et al*., 2006; Xie *et al*., 2008). The high toxicity effect associated with insoluble uranium compounds is largely due to lung irradiation by inhaled particles. After entering the bloodstream, the adsorbed insoluble uranium compounds tend to bioaccumulate and stay for years in bone tissue because of uranium affinity for phosphate. Additionally, the accumulation of these insoluble uranium compounds in lungs over time may lead to increased risk of cancer (WHO, 2001).

2.9.2 Radiological Toxicity

Several human health effects are also associated with exposure to radiation from uranium. In general, U-235 and U-234 pose much greater radiological health risk than U-238 as they have much shorter half-life, decay quicker, and therefore are more radioactive. All uranium isotopes (U^{234}, U^{235}, U^{238}) emit (alpha) α-particles that have little penetrating ability that are unable to penetrate even the superficial keratin layer of human skin. This is because the particles are relatively large and have a positive charge. Therefore, radiation hazard from soluble uranium compounds primarily occurs when uranium compounds are ingested or inhaled, representing an internal radiation hazard (Craig, 2001).

Uranium isotopes may also emit beta and gamma particles during their decaying process to stable lead isotopes. Beta-particles have greater ability to penetrate the skin than alpha particles while gamma rays are have extremely high penetrating ability than both alpha and

beta particles, and may present both an internal and external hazard. Consequently, exposure to low levels of external radiation emanating from uranium decay products in the vicinity of large quantities of uranium in storage or in processing facility may result to radiation hazard. At the exposure levels associated with the handling and processing of uranium, the primary radiation health effect of concern is associated to the increased probability of developing cancer over time as the uranium uptake increases (UNSCEAR, 1999; Mtimunye and Chirwa 2013). Uranium is also known as a teratogen as it can cause birth defects.

The huge volume of radiotoxic waste on soil, surface water, and groundwater systems associated with improper disposal of spent fuel waste from the nuclear reactor has led to multidisciplinary studies that evaluate the impact of uranium and its decay products in the environment.

2.10 Remediation Strategies

Treatment is performed on nuclear waste to achieve one or all of the four targets for handling of waste: waste minimization, toxicity reduction, volume reduction, and/or security (deterrence of proliferation). The targets can be achieved through physical, chemical, or biological processes that may be applied either *in situ* or *ex situ*.

2.10.1 Physical-Chemical Treatment

Physical-chemical treatment strategy for uranium and other radioactive waste involves the physical extraction of the radioactive component based on its chemical charge or size to reduce the volume of radioactive waste followed by treatment of the bulky waste using conventional methods (Chirwa, 2011). Processes that have been tried include ion exchange, chemical oxidation, membrane, and adsorption processes.

Ion exchange Process

Ion exchange is a unit process by which ions of given species are displaced from an insoluble exchange material by ions of a different species in a solution. In the ion exchange process uranium-containing solution enters one end of the column under pressure and passes through a resin bed which separates the uranium from the solution. Most ion exchange resins are not selective and therefore may not be effective in removing metallic elements from nuclear waste. Several specially designed resins that target specific species by manipulating the composition of the functional groups have been tested for removal of uranium from waste

streams (VanLam *et al*., 2000; Zaganiaris, 2009). Although, proven to be successful on pilot scale, full implementation of ion exchange for uranium separation is hindered by high cost. Additionally the ion exchange resin surfaces are not self-regenerating, and therefore have limited capacity for adsorption (Zaganiaris, 2009).

Membrane Processes

A membrane is a semi-permeable barrier between two phases, which restrict the movement of molecules in a very strict manner. These movements are based on size exclusion, differences in diffusion coefficients, electrical charge, and solubility. Conventional membrane systems used in treating uranium includes, nano-pore filtration, ultrafiltration, microfiltration, and reverse osmosis (Pabby *et al*., 2008). Nano-pore membrane technologies have high potential due to their ability to separate radioisotopes from water or gas streams. Membrane processes are quite dependable and possess significant processing capabilities such as the ability to capture pollutants for cleaning and recycling. Lately, the economic viability of these processes has improved due to the decline in cost of membranes. However, the common limitation associated with the membrane processes is the generation of considerable quantities of radioactive solid waste in the brine. Furthermore, the treated liquid effluent is not pure enough for environmental discharge or recycling.

Chemical Extraction

Chemical extraction processes involve the use of sodium carbonate/bicarbonate and citric acid to extract uranium from contaminated soil (Phillips *et al*., 1995; Gramss *et al*., 2004). Although this process is proven to be effective in recovering or extracting uranium from the contaminated soil, extra care should be taken with quantity of citric acid or sodium carbonate used, because additional quantities may result into further uranium migration which may heavily pollute many natural ecosystems (Gramss *et al*., 2004; Kantar and Honeyman, 2006). On the other hand, oxidizing/reducing agents added to matrix to treat one metal could transform other metals in the system into mobile and toxic forms (NAS, 1974). Additionally, the long-term stability of reaction products is of concern since changes in soil and water chemistry might create conditions where the detoxified forms are reversed back to toxic forms.

2.10.2 Biological Treatment Process

Biological methods have been proposed to improve or substitute the conventional physico-chemical methods for the remediation of contaminated environments. Biological methods can be applied either *in situ* or *ex situ*. However, for areas that have already been contaminated, *in situ* treatment options are preferred for preventing further migration of the pollutants. *In situ* treatment options are considered as environmentally friendly waste management methods as they cause fewer disturbances on site and also minimize the risk associated with toxic waste transportation (Doherty *et al*., 2006; Gavrilescu, 2006; Olexsey and Parker, 2006).

Unlike organic compounds, toxic metals cannot be degraded or destroyed but can only be reduced from a high oxidation state to a lower oxidation state. Microbes have the potential to interact with metals and radionuclides in natural and synthetic environments altering their physical and chemical state such as its oxidation state, solubility, and sorption properties. Different mechanisms by which microbes remove or immobilize metals and radionuclides include (i) biosorption to cell components or extracellular polymeric substance (EPS), (ii) bioaccumulation, (iii) bioprecipitation by reaction with inorganic ligands such as phosphate, and (iv) bioreduction of soluble metal to insoluble metal (Suzuki and Banfield, 2004; Nancharaiah *et al*., 2006; Merroun *et al*., 2006; Nedelkova *et al*., 2007; Sivaswamy *et al*., 2011).

Biosorption

Biosorption is the term used to describe the uptake or binding of heavy metals or radionuclides to cellular components. This biosorption process involves both adsorption and absorption mechanisms. In this process uranium-bearing water is brought into contact with either living or dead biomass functional groups such as (carboxyl, hydroxyl, amine, and phosphate group) on their surface wall. Since the cell surface layer is in direct contact with the external environment, the charged groups on the surface layer are able to interact with ions or charged molecules present in the uranium-bearing water. As a result, metal cations become electrostatically attracted and bound to the cell surface layer. Some bacterial species may produce micro-molecules outside their own cell wall called extracellular polymeric substances (EPS) capable of immobilizing metals (Comte *et al*., 2008). Different studies on biosorption demonstrated that uranium biosorption is reversible, species-specific, and depends upon the chemistry and pH of the solution, physiological state of cells as well as the

presence of the extracellular soluble polymers (Francis *et al*., 2004; Nakajima and Tsuruta, 2004).

The biosorbents used in the biosorption process may be viewed as the natural ion-exchange materials that may avoid the potential problems encountered with ion-exchange resin such as incapability of resin regeneration. In this process desorption and recovery of heavy metals and radionuclides from biosorbents using sulphuric acids, hydrochloric acid, sodium hydroxide, or other complexing reagents for further reuse is easy (Kratchvil and Volesky, 1998; Valls and deLorenzo, 2002). Additionally, biological process improvement through genetic engineering of cells using live cells as biosorbents is possible. Although, biosorption of radionuclides to the cell surface and polymer substance is a promising technology for remediation of contaminated waters, the effectiveness of this process is highly affected by pH of the solution and saturation of the biosorbent when metal interactive sites are occupied and also the complexation of metal with carbonates which may result in slower biosorption rates.

In previous studies by Sar and DSouza (2002) and Jroundi *et al*. (2007) it was observed that biosorption under acidic conditions is not favoured in several species of bacteria. This is because at low pH, the protons (H^+) compete with UO_2^{2+} for sorption sites (surface hydroxyl groups–SOH), thus indicating poor selectivity of the biosorbent surface against competing ions. The other limitation associated with biosorption process is that the biosorbents rarely facilitate the change in the valence state of target species (Mtimunye and Chirwa, 2013).

Bioaccumulation

Bioaccumulation is an active process wherein metals are taken up into living cells and sequestrated intracellularly by complexing with specific metal-binding components or by precipitation. Intracellular accumulation of metals occurs among all classes of microorganisms as chemical surrogates by an energy-dependent transport system. Unlike metabolically essential metals such as Fe, Cu, Zn, Co, and Mn, which accumulates intracellularly via energy transport system, uranium has no known essential biological function and may be transported into microbial cells only due to increased membrane permeability resulting from uranium toxicity in the living cell (Francis *et al*., 2004; Suzuki and Banfield, 2004; Geissler *et al*., 2010). Therefore, intracellular accumulation of uranium is considered as metabolism-independent process as there is no direct evidence of uranium transporters in microorganisms.

It has been demonstrated in many studies that bacterial cells can intracellularly immobilise uranium through chelation by polyphosphate bodies. However, the major drawback associated with the use of active uptake systems is the requirement of metabolically active cells and also the challenge in metal desorption and recovery (Macaskie *et al*., 2000). For metal recovery, the cells will need to be destroyed in order to release the metal either by lysis or by incineration. Therefore, in this case, the media or the cell used for the uptake of metals cannot be reused.

Bioprecepitation

Bioprecipitation also known as biocrystallization or biomineralization is the process by which metals and radionuclides can be precipitated with microbial generated ligands such as phosphate (PO_4^-), sulphide (S^{2-}), oxalate ($C_2O_4^{2-}$), or carbonate (CO_3^{2-}) (Macaskie *et al*., 1992; Joeng *et al*., 1997). In these processes bacteria interact strongly with metals and radionuclides, eventually precipitating them as carbonates and hydroxide minerals at the surface of the cell (VanRoy *et al*., 1997). Macaskie and other researchers investigated the accumulation of UO_2^{2+} as U-phosphate on *Citrobacter sp*., using enzymatically liberated inorganic phosphate ligand (Macaskie *et al*., 1992; Merroun *et al*., 2006; Beazley *et al*., 2007; Jroundi *et al*., 2007). Cells showed no saturation constrains and it could accumulate several times their own weight of precipitated metal.

The above method showed that the secretion of inorganic compounds such as orthophosphate groups can directly bind U(VI) and form insoluble polycrystalline uranyl hydrogen phosphate ($UO_2HPO_4.4H_2O$) or meta-autunite-like mineral phase ($Ca(UO_2)_2(PO_4)_2.3H_2O$). Accumulation of these uranyl phosphate groups within certain cell-surface lipopolysaccharides (LPS) provides a nucleation site for precipitation, resulting in efficient removal of radionuclides in the solution and also preventing fouling of the cell surface (Renshaw *et al*., 2007). This indicates that precipitation and biosorption are overlapping phenomena, and it can be difficult to assign the contribution of each to metal immobilization. In addition to direct precipitation by microbially generated ligands, actinides can also be removed from solution by chemisorption to biogenic minerals (Macaskie *et al*., 1994).

The limitations of this method during application in industrial processes could be similar to those encountered in biosorption. Firstly, the process is hindered by the formation of negatively charged uranyl carbonate complexes, arising from microbial metabolism of the carbon source under anaerobic conditions and the U(VI)-carbonate complex formed may also

enhance U(IV) oxidation over time (Ginder-Vogel and Fendorf, 2008). Additionally, these processes may precipitate metals other than uranium and forms insoluble uranyl-complex on the cell surface, which may eventually result in cell surface saturation.

Bioreduction

Reduction of the highly toxic and mobile U(VI) to the sparingly soluble U(IV) using appropriate microbes in the form of bio-flocs has been proposed as a mechanism for preventing the migration of U(VI) in groundwater (Lovley *et al*., 1992; Gorby and Lovley, 1992). An electron donor such as acetate, lactate, ethanol, or glucose could be introduced into the polluted environments to stimulate U(VI) reduction by native microbial species at the site (Anderson and Pedersen, 2003). Where native cultures do not have the U(VI) reducing capability, processes such as molecular bioaugmentation have been proposed whereby genetic material from U(VI) reducing bacteria is introduced into the environment using broad spectrum plasmids that can be easily taken up by some of the native bacteria (Chirwa, 2011).

Microorganisms are known to have evolved biochemical pathways for degradation or transformation of toxic compounds from their immediate environment either for survival or to derive energy by using toxic compounds as electron donors or acceptors (Istok *et al*., 2004; Merroun and Solenska-Pobell, 2008). This process has been conserved over billions of years, such that, to this day, all life on earth depends on variants of this pathway (Nealson, 1999; Bush, 2003). The overall transfer of electrons from a carbon source such as lactate to active uranium species can be represented as follows (Figure 2-2):

Microbial U(VI) reduction was first reported in crude extracts from *Micrococcus lactilyticus* by assaying the consumption of hydrogen which was dependent on the presence of U(VI) (Woolfolk and Whiteley, 1962). To date, U(VI) reduction capability has been identified in more than 25 species of phylogenetically diverse prokaryotes. Examples of these are the mesophilic sulphate-reducing bacteria (*Desulfovibro sp*.) (Lovley and Phillips, 1992), Fe(III)-reducing bacteria (*Geobacter* and *Shawanella sp*.) (Coates *et al*., 2001), fermentative bacteria from *Clostridium sp*., (Francis *et al*., 1994), *Acidotolerant bacteria* (Shelobolina *et al*., 2004), *Thermoterabacterium* (Khijniak *et al*., 2005), *Myxobacteria sp.* (Wu *et al*., 2006) and others as shown in Table 2-1 below.

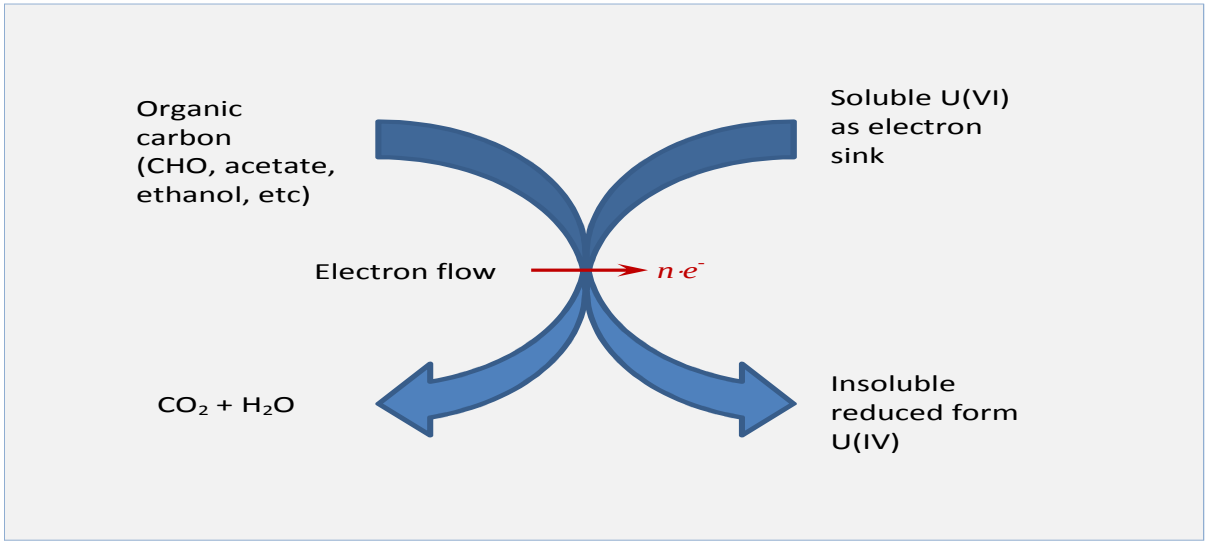

$$U^{4+} + 4OH^- \rightarrow U(OH)_{4(s)}\downarrow$$

Figure 2-2: Microbial reduction of U(VI) to U(IV). Energy Transduction and Metal Reduction (Mtimunye and Chirwa, 2013).

An example of a balanced stoichiometric relationship during U(VI) reduction using lactate as an electron donor is represented as follows:

$$UO_2^{2+} + 0.5CH_3CH_2COO^- + 0.5H_2O \xrightarrow{URB} UO_2 + 0.5CH_3COO^- + 0.5CO_2 + 2H^+ \quad (2\text{-}1)$$

where: URB represent U(VI) reducing bacteria or enzyme. It can be seen in Equation 2-1 that UO_2^{2+} needs to accept two electrons in order to be converted to UO_2.

Researchers such as Lovley and co-workers (1991) were the first to demonstrate the importance of dissimilatory metal-reducing bacteria (DMRB) in reducing toxic form of uranium (U), iron (Fe), manganese (Mn), and other toxic metals (Lovley *et al*., 1991; Wade and DiChristina, 2000; Lloyd *et al*., 2003). In this process energy is conserved for anaerobic growth of these organisms (Lovley *et al*, 1993; Wu *et al*., 2006). Since the ability to reduce U(VI) enzymatically is not restricted to Fe(III)-reducing bacteria, other organisms such as *Clostridium*, *Desulfovibrio desulfuricans*, *Desulfosporosinus sp*., *Desulfovibrio vulgaris*, and *Anaeromyxobacter Dehalogenans* were also able to reduce uranium via a respiratory process that does not conserve energy to support anaerobic growth (Lovley and Phillips, 1992 and 1994; Francis *et al*., 1994; Suzuki *et al*, 2004; Wu *et al*., 2006).

Table 2-1: U(VI) reducing bacteria, their source, and preferred environmental conditions

Bacterium	Source of Culture	Growth Condition, Energy Source
Anaeromyxobacter dehalogenans str. 2CP-C	Stream sediments	Anaerobic, 2-chlorophenol
Cellulomonas flaigena ATCC 482	Sugar cane field	Aerobic/anaerobic, glucose and others
Clostridium sphenoides ATCC 19403	Mine pit water	Anaerobic, glucose, citric acid
Desulfomicrobium norvegicum DSM 765	Sediment core	Anaerobic, acetate and others
Desulfotomaculum reducens	Salt water, USA	Anaerobic, lactate and others
Desulfovibrio baarsii DSM 2075	Ditch mud, Germany	Anaerobic, ethanol and others
Desulfovibrio desulfuricans strain ATCC 29577	Tar sand mixture, UK	Anaerobic, acetate and lactate
Desulfovibrio desulfuricans strain G20	Oil reservoir, Alaska	Anaerobic, acetate, lactate, glucose
Desulfovibrio sp. UFZ B 490	Uranium dump, Germany	Anaerobic, ethanol, TCA metabolites
Desulfovibriovulgaris Hildenborough	Wealden clay, England	Anaerobic, lactate
Geobacter metallireducens GS-15	Sediment, Potomac River, USA	Anaerobic, acetate, formate, phenol
Geobacter sulfurreducens	Sediments, Norman	Anaerobic, acetate, formate
Pseudomonas putida	Uranium mill tailing sites	Anaerobic, glucose, pyruvate
Pseudomonas sp. CRB5	Chromate containing sewage	Anaerobic, lactate and others
Pyrobaculum islandicum	Iceland geothermal power plant	Anaerobic, elemental sulphur, iron, thiosulfate
Shewanella alga BrY	Estuary sediment, New Hemisphere	Facultative anaerobic, insoluble mineral oxides
Shewanella oneidensis MR-1	Sediment, Onedia Lake, New York	Anaerobic, lactate
Shewanella putrefaciens strain 200	Oil pipe line, Canada	Anaerobic, formate, lactate
Thermoanaerobacter sp	Geothermal spring	Anaerobic, glucose, peptone, pyruvate
Thermus scotoductus	Hot tap water, Iceland	Aerobic, acetate
Thermoterrabacterium ferrireducens	Hotspring in Yellowstone, USA	Anaerobic, citrate, glycerol

*Adapted from (Chirwa, 2011)

The unique physiological property of DMRB, (*Geobacter* and *Shawanella*) is that they are obligate anaerobes that are required to respire anaerobically on their terminal electron

acceptor such as Fe(III) and Mn(IV) oxide. DMRB respiring solid such as Fe(III) and Mn(IV) oxide as anaerobic electron acceptor, are presented with unique physiological problem of engaging electron transport system with poorly soluble minerals. Therefore, in order to overcome the problem of respiring solid electron acceptor which are unable to contact inner membrane (IM) localized electron transport system, Fe(III) and Mn(IV) respiring DMRB are postulated to employ a variety of novel respiration strategies not found in other gram-negative bacteria that respire on soluble electron acceptors such as O_2, NO_3^-, SO_4^{2-}, CO_2.

Radionuclides such as U(VI) and Tc(VII) are relatively soluble in the environment, typically as anionic uranyl-carbonate complexes. The solubility of the radionuclides U(VI) and Tc(VII) under natural pH, indicate that these soluble species are more bioavailable than the (Fe(III) and Mn(IV)) oxide as they may easily enter the cell periplasm through porins or channels in the outer membrane.

2.11 Enzymatic U(VI) Reduction

Members of genera *Shewanella*, *Geobacter*, *Clostridium*, *Desulfovibrio*, and *Desulfosporosinus* have been used in the reduction of U(VI) under both aerobic and anaerobic growth conditions (DiChristina *et al*., 2005). The mechanism by which *Shewanella* and *Geobacter* species enzymatically reduce U(VI) to U(IV) involves a dissimilatory respiratory process where energy is conserved for cell growth (Lovley *et al*., 1993). In the above organisms, the electron transport pathway is believed to include *c*-type cytochrome on the membrane (Lloyd *et al*., 2002). The enzymatic U(VI) reduction activity is affected by U(VI) chemical speciation, electron donors, complexing-ligands, and competing electron acceptors.

2.11.1 Geobacter Reductase

Several genes of *Geobacter sulfurreducens* which include trihaeme periplasmic cytochrome, *c7*, diheme periplasmic cytochrome, and tetraheme cytochrome, *c3*, display U(VI) reductase activity *in vitro*. However, mutants deficient in either cytochrome-*c3* or cytochrome-*c7* preserve U(VI) reduction activity *in vivo* (Lloyd *et al*., 2003). These findings suggest that either cytochrome *c3* and *c7* are not the physiological U(VI) reductases in *G. sulfurreducens* or that the electron transport pathway to U(VI) is highly branched and consist of multiple U(VI) terminal reductases. The highly branched nature of the U(VI) reduction pathway in *G. sulfurreducens* is reflected by the finding that Fe(III) reduction deficient *c7* mutants are also

deficient in U(VI) reduction activity (Lloyd *et al*., 2003; DiChristina *et al*., 2005).

Interestingly, although this organism is proficient at reducing a broad range of extracellular Fe(III) and Mn(IV) minerals, and UO_2^{2+}, it was observed to be inefficient in reducing, NpO_2^{+}, the reduced species of neptunyl (NpO_2^{2+}) exiting in the spent fuel nuclear waste (Renshaw *et al*., 2005; Geissler *et al*., 2010). The latter authors suggested that the enzyme system responsible for uranium reduction in *G. sulfurreducens* is specific for hexavalent actinides and is capable of transferring one electron to an actinyl ion, and the instability of the resulting U(V) then generates U(IV) via disproportionation.

2.11.2 Shewanella Reductase

To date, only four strains of bacteria have been reported to conserve metabolic energy from dissimilatory U(VI) respiration to support growth, i.e., *Shewanella putrefaciens* (formally known as *Pseudomonas sp*.), *G. metallireducens*, *Desulfotomaculum reducens*, and *Thermoterrabacterium ferrireducens* (Lovley and Phillips, 1992; Kennedy *et al*., 2004; Shelobolina *et al*., 2004; Wall and Krumholz, 2006). Early work with *S. putrefaciens* showed that cells limited for Fe were unable to use Fe(III) as a terminal electron acceptor (Obuekwe and Westlake, 1982; Wall and Krumholz, 2006). These cells lost their orange colour under Fe(II) conditions which indicated a major decrease in *c*-type cytochrome content (Kennedy *et al*., 2004). The interpretation of these observations was that cytochromes were involved in the transfer of electrons to the terminal electron acceptor or were the terminal reductases. Subsequently, various cytochromes of *S. putrefaciens* were shown to localize in the periplasm with either the cytoplasmic or the outer membrane (Myers and Myers, 1992).

Comparison of uraninite ($UO_{2(s)}$) deposition by mutants lacking outer membrane decaheme *c*-type cytochromes (MtrC) showed accumulation predominantly in the periplasm versus the deposition of $UO_{2(s)}$ external to wild-type cells (Kennedy *et al*., 2004). This result indicate that U(VI) reduction is not eliminated by any of the single mutants analysed and also supports the hypothesis that uranium reductase are likely nonspecific low potential electron donors present in both the periplasm and outer membrane. It remains to be determined whether the mutants altered for U(VI) reduction are similarly affected in their ability to use U(VI) as terminal electron acceptor for growth.

2.11.3 Electron Donors and Competing Electron Acceptors

U(VI) reduction by *Shawanella* is couple to oxidation of various electron donors such as hydrogen, lactate, formate or pyruvate (Lovley *et al*, 1991). It has been reported by Liu and co-workers (2002) that hydrogen is the most preferred electron donor as higher U(VI) reduction was observed with H_2 as an electron donor (Aubert *et al*., 2000; Liu *et al*., 2002). The observed increased U(VI) reduction rate coupled to H_2 oxidation rather than lactate oxidation was attributed to (i) the rapid flow of electrons from the periplasmic H_2-hydrogenase through the electron transport chain to the terminal electron acceptor; and (ii) the faster mass flux of neutrally charged H_2 to the enzymatic site of oxidation which does not require an active transport system.

The presence of competing terminal electron acceptors such as O_2, NO_3^-, Fe(III), and Mn(IV) may interfere with microbial U(VI) reduction in a system. To evaluate the interference of U(VI) in the presence of various competitive electron acceptors, competition between SO_4^{2-} and U(VI) reduction was explored in different approaches with the SRB (Spear *et al*., 2000). On the first approach Spear and co-workers (2000) reported that a mixed culture of SRB and a pure culture of *D. desulfuricans* was able to simultaneously reduce SO_4^{2-} and U(VI) when provided at equal molar concentrations or equal electron equivalent concentrations. On the second approach similar competition experiment was carried out with *D. vulgaris* in the presence of Fe(III), SO_4^{2-}, and U(VI) (Elias *et al*., 2004). The results showed that, in the presence of lactate as electron donor, the reactions were discreet with Fe(III) reduced first, followed by U(VI), and finally SO_4^{2-}. However, when H_2 was used instead of lactate as electron donor, Fe(III) was reduced first again and U(VI) and SO_4^{2-} appeared to be simultaneously reduced.

2.12 Cellular Localization

The subcellular location of enzymatic U(VI) reduction in DMRB has been examined recently using TEM. TEM analysis confirmed precipitated uraninite ($UO_{2(s)}$) both outside of the cell and within the periplasm of gram-negative DMRB (Lovely and Phillips, 1992; Lloyd *et al*., 2003; DiChristina *et al*., 2005; Wall and Krumholz, 2006), suggesting that U(VI)-complexes do not generally have access to intracellular enzymes. Interestingly, for the gram-positive bacterium *Desulfosporosinus*, uraninite was found in an analogous location concentrated in the region between the cytoplasmic membrane and cell wall (Suzuki *et al*., 2004). These

findings suggest that U(VI) reductases may be localized on the periplasmic of the cytoplasmic membrane or in the periplasm its self or both. Identification of U(VI) reduction products of *Desulfosporosinus* as nano-meter sized $UO_{2(s)}$-particles further suggest that the localization of the reduced uranium species within the cell cytoplasm may be associated to the diffusion of the nano-size $UO_{2(s)}$-particles from the cell periplasm.

Cytoplasmic uraninite deposit location has also been reported in few studies in *Pseudomonas sp*, and *D. desulfuricans* strain G-20 (McLean and Beveridge, 2001; Sani *et al*., 2004; Merroun and Selenska-Pobell, 2008). When TEM thin sections of *Pseudomonas* isolates were examined, U(IV) was found inside as well as concentrated at the envelope. Because uranium has no biological known function, the mechanisms of intracellular uraninite precipitation are still not well understood. McLean and Beveridge (2001) speculated that the presence of uranium precipitate in the cytoplasm of *Pseudomonas* may be due to the presence of polyphosphate granules observed in the cell which might protect the cell by forming strong complexes with uranium, thus sequestering it in cytoplasm.

In the case of *D. desulfuricans* G-20 the internal deposition of uraninite observed in cells that had been grow in a medium intended to limit heavy metal precipitation and maximize toxicity (Sani *et al*., 2004). To prevent the formation of strong complexes, the medium had no specifically added carbonate or phosphate. Such modifications may also alter the physiology of the bacterium and stimulating uptake of the toxic metal to the cytoplasm. This findings indicate that the cytoplasmic deposition of U(IV) in *Desulfovibrio* may be associated to nutritional stresses on U(VI) reduction.

With the exception of these rare reports of cytoplasmic uraninite, the localized precipitation of insoluble U(IV) in the periplasm and outside of both gram-negative and gram-positive cells suggests that U(VI) complexes do not generally have access to intracellular enzymes. The best candidates for the reductases would be electron carrier proteins or enzymes exposed to the outside of the cytoplasmic membrane, within the periplasm, and/or in the outer membrane (Wall and Krumholz, 2006).

2.13 Emerging Treatment Technologies

2.13.1 Biofilm Systems

In natural environment such as groundwater aquifers microbial community generally exist as biofilms or bio-flocs which are significant for potential metal immobilization (Chirwa, 2011).

Biofilm are formed when bacterial species adhere to surfaces in moist environments by excreting a slimy, glue-like substance, extracellular polymeric substances (EPS). The EPS which composed of polysaccharides, proteins, free nucleic acid, and water allows the complex development of the biofilm structure. The complex nature of the biofilm structure makes the organism to be more resistant to environmental changes. At the initial stage the formation of the biofilm is believed to be an active process coupled to the cell's central metabolism (Kjelleberg and Hermanson, 1984; Paul, 1984). Within the biofilm system, complex processes such as nutrient cycling, mass transport resistance, cell and substrate diffusion, and biofilm loss at the surface may take place.

Unlike most activated sludge systems, biofilm systems have the advantage of lower-carry over biomass. Thus imply that the microbes in the biofilm reactor may be retained at flow rates greater than the washout flow rates and immobilized as the dense layer growth attached to the solid surface. Biofilm is also play an important role in the cell division cycle. Meadows (1971) observed that *Pseudomonas fluorescens*, and *Aeromonas liquifaciens* cells undergo cell division only during their most stable attachment phase. The complexity in biofilms processes presented above, sometimes presents an advantage when complex metabolic processes and co-operation between different species in the community of organisms is required to remove a particular compound. Studies by Nkalambayausi-Chirwa and Wang (2001), showed the effectiveness of biofilm systems in removing two pollutants simultaneously. Optimum removal of the two pollutants was achieved in the reactor which was inoculated with both slightly facultative Cr(VI)-reducers, *Escherichia coli*, and the obligate aerobic phenol degraders, *Pseudomonas putida*. Results from this study showed that biofilm systems are self-optimised system in which metabolites formed from phenol degradation in aerobic layer supported the growth of Cr(VI) reducing bacteria in deeper layer of the biofilm.

2.13.2 Reactive Barrier Systems

Waste from nuclear power generation and other radionuclide processing facilities is usually stored in specifically engineered facilities for decade's prior final disposal (Merroun and Seleska-Pobell, 2008). In underground repositories the main concern is high probability of radionuclides escape into groundwater systems causing groundwater contamination. In areas where contamination has actually occurred further migration of the pollutants is prevented *in situ* using permeable reactive barriers (PRB). Permeable reactive barriers (PRB) are created

by extending the permeable reactive material to intercept a plume of contaminated groundwater (Figure 2-3). The wall of the PRB is engineered to be at least as permeable as the surrounding aquifer materials such that it allows passage of groundwater while treating groundwater contaminants *in situ*. Treatment of pollutants in groundwater can be both biotic and abiotic. Abiotic PBR treatment involves the use of neutralizing agents such as lime, adsorbents, and zero-valent iron (Fe^0) while biotic PBR use microbes as a permeable reactive material. The processes by which the biological permeable reactive barrier promotes *in situ* containment and stabilization of contaminants in groundwater systems include degradation, adsorption, precipitation, and reduction.

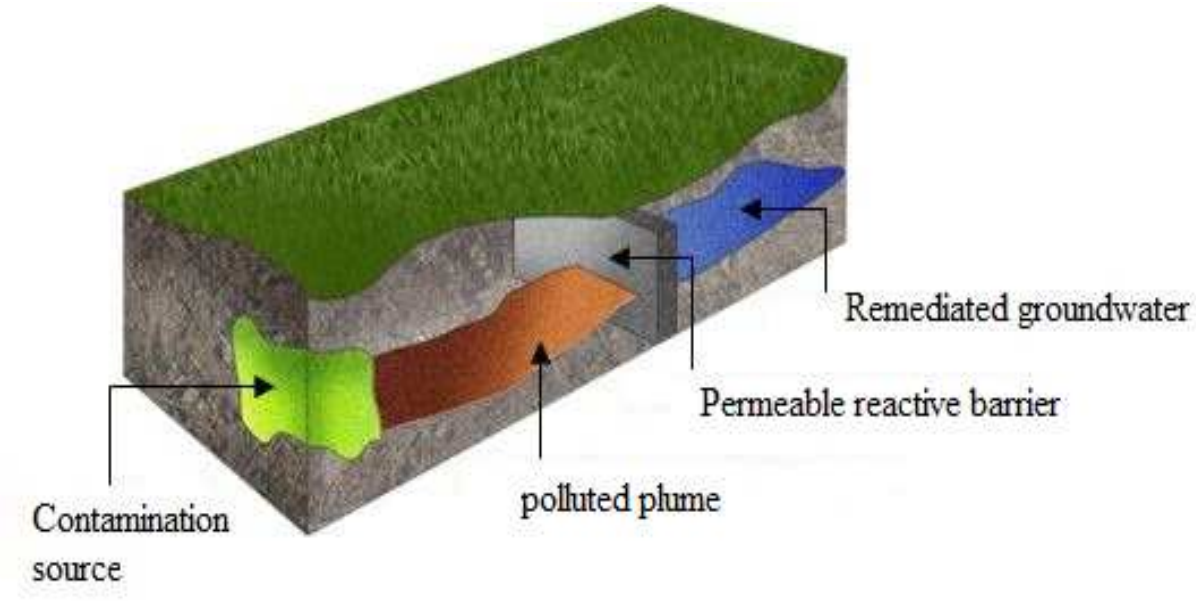

Figure 2-3: Theoretical representation of the permeable reactive barrier system as an intervention for U(VI) pollution in an unconfined aquifer system.

Chemical PRB has been tested in batch studies using fine grinned zero valent iron (Fe^0) as a reactive material (Thijs *et al*., 2004; Gavrilescu *et al*., 2009). Results from the later study demonstrated the effectiveness of Fe^0 in uranium removal, with the removal efficiency of more than 99.9%. The problem associated with the use of Fe^0 as a reactive barrier material in PRB's is that they do not provide a permanent solution as the use of chemicals to treat certain pollutants in groundwater systems may also form toxic species as a result of incomplete chemical reaction. Furthermore, the replacement of the reactive barrier material and the disposing of the spent reactant may drive up the cost of the process.

2.14 Summary

The remediation of uranium-contaminated water systems utilizing both physico-chemical and biological methods have been evaluated in this study. The remediation of uranium contaminated sites using traditional physico-chemical methods such as pump-and-treat or excavation followed by chemical treatment has been shown to be costly and disruptive to ecosystems. Biological methods on the other hand are of great interest as they are cost-effective, and environmentally friendly. Microorganisms play important roles in the environmental fate of toxic metals with prosperity of physical-chemical and biological mechanisms effecting transformations between soluble and insoluble phases. As an endeavor to solve the problem of soil and groundwater contaminated with uranium and other toxic metals, studies on *in situ* bioremediation of toxic metals have been conducted.

The main limitation associated with *in situ* bioremediation of uranium and other toxic metals is that unlike organic compounds, metals are not destroyed but rather trapped in the aquifer matrix in a reduced state. The fate of such reduced metals in a system and foreseeable blockage by hydroxide species remains a challenge. This is mainly because removal of reduced metal precipitate trapped in aquifer matrix during *in situ* treatment is a scientific intensive procedure that requires detailed investigation. While detailed investigations concerning the fate of the reduced metal precipitate in aquifer systems are still underway, pump-and-treat approach using bioreactor systems could serve as a prospective measure in preventing further U(VI) contamination to surrounding aquifers.

CHAPTER 3

EXPERIMENTAL METHODS

3.1 Bacterial Culture

3.1.1 Source and Isolation of U(VI) Reducing Microorganisms

Microorganisms were isolated from soil samples collected from the tailing dumps of an abandoned uranium mine in Phalaborwa, Limpopo (South Africa). The samples were collected in sterile containers and stored at 4°C in the refrigerator until used. Bacteria cultures were isolated from the soil samples using the enrichment culture technique. To isolate the U(VI) tolerant species, a gram (1 g) of soil sample was added to 100 mL of sterile basal mineral medium (BMM). The medium was amended with D-glucose as sole added carbon source and 75 mg/L of U(VI). The inoculum was grown under anaerobic conditions for 24 hours at 30±2°C in 100 mL serum bottles purged with nitrogen gas (99.9% N_2) and sealed with rubber stoppers and aluminium seals. After 24 hours enriched bacterial strains were isolated by serial dilution.

3.1.2 Purification of Indigenous Bacteria

Individual colonies were obtained by depositing 0.1 mL of ten times serially diluted sample from the 7^{th} to the 10^{th} test tube into the petri dishes containing sterile nutrient agar (NA) using the spread method. The plates were then incubated for about 24-48 hours at 30±2°C in anaerobic gas packs to develop separate identifiable colonies. Individual colonies based on their colour and morphology were then sub-cultured into a 100 mL sterile nutrient broth (NB) using a heat sterile wire loop. Cells were allowed to grow for 24 hours and then 1mL of 24 hours grown culture was serially diluted and then 0.1 mL of diluted sample from 7^{th} to the 10^{th} tube was deposited on a nutrient agar plates. This preparation was conducted inside anaerobic glove bags filled with 99.9% pure N_2 gas. The plates were thereafter transferred into anaerobic gas packs followed by incubation for 24-48 hours at 30±2°C. The process was repeated at least three times in order to achieve close to pure culture for each identified species. The pure cultures were then preserved at 4ºC on sealed agar slants under a nitrogen environment and were sub-cultured monthly to preserve viability. Several species of bacteria were un-culturable under the above conditions, but the target was to isolate U(VI) tolerant organisms with a high probability of being able to reduce U(VI).

3.2 Growth Media

3.2.1 Basal Mineral Media

Basal Mineral Medium (BMM) was prepared by dissolving: 10 mM NH_4Cl, 30 mM Na_2HPO_4, 20 mM KH_2PO_4, 0.8 mM Na_2SO_4, 0.2 mM $MgSO_4$, 50 µM $CaCl_2$, 0.1 µM $ZnCl_2$, 0.2 µM $CuCl_2$, 0.1 µM NaBr, 0.05 µM Na_2MoO_2, 0.1 µM $MnCl_2$, 0.1 µM KI, 0.2 µM H_3BO_3, 0.1 µM $CoCl_2$, and 0.1 µM $NiCl_2$ into 1 L of distilled water as according to Roslev et al. (1998). The medium was then amended with 25 mL of glucose solution prepared by dissolving 5 g D-glucose in 1L distilled water. The glucose solution was amended to act as a carbon and energy source for the bacteria. The prepared medium was sterilized before use by autoclaving at 121°C at 115 kg/cm^2 for 15 minutes.

3.2.2 Commercial Broth and Agar

The first three media, nutrient broth (NB), nutrient agar (NA), and Plate count (PC) agar (Merck, Johannesburg, South Africa) were prepared by dissolving 31 g, 16 g, and 23 g of powder, respectively in 1000 mL of distilled water. The nutrient agar and plate count agar media were cooled at room temperature after sterilization at 121°C at 115 kg/cm^2 for 15 minutes and then dispensed into petri dishes to form agar plates for colony development.

3.3 Characterisation of Microbial Community

The phylogenetic characterization of cells was performed on isolated individual colonies of bacteria from the 7th to the 10th tube in the serial dilution preparation. Individual colonies from the purified cultures were then prepared for 16S rRNA (16 Svedburg unit *ribosomal* Ribo-Nucleic-Acid) genotype fingerprinting. Genomic DNA was extracted from the purified colonies according to the protocol described for the Wizard Genomic DNA purification kit (Promega Corporation, Madison, WI, USA). 16S rRNA genes were then amplified by using a reverse transcriptase-polymerase chain reaction (RT-PCR) using primers pA and pH1 (Primer pA corresponds to position 8-27; Primer pH to position 1541-1522 of the 16S gene under the following reaction conditions: 1 minute at 94ºC, 30 cycles of 30 s at 94ºC, 1 minute at 50ºC and 2 minutes at 72ºC, and a final extension step of 10 minutes at 72ºC). PCR fragments were then cloned into pGEM-T-easy (Promega) [Promega Wizard® Genomic DNA Purification Kit (Version 12/2010)]. The 16S rRNA gene sequences of the strains were aligned with reference sequences from *Desulfovibrio spp.*, *Geobacter sp.*, *Acinetobacter spp.*, *Anthrobacter spp.*, and *Shewanella putrefaciens* using Ribosomal Database Project II

programs. Sequence alignment was verified manually using the program BIOEDIT. Pairwise evolutionary distances based on an unambiguous stretch of 1274 bp were computed by using the Jukes and Cantor (1969) method.

3.4 Chemical Reagents and Standards

Sodium chloride solution (0.85% NaCl) was prepared by dissolving 0.85 g of sodium chloride salt in 100 mL distilled water and sterilized by autoclaving at 121°C for 15 minutes. All chemicals used were of analytical grade obtained from Sigma Aldrich, Johannesburg, South Africa.

3.4.1 Uranium Stock

U(VI) stock solution (1000 mg/L) was purchased from (Sigma, South Africa) as uranyl nitrate ($UO_2(NO)_3.6H_2O$). The U(VI) stock solution was used throughout the experiments to serve as U(VI) source. The standard solutions of U(VI) were prepared from the U(VI) stock solutions in 50 mL volumetric flasks by diluting a specific volume of U(VI) stock solution with BMM amended with D-glucose to give desirable final U(VI) concentration ranging from (0-80 mg/L).

3.4.2 Arsenazo III Reagent

Arsenazo III reagent was prepared by dissolving 0.07 g (1,8-dihydroxynaphthalene-3,6 disulphonic acid-2,7-bis[(azo-2)-phenylarsonic acid]) in 24.8 mL of 70% perchloric acid ($HClO_4$) (Merck, SA) and then filled the volumetric flask up to 2 L with distilled water to give a red-pink color. The solution was kept at 4°C until further use.

3.5 Experimental Batches

3.5.1 Preliminary U(VI) Reduction Studies

Preliminary U(VI) removal kinetic studies were conducted in batch reactor systems to evaluate the efficiency of each isolate in reducing U(VI) as individual species. The isolates were grown overnight as individual pure isolates in a sterile nutrient broth. The overnight grown cells were then harvested by centrifuging at 6000 rpm (2820 *g*) for 10 minutes. The supernatant was decanted and the remaining pellet was washed three times with sterile 0.85% NaCl solution. The washed pellet was then re-suspended into different serum bottles containing sterile BMM amended with D-glucose and U(VI) concentration ranging from (30-

75 mg/L). The serum bottles were then purged with 99.9% pure N_2 gas for about (5-10 minutes) to expel residual oxygen in the serum bottles prior sealing the bottles with rubber stoppers and aluminium seal. The serum bottles were then incubated on a rotary shaker at 30±2°C with continuous shaking on a lateral shaker (Labotec, Gauteng, South Africa) at 120 rpm. To determine U(VI) concentration over time, aliquots of 2 mL were taken from different serum bottles, centrifuged using a 2 mL eppendorf tube at 6000 rpm (2820 *g*) in a Minispin Microcentrifuge (Eppendorf, Hamburg, Germany). The supernatant was then used for U(VI) concentration analysis.

3.5.2 U(VI) Reduction on a Mixed-Culture of Bacteria

U(VI) reduction experiments on a mixed-culture of bacteria which was grown over night in a sterile nutrient broth under anaerobic conditions were conducted. The overnight grown cells were harvested by centrifuging at 6000 rpm (2820 *g*) for 10 minutes. The supernatant was decanted and the remaining pellet was washed three times with sterile 0.85% NaCl solution under an anaerobic glove bag purged with 99.9% (N_2) gas. Anaerobic U(VI) reduction experiment were conducted in 100 mL serum bottles by adding U(VI) stock solution into the BMM amended with D-glucose to give the desirable effective final U(VI) concentration ranging between (100-600 mg/L).

Prior to inoculating the serum bottles with the washed cells, 2 mL of a sample was withdrawn from each serum bottle at various U(VI) concentration to determining the absorbance of U(VI) before inoculating the bottles with viable cells. The washed cells were then re-suspended into 100 mL serum bottles under an anaerobic glove bag purged with 99.9% (N_2) gas. The samples in the bottles were then directly purged with 99.9% (N_2) gas for about 10 minutes to expel any oxygen gas before sealing with silicon rubber stopper and aluminium seals. The samples were then incubated at 30±2°C with continuous shaking on a lateral shaker at 120 rpm. U(VI) reduction was monitored by withdrawing 2 mL of the sample at regular time intervals using a sterile syringe. The withdrawn samples were then centrifuged using a 2 mL eppendorf tube at 6000 rpm (2820 *g*) for 10 minutes in a Minispin Microcentrifuge before U(VI) analysis to remove suspended cells.

3.5.3 Abiotic U(VI) Reduction Experiments

Cell free medium and heat-killed cultures were used to determine the extent of abiotic U(VI) reduction in batch experiments. Overnight grown cells were heat killed by autoclaving at

121ºC for 20 minutes in several cycles. The heat-killed culture cells were then harvested by centrifuging at 6000 rpm (2820 *g*) for 10 minutes and then washed three times with sterile 0.85% NaCl solution followed by res-suspension into serum bottles containing BMM amended with D-glucose and U(VI) solution to the desirable U(VI) concentration of 100 mg/L. The cell-free control contained only fresh BMM amended with D-glucose and U(VI) solution to the desirable concentration of 100 mg U(VI)/L. The 100 mL serum bottles were then purged with 99.9% (N_2) for about (5-10 minutes) to expel residual oxygen prior closing and sealing with a silicon rubber stopper. All experiments biotic and abiotic were conducted in triplicates at 30±2ºC with continuous shaking on lateral shaker at 120 rpm.

3.5.4 U(VI) Reduction Pathway Targets and Inhibitors

To evaluate the effectiveness of enzymatic U(VI) reduction process, overnight grown cells were harvested by centrifuging at 6000 rpm (2820 *g*) for 10 minutes. One set of overnight grown cells was exposed to (0.1%) of rotenone ($C_{23}H_{22}O_6$), a compound that inhibits the flow of electrons from NADH to the ubiquinone (Q) in the cell membrane of many bacterial cells by binding to the (Q) binding site of NADH-dehydrogenase (Gomes *et al*., 2001; Vehovszky *et al*., 2010). The other set of overnight grown cells was exposed to (0.1%) cadmium chloride ($CdCl_2$), the known inhibitor of thioredoxin which is responsible for a number of different important cellular functions of all living organisms including humans (Zeller and Klug, 2006). Cadmium has been shown to inhibit thioredoxin by binding at Cys32 and Asp26 residues of *E. coli* thioredoxin (Rollin-Genetet *et al*., 2004; Li and Krumholz, 2009). The experimental conditions were kept the same (100 mL serum bottles containing BMM amended with D-glucose and 100 mg U(VI)/L solution, and incubated at 30±2ºC under anaerobic conditions).

3.6 Continuous Flow Suspended-Cell Bioreactor

3.6.1 Reactor Setup

The continuous flow reactor was constructed from a 10 L flat-bottomed glass flask (Figure 3-1). The glass reactor was used instead of the plastic to minimize the adsorption of uranium by the reactor itself. A rubber stopper was plugged on the opening at the top of the reactor to maintain anaerobic conditions. Four holes fitting glass tubes were drilled in the rubber stopper. The four ports on the rubber stopper include (i) the influent port, (ii) nitrogen inlet port, (iii) the outlet port that was used to maintain the reactor volume of 8L by allowing

excessive volume to escape as waste, and (iv) the effluent port. Additional port was drilled to directly insert the probe which measures the pH, ORP, and temperature (pHC101, MTC101, Hach, USA) simultaneously in a system. The reactor was placed on a magnetic stirrer (Velp Scientifica, Labex Pty Ltd, South Africa) and a sterile magnetic stirrer bar was inserted into a reactor prior closing it with the rubber stopper to achieve completely mixed conditions at 30±2°C.

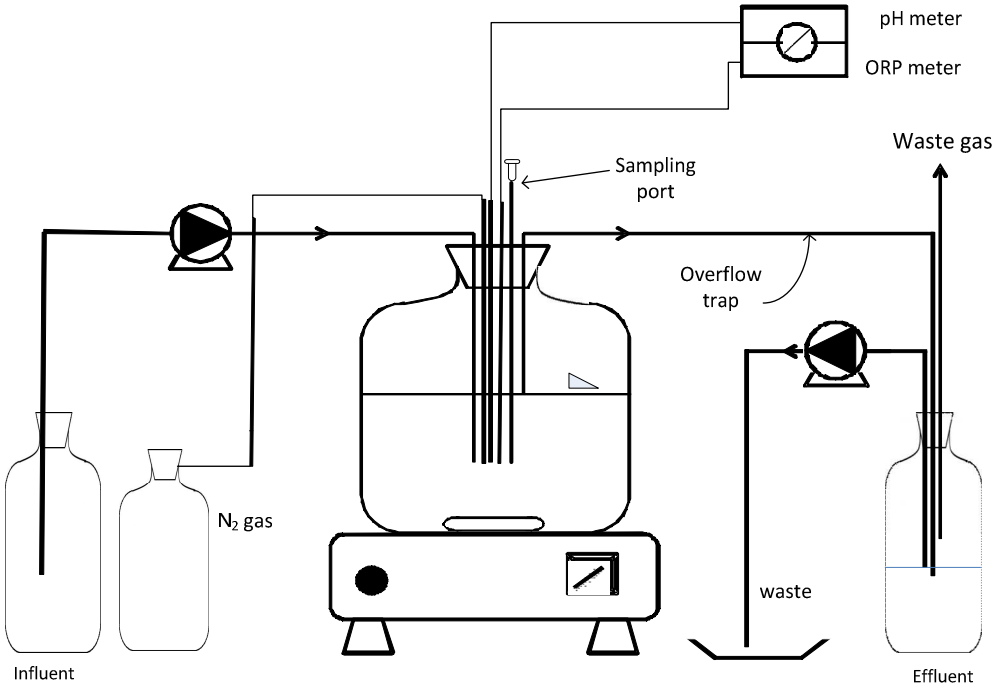

Figure 3-1: Laboratory set-up of a suspended cells continuous flow reactor.

3.6.2 Start-up Culture

A mixed-culture of bacteria from the soil samples of the tailing dumps of the abandoned uranium mine was cultivated for 24 hours in the sterile nutrient broth. The cultivated cells were then harvested by centrifuging at 6000 rpm (2820 g) for 10 minutes. The supernatant was decanted and the remaining pellet was washed three times with sterile 0.85% NaCl solution. The washed pellet was then mixed with sterile BMM amended with D-glucose as carbon source and directly re-suspended in 10 L flat-bottomed glass flask containing sterile BMM amended with D-glucose using the inlet port.

3.6.3 Reactors Operation

During the experimental run, sterile BMM amended with D-glucose and U(VI) solution of specific or target concentration ranging from (100-400 mg/L) was fed into a 10 L glass flask sealed with a rubber stopper through ports using pre-calibrated peristaltic pump which was initially calibrated to maintain a hydraulic retention time of approximately 24 hours (Masterflex, Cole-Palmer Inst. Co., Niles, Illinois). The flask was thoroughly purged with 99.9% (N_2) over time to expel residual oxygen in the flask which is continuously operated. The oxidation reduction potential (ORP) and the pH of the solution was measured continuously using ORP and pH probe (pHC101, MTC101, Hach, USA). The experiments were conducted at 30±2ºC. Samples were then withdrawn from the effluent port for U(VI) analysis.

3.7 Continuous Flow Biofilm Rector System

3.7.1 Reactor Set-up

Two columns constructed from a Plexiglas (PVC glass), (1 m long, 0.1 m internal diameter) were installed in a laboratory as continuous flow columns. Each column consisted of an influent port, four equally space intermediate sampling ports with bed heights of (0.2 m, 0.4 m, 0.6 m, and 0.8 m), and the final effluent port as shown in Figure 3-2. The columns were packed with bio-cell filters (Happykoi, South Africa) and then closed on both ends with PVC caps. A provision for biomass analysis on the biomass growth support medium was made on PVC cap placed on the top end of the column. The two packed columns were then installed vertically on the stand by clamping. The temperature in the control room where the columns were operated was maintained at 30±2°C. The pore volume which is essential for studying the movement of solute through a support media was calculated as a difference between the weight of the saturated sample and the weight of a dry sample in a column.

3.7.2 Start-up Culture

Reconstituted mixed-culture of bacteria from the soil samples of the tailing dumps of the abandoned uranium mine was cultivated for 24 hours in the sterile nutrient broth. The cultivated cells were then harvested by centrifuging at 6000 rpm (2820 g) for 10 minutes. The supernatant was decanted and the remaining pellet was washed three times with sterile 0.85% NaCl solution. The washed pellet was then mixed with diluted sterile BMM amended with diluted D-glucose solution as carbon source.

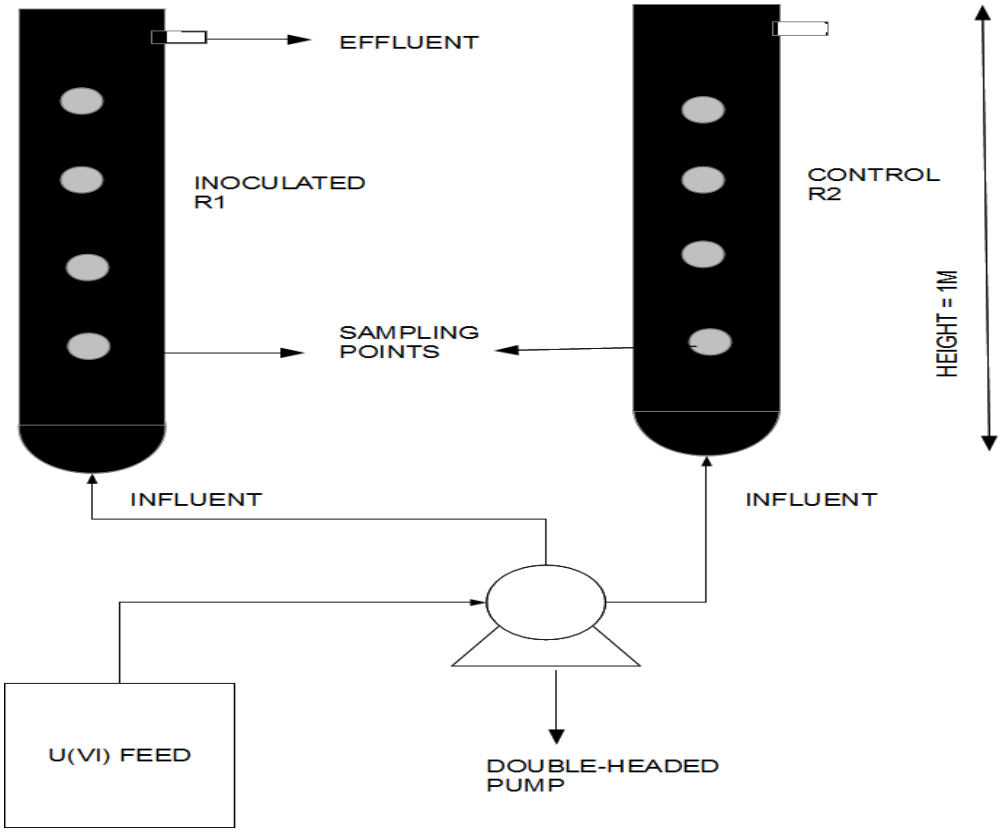

Figure 3-2: Laboratory set-up of a fixed-film continuous flow reactor.

3.7.3 Reactor Start up

Prior experimental run, distilled water was fed through each column from the bottom inlet through a peristaltic pump to check for leaks in the columns and saturate pores with water. Flow rates were also measured and adjusted to establish the hydraulic residence time (HRT) of approximately 24 hours in each reactor. One reactor columns (R1) was then seeded with viable cells solution amended with BMM and D-glucose. The viable cells solutions was fed into (R1) for 2.5 weeks through re-circulation using a pre-calibrated peristaltic pump without disturbance to allow near uniform distribution and attachment of cells to the bio-cell filter and also to sustain the growth of microorganisms in the reactor.

3.7.4 Reactors Operation

During the experimental run, sterile BMM and U(VI) solution of specific or target concentration ranging from (75-100 mg/L) was continuously fed into the reactors which were operated as packed beds. One column (R1) was seeded with the mixed-culture of bacteria and operated as a biofilm reactor, while the other column (R2) was operated as control reactor

without the addition of any cells. The microbial activity in the biofilm reactor was confirmed through protein concentration analysis prior feeding simulated U(VI) containing plume water into R1. U(VI) containing plume water was continuously and simultaneously fed into both column reactors (R1 and R2) from the bottom inlet using a pre-calibrated double headed peristaltic pump. The experiments were conducted for 99 days under oxygen stressed and nutrient deficient conditions. Samples were then withdrawn from each sampling port over time for U(VI) analysis. The column and the packing specification are given in Table 3-1.

Table 3-1: Biofilm Reactor Specification

Column and packing material properties	Value
Height of the column	1 m
Diameter of column	0.1 m
Total volume of reactor	7.85 L
Total surface area of column	0.3298 m^2
Name of packing material	Bio-cell filters
Particle size	0.013 m×0.01 m
Specific surface area	650 m^2/m^3
Density	0.179 kg/L
Packing Weight in the column	1.404 kg
Porosity	95%

3.8 Evaluation of Biomass Yield

3.8.1 Total Biomass

In a suspended cell system samples (5 mL) were withdrawn at regular time intervals, centrifuged for 10 minutes at 6000 rpm (2820 *g*). The supernatant was used to analyse U(VI) concentration and the settled pellet was used for biomass analysis. The centrifuged sample was filtered through a pre-weighed Whatman filter paper No.41 of 20 µm. The filter paper containing a wet biomass was dried in the oven at 75-80°C and cooled to room temperature in a desiccator and weighed until a constant weight was achieved. The difference between the

dried filter paper with cells and the empty filter paper was considered as a biomass concentration per 5 mL.

For measurement of the attached cells in a biofilm reactor, sample (biofilm support media) was extracted from the column using sterile tweezers. The sample was then washed with gentle shaking for about 15 minutes in 10 mL distilled water to remove sorbet medium. The washed sample was then dried in an oven at 45±5°C for about 5 hours, cooled to room temperature in a desiccator. The sample was then washed again with distilled water three times for 15 minutes by vigorous shaking, and the dehydrated into 30% ethanol to ensure cell detachment. The sample was then allowed to further dry in oven over nigh at 50±5°C, cooled to room temperature in a desiccator. Cell detachment on the sample was confirmed using microscope (Zeiss, Germany). The total biomass was calculated as a difference between the bio-cell filter with biomass and bio-cell filter without biomass.

3.8.2 Viable Biomass Analysis

Samples (1 mL) were withdrawn from experimental batches at regular time intervals of 0-72 hours for the analysis of viable cell concentration. The withdrawn samples from each batch reactor over time were then serially diluted in 10 test tubes containing 9 mL of sterile 0.85% NaCl solution. The diluted sample (0.1 mL) from the 7^{th} to the 10^{th} tube was then transferred into a PC agar plate using the spread method. The PC agar plates were then incubated for 18-24 hours at 30±2°C. Colonies were counted after incubation and multiplied by a dilution factor. The bacterial count was reported as colony forming units (CFU) per mL of sample.

For the biofilm reactor the sample (biofilm support media) was extracted from the column using sterile tweezers. The sample extracted from the column was initially weighed and then placed into a 9 mL sterile buffered solution (Ringer's solution) solution which was prepared by dissolving 2 Ringer's tables into 1 L distilled water as per manufacture instruction (Merck, Johannesburg, South Africa). The solution containing the bio-cell filter was then agitated over several times to dislodge most of the microbes without destroying them. The supernatant was serially diluted up to 10 times dilution factor. From each tube, 0.1 mL of the solution was transferred into the agar plate using a spread method. This was done in triplicate for each dilution to have statistical representivity. The plates were then incubated for (2-5) days at 30±2°C. The number of colonies were then counted and multiplied by a dilution factor. The bacterial count was reported as colony forming units (CFU) per mL of sample.

3.8.3 Protein Concentration

Proteins make up a large fraction of the biomass of actively grown microbes. Total protein concentration in a cell was determined in a UV/ Vis spectrophotometer at the wavelength of 595 nm using Coomassie dye as a complexing agent to facilitate protein detection. The accuracy and the precision of the method were determined by measuring the concentration of the Bovine Serum Albumin (BSA) standard solutions according to the protocol described for the Coomassie Plus Brandford Assay Kit. To measure protein concentration 2 mL of the unfiltered sample was withdrawn and then diluted with 0.1 M of HNO_3 for about 15-20 minutes in order to facilitate protein extraction. The well mixed aliquot of 0.5 mL was pippeted in an eppendorf tube, mixed with 1.5 mL of the Comassie Plus Reagent, allowed to stand for 5-10 minutes and centrifuged for 10 minutes in order to settle the available pellet prior analysing in a UV/ Vis spectrophotometer. The amount of protein was estimated by interpolation from standard curve prepared with BSA.

3.9 Analytical Methods

3.9.1 Elemental Analysis by ICP-MS

Metallic elements of the soil samples collected from the tailing dumps of the abandoned uranium mine in Phalaborwa, South Africa were characterised using Inductively-Coupled Plasma-Mass Spectrometry (ICP-MS) Spectromass 2000 (Spectro Analytical Instruments, Kleve, Germany). The elements were extracted from the soil sample as according to Zhou and Gu (2005). The pre-weight 5 g of soil sample was suspended in 25 mL of 0.1 M $NaHCO_3$ under room temperature (20±5°C). The soil sample was thoroughly mixed with $NaHCO_3$ by vortex and then allowed to stand for 24 hours. After 24 hours the sample was centrifuged for 10 minutes in three cycles at 6000 rpm to remove soil particles and elemental precipitates formed in the aliquot. The aliquot was then diluted with deionized water up to 50 mL. The sample was then analysed using ICP-MS for total uranium and other elements in the Laboratory at NECSA Limited, Phelindaba, South Africa. This analysis was mainly performed to confirm the background uranium concentration at the study site and also to reveal other elements present in the soil sample. Background uranium concentration in the samples was detected at levels as high as 29 mg/kg (72 mg/L) much higher than the values observed in natural soils (0.3-11.7 mg/kg). Table 3-2 shows elementary soil composition of significant presence.

Table 3-2: Mineral composition of the tailing dumps soil samples

Element	Symbol	Mass concentration (mg/L)
Aluminium	Al	8.2096
Bismuth	Bi	8.5385
Boron	B	0.3472
Calcium	Ca	677.54
Iron	Fe	299.65
Magnesium	Mg	216.90
Manganese	Mn	6.0716
Sodium	Na	3.4397
Potassium	K	4.2016
Uranium	U	72

3.9.2 Determination of U(VI)

U(VI) reductase activity was determined by measuring the decrease in U(VI) in the solution using UV/Vis spectrophotometer (WPA, Light Wave II, and Labotech, South Africa). Arsenazo III (1,8-dihydroxynaphthalene-3,6 disulphonic acid-2,7-bis [(azo-2)-phenylarsonic acid]), a non-specific chromogenic reagent, was selected as the complexing agent for facilitating U(VI) detection (Bhatti *et al*., 1991). Measurement of U(VI) was carried out by sampling 2 mL of solution from the reactors using disposable syringes. The withdrawn sample was then centrifuged at 6000 rpm (2820 *g*) for 10 minutes using Minispin-Microcentrifuge. The centrifuged sample (0.5-1 mL) was then diluted with 0.4 mL of 2.5% diethylene-triaminepenta acetic acid (DTPA) and diluted up to mark with BMM in a 10 L volumetric flask. The homogenous solution was the mixed with 2 mL of complexing reagent (Arsenazo III), allowed to stand for full colour development prior analysis for U(VI) at 651 nm. In the presence of hexavalent uranium the reddish-pink complexing reagent changed into blue color. DTPA was added to mask the interference caused by other cations (Shrivastsva *et al*., 2013).

3.9.3 Determination of Total Uranium

For total uranium analysis, an unfiltered sample (0.5 mL) withdrawn from the reactor was digested with 1 mL of 2 M HNO_3, centrifuged for 10 minutes at 6000 rpm (2820 *g*). The supernatant was collected and diluted up to mark with BMM. Total uranium was then measured using inductively-coupled plasma mass spectrometry (ICP-MS) which was previously calibrated against the uranium atomic adsorption standard solutions ranging from (0-100 mg/L). The linear graphs/calibration curves with the regression of 99.5% were then obtained by plotting absorbance versus the known concentration data of uranium.

3.9.4 X-ray Powder Diffraction Analysis (XRD)

To ascertain the chemical nature of radionuclides bound to the biomass the XRD analysis of metal loaded sample was conducted in the Laboratory at NECSA Limited, South Africa. After the bio-removal process the metal loaded sample was concentrated by centrifuging at 600 rpm for 10 minutes. The supernatant was decanted and the remaining pellet was dried at 60±10°C for 72 hours. The dried sample of uranium loaded biomass was grinded to near even fine particle using mortar pestle method and then loaded into sealed sample holder to prevent sample and equipment contamination. The sample was then analysed in XRD using Bruker powder diffraction meter (Model D8 Advanced) with Cu-Kα radiation. The diffraction pattern was recorded from 8-84° (2θ) with step size of 0.04° and time per step size 8.1 s. The chemical nature of uranium crystals was determined by comparison with the powder diffraction standard files in 2007 PDF-2 database.

3.9.5 Fourier Transform Infrared spectroscopy (FTIR)

To elucidate the chemical or functional groups involved in metal binding on the bacterial surface the FTIR analysis of control (metal-free) and uranium-loaded sample was conducted. For FTIR analysis cells were incubated with and without uranium for 24 hours. After 24 hours of incubation the cells were the harvested by centrifuging at 6000 rpm for 10 minutes. The supernatant was discarded and the remaining pellet was dried at 60±10°C in an oven for about 72 hours. The dried samples were then grinded using mortar pestle method to near even particle size prior analysis on the (ATR-FTIR). Infrared spectra of uranium-free and uranium-loaded biomass were recorded within a range of 400-4000 cm^{-1} using a Bruker Tensor 70 FTIR spectrometer. The ATR-FTIR instrument resolution was set at 4 cm^{-1}. The reflectance spectra were recorded and averaged over 32 scans, using the total internal reflectance

configuration with a Harrick™ Mvp-pro cell consisting of a diamond crystal. Spectra were viewed in OMNIC software.

3.9.6 Raman Spectroscopy

For detailed and conclusive sample characterisation, Raman spectrum analysis for the previously prepared powder sample was conducted. Compared to the Infrared spectra, Raman spectrum is very specific, effective in analysing inorganic material and it is also not affected by the presence of water molecules in a sample. The Raman spectra of the sample were obtained with a Ram II (FT-Raman) spectrometer (Bruker), fitted with a Germanium detector cooled with liquid nitrogen. The 1064 nm wavelength radiation was used with a 50 mW laser power setting. The spectral resolution on the instrument was set at 4 cm^{-1}.

3.9.7 U(VI) Deposition Analysis using TEM

In order to establish whether cells were deposited on the surface or inside the cells Transmission Electron Microscopy (TEM) of bacterial cells was performed in the Microscopy Laboratory, University of Pretoria following the methodology by Mathews (1986) and Hayat (1981). Metal free (control) and metal loaded bacterial cells were concentrated by centrifugation and then fixed in 1-2% glutaraldehyde. Thereafter, the material was washed three times with phosphate buffer (pH 7) followed by fixing in 0.5 % osmium tetraoxide stain for 2 hours.

Cells were dehydrated through a graded ethanol series (30%, 50%, 70%, 90%, 100%, 100%, and 100%), infiltrated with 50% Quetol epoxy resin and embedded in pure Quetol epoxy resin for 3 hours (Glauert, 1975). Cells were then polymerised at 60°C for 39 hours and cut into ultrathin sections using Reichert Ultracut E Ultra-microtome (Reichart, Germany). The sections were loaded in carbon coated copper grid and stained with uranyl acetate and Reynolds' lead citrate for 2 minutes, and then rinsed in water. The ultra-thin copper coated samples were then observed under a TEM (Joel JEM-2100F, Joel, Tokyo, Japan) equipped with Energy-Dispersive X-ray spectroscopy (EDX) (Oxford Instrument, UK).

3.9.8 Elemental Scan using EDX

EDX spectroscopy of the metal-free and metal-loaded sample was conducted to achieve the conclusive identification or characterisation of the deposited elements on the cell surface. The EDX was set at the acceleration voltage of 200 kV. For accurate prediction of each element

in the sample a threshold was set to zero for all quantitative results with sigma below 1. To stimulate the emission of characteristic X-rays from a specimen, a high-energy beam of X-ray is focused to the ultra-thin sample (100 nm) with density of (10 g/cm^3). The X-ray energy released by focusing the X-ray beam to the sample allowed the characterization of elemental composition of the specimen to be measured. EDX characterization capabilities were due to the fundamental principle that each element has a unique atomic structure allowing unique set of peaks on its X-ray emission spectrum. The weight % of each element in the sample was determined by measuring the line intensity of each element in the sample.

3.9.9 Scanning Electron Microscopy (SEM)

Surface morphology of the culture attached to the support material and grown as a biofilm was evaluated using Scanning electron microscopy (SEM) (Joel, JSM-5800LV). The biofilm on the support material was fixed in a 2.5% glutaradehyde in 0.1 M phosphate buffer (pH 7.0) solution. The fixative solution was decanted off and cells attached to the support material were then washed in a phosphate buffer, prior dehydrating in a series of ethanol solutions (30%, 50%, 70%, 80%, and 90%). Samples were dried in liquid CO_2 and then mounted on stubs with double sided tape, coated with gold, and then observed under SEM.

3.10 Statistical Methods

3.10.1 Reliability Analysis

The required number of determinations for each sample was established using Statistical Reliability Test as describe by Sawyer and co-workers (2003). A grid of three determinations by five different operators was obtained for each method and the reliability factor R_m was determined from variances using the equation below:

$$R_m = \frac{S^2{}_B - S^2{}_W}{S_B{}^2 (n-1) S_W{}^2}$$

where: R_m= interclass correlation coefficient, n = number of experimental units (classes), S^2_B= between experimental unit variability, and $S_W{}^2$= pooled within experimental unit variability. To achieve a target reliability of R^2=0.95 (95%) the required number of determination was obtained by factoring the reliability based on the power test below:

$$m = \frac{R^*(1-R_m)}{R_m(1-R^*)}$$

where: number of repetition required to obtain the target reliability, R*= target reliability coefficient, R_m = calculated reliability coefficient (interclass). For the uranium solution triplicate determination were required to achieve reliability factor of 0.95.

3.10.2 Quality Assurance

Prior to U(VI) analysis the UV/Vis spectrophotometer was calibrated. The calibration curve was prepared in a BMM solution using the Arsenazo III method at λ = 561 nm. From the stock solution of 1000 ppm uranyl nitrate serial dilution of known uranium concentrations ranging from 0-80 mg/L were prepared and their absorbance was measured at 651 nm. The intermediate precision of the method was evaluated using two different systems in the same laboratory to measure same samples. The relative standard deviation obtained for two systems using the same samples were 0.34 and 0.36, respectively.

The linearity of the method was evaluated using U(VI) standard concentrations of 0, 2, 10, 20, 30, 40, 50, 60, and 80 mg U(VI)/L, but the linearity was found to be at 0, 20, 30, 40, 50, 60, and 80 mg/L. The linear graphs/calibration curves with the regression of 99.7% were then obtained by plotting absorbance versus the known concentration data of U(VI). The equation of the calibration curve obtained was found to be linear in the standard uranium concentration and was used for calculating unknown uranium concentration. To ensure that U(VI) analysis method is dependable over a long term, routine analysis of three randomly selected uranium standards were read in the pre-calibrated instrument. The absorbance's of randomly selected uranium standards were then compared to those in the linear standard curve with (R^2=99.7%). If the absorbance of uranium standards with the same concentration read significantly different from one another then the instrument was re-calibrated prior further analysis.

In the case of protein analysis the calibration curve was prepared using BSA standard solutions. It was observed that under standard assay conditions, the absorbance measurements at λ=590 nm with the range of (0-0.645) was linear to protein concentration ranging from 0-750 mg/L. With this range the correlation coefficient was 0.997 (R^2=99.7%). This method could directly measure proteins solution without dilution at concentration ranging from 10-1000 mg/L (Lopez *et al*., 2010). This simple procedure increased the accuracy of assay by minimizing the error that may occur when diluting unknown protein concentration. For the greatest accuracy in estimating total protein concentration in unknown sample a standard curve was prepared each time the assay is performed.

CHAPTER 4

RESULTS FROM BATCH KINETIC STUDIES

4.1 Overview

The leakage of nuclear spent fuel waste from underground repositories and the leachate of uranium from deposits have led to huge amount of uranium contamination in water systems. As a first step towards addressing the problem of U(VI) contamination in water bodies, studies on radioactive waste treatment using biological processes have been widely and successfully conducted in batch reactor systems, such as closed and sealed serum bottles (Chabalala and Chirwa, 2010, 2011; Reed *et al*., 2007; Luo *et al*., 2007). Batch reactor systems were observed to be effective in treating U(VI) in aqueous solutions under controlled environmental conditions. Although batch studies were observed to be effective in treating U(VI), the results obtained from batch kinetics studies cannot be directly extrapolated into the actual site for *in situ* bioremediation. This is because U(VI) transport through a saturated porous media is highly dynamic process that cannot be fully defined through batch kinetic studies.

As an initial step towards understanding the complex process associated with subsurface U(VI) reduction, continuous flow systems were evaluated in this study. This is mainly because unlike batch systems, continuous flow systems take hydrodynamic issues into consideration. The performance of the microbial batch systems in removing U(VI) under oxygen stressed conditions was evaluated using the pseudo-second order reaction kinetic model. The kinetic parameters obtained from the batch kinetic studies were then adjusted and used as an initial tool for easy development and evaluation of continuous flow system; this is discussed in Chapter 5 and Chapter 6.

4.2 Microbial Analysis

Thirteen species of U(VI) tolerant bacteria were identified from the 16S rRNA gene analysis of cultures isolated from the uranium mine tailing dumps. Of the 13 isolated U(VI) reducing and tolerant bacteria under anaerobic conditions at 75 mg U(VI)/L, only nine species could be sub-cultured under facultative anaerobic conditions. The other four species although produced a fingerprinting during analysis they could not be sub-cultured under facultative

anaerobic conditions, suggesting that they are strictly anaerobes. Phylogenetic characterization yielded 93 to 99% homologs associated with the *Bacilli*, *Microbacterieceae*, *Anthrobacteriae*, and *Acinetobater* groups as shown in Table 4-1.

Among the identified homologs, were species previously reported to exhibit U(VI) reducing activity and resistance to toxic effects of a range of metals. Fowle and co-workers (2000) showed that some *Bacillus* species are effective biosorbents of uranium. Additionally, Suzuki and Banfield (2004) observed intracellular accumulation of uranium in *Anthrobacter* species isolated from a uranium-contaminated site. In the study by the later authors, the precipitation of the uranium species inside the cells was localised around polyphosphate granules as UO_2^{2+}-phosphate complexes showing that the polyphosphate played a role in removal of uranium from solution.

Table 4-1: Partial sequencing of URB isolated from soil samples of abandoned uranium mine under facultative anaerobic conditions.

Pure Culture	**NCBI Blast**	**% Identity**
Y1	*Kocuria turfanesis*	99 Actinomycetes from Micrococcaceae
Y3	*Arthrobacter creatinolyticus*	93
Y5	*Microbacterium aerolatum*	100
Y6	*Bacillus licheniformis*	100
Y7	*Bacillus altitudinis*	100
Y8	*Anthrobacter sulfonivorans*	100
Y9	*Acinetobacter baumanii*	100
Y10	*Chryseobacterium indoltheticum*	100
Y11	*Bacillus pumilus*	100

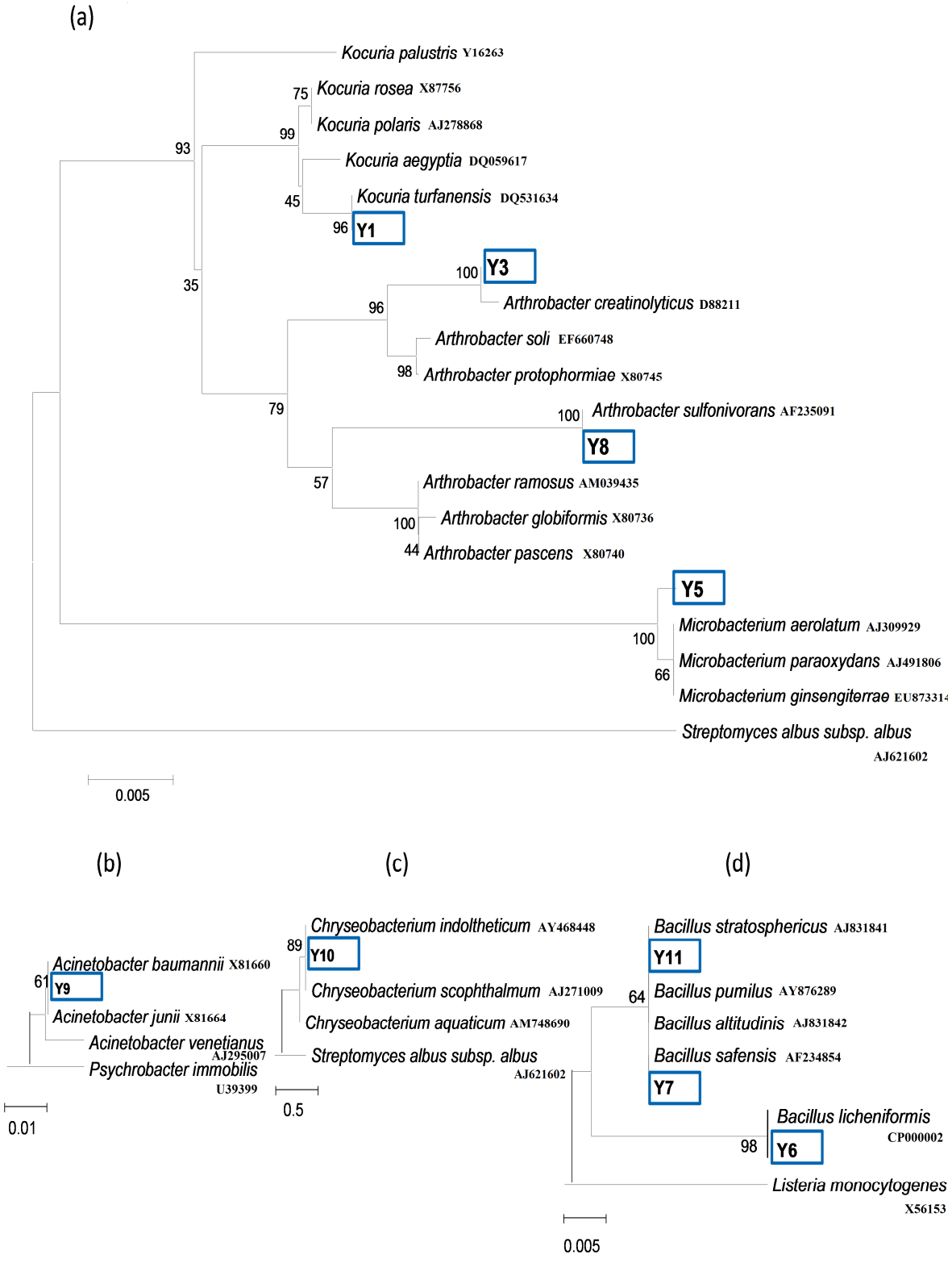

Figure 4-1: Phylogenetic analysis results showing the predominance of (a) *Microbacterieceae* and *Anthrobacteriae*, (b) *Acinetobacter*, (c) *Chryseobacrerium*, and (d) *Bacillus* species under U(VI) exposure.

A phylogenetic tree with closest association to know the purified cultures grown under micro-aerobic conditions based on a basic BLAST search of rRNA sequencing in the NCBI database was constructed (Figure 4-1a-d). Colonies Y10 in Figure 4-1c is not reported in literature as any metal reducing species. Another uranium (VI) reducing species, Y6, was also identified among the Bacilli shown in Figure 4-1d. In the phylogenetic analysis, the scale indicated at the bottom of the plots represents the genetic distance, while the percentage numbers at the nodes indicate the level of bootstrap based on neighbour-joining analysis of 1000 replicates.

4.3 Preliminary U(VI) Reduction Studies

Preliminary experiments on different bacterial species isolated from the tailing dumps of the abandoned uranium mine were conducted to evaluate the effectiveness of each isolate in reducing U(VI). Uranium (VI) reduction experiments on individual bacterial species were initially conducted at low U(VI) concentration of 30 mg/L. All the experiments were conducted in triplicates at 30±2°C. Data in Figure 4-2a and Figure 4-2b shows that all tested isolates (Y1, Y3, Y5, Y6, Y7, Y8, Y9, Y10, Y11) were able to reduce U(VI) in the solution effectively as individual pure isolates. These figures also demonstrate that significant U(VI) removal in all tested isolates was achieved within the first few hours of incubation ranging from 1 to 4 hours. Instantaneous U(VI) removal observed within the first few hours of incubation at the initial U(VI) concentration of 30 mg/L was attributed to physical chemical processes taking place in the system at near neutral pH in the presence of high nutrients concentrations.

Although significant U(VI) removal in all tested species was observed within the first few hours of incubation, Figure 4-2b shows the increase in U(VI) concentration in other species (Y7, Y8, Y9, Y10, and Y11) after 4 hours of incubation. The species (Y7, Y8, and Y9) were determined among nitrate reducing species that can release enzymes that oxidizes U(IV) to U(VI) under anaerobic conditions in the presence of nitrate (Selenska-Pobell *et al*., 2008; Akob *et al*., 2007). Therefore, the increase in U(VI) concentration observed in these species was associated to the possibility of enzymatic U(IV) re-oxidation to U(VI).

The effectiveness of each isolate in reducing U(VI) was further evaluated at higher initial U(VI) concentration of 75 mg/L, which is the background uranium concentration at the study site. Results in Figure 4-2c show U(VI) removal efficiency of more than 50% in Y1, Y3, Y5,

and Y6 within 48 hours of incubation. The reduced U(VI) removal efficiency achieved in other tested species (Y7-Y11) at the initial U(VI) concentration of 75 mg/L was associated to the frequent U(IV) oxidation observed and also to susceptibility of these species to U(VI) toxicity at higher U(VI) concentrations. The susceptibility of these species to U(VI) toxicity was confirmed by significant decrease in microbial activity observed after 48 days of incubation at initial U(VI) concentration of 75 mg/L.

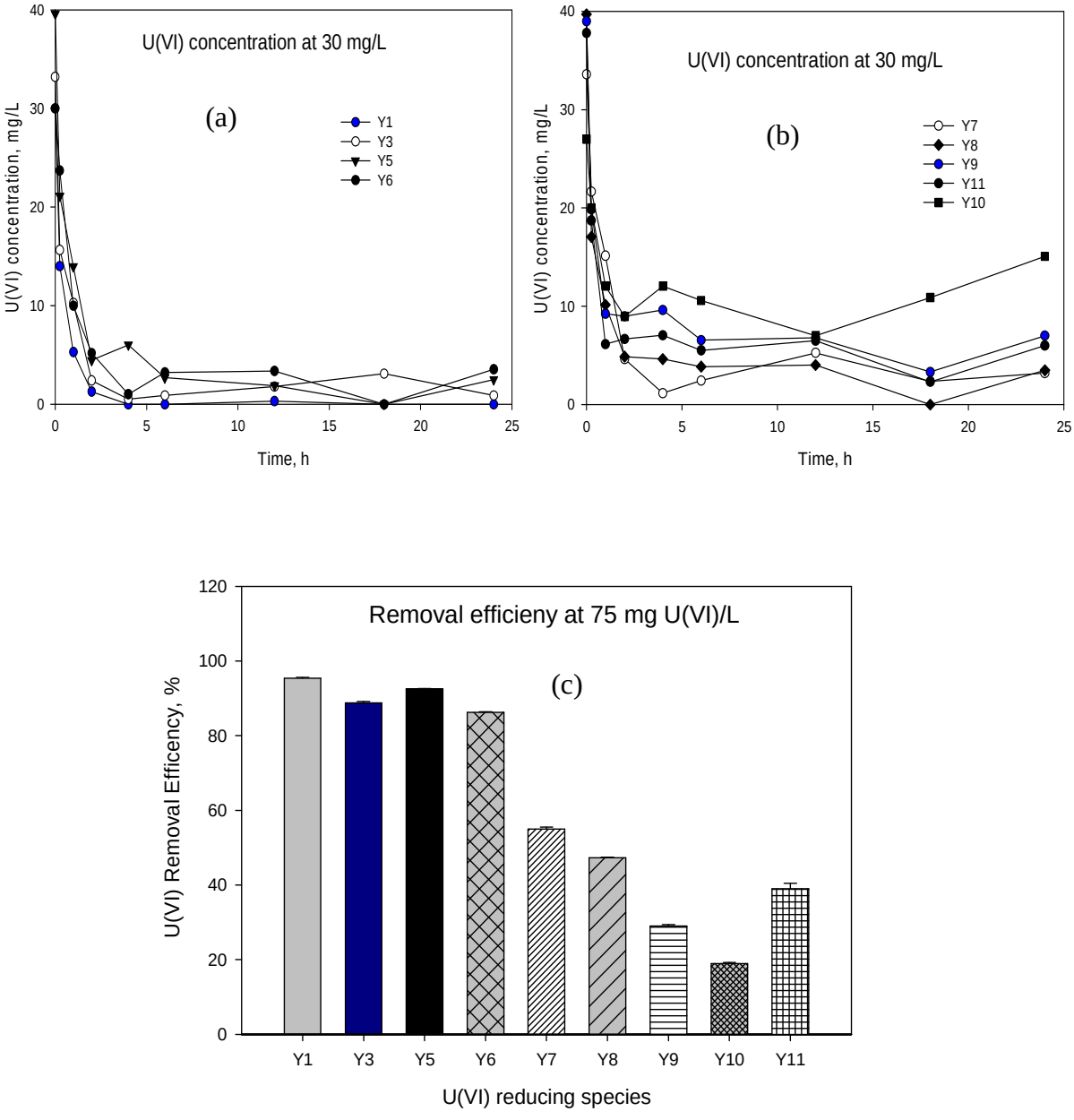

Figure 4-2: U(VI) reduction by individual species at the initial U(VI) concentration of (a), (b) 30 mg/L, and (c) 75 mg/L after 48 hours of incubation.

4.3.1 Performance Evaluation of Individual Isolates.

The performance of each isolate (Y1-Y11) in reducing U(VI) was evaluated over time at lower and higher U(VI) concentration of 30 mg/L and 75 mg/L, respectively (Table 4-2). Results show higher U(VI) removal efficiency of more than 50% on species Y1, Y3, Y5, and Y6 at initial U(VI) concentrations up to 75 mg/L. In other tested species (Y7, Y8, Y9, Y10, and Y11) higher removal efficiency of more than 50% was achieved at lower initial U(VI) concentration of 30 mg/L. However, increasing U(VI) concentration to 75 mg/L, significant decrease in U(VI) removal efficiency was achieved.

Table 4-2: Performance of individual species of isolates in reducing U(VI)

Pure Culture	Initial U(VI) Concentration (mg/L)	Initial Protein concentration (mg/L)	Protein concentration after operation(mg/L)	Removal Efficiency after operation (%)
Y1	30	---	---	100
	75	36.56	9.4	95.4
Y3	30	---	---	100
	75	39.89	7.3	88.8
Y5	30	---	---	94
	75	44	10.7	92.5
Y6	30	---	---	88.2
	75	50.17	10.5	86
Y7	30	---	---	93.5
	75	53.2	1.47	55
Y8	30	---	---	91.2
	75	48.78	2	47.3
Y9	30	---	---	82
	75	54.3	0	29
Y10	30	---	---	84
	75	44.33	0	19
Y11	30	---	---	60
	75	48	1.3	40

--- no data

It is also demonstrated in Table 4-2 that after 48 days of operation at 75 mg/L the decrease in protein concentration was observed in all species but more pronounced in Y7, Y8, Y9, Y10,

and Y11. The highest performing pure isolates with removal efficiency of at least 60% and with insignificant re-oxidation observed at 75 mg U(VI)/L were then used in this study for further U(VI) reduction kinetic studies.

4.4 Mixed-Culture Performance

4.4.1 Abiotic U(VI) Removal

Abiotic U(VI) reduction activity was evaluated by conducting the experiments at 100 mg U(VI)/L using cell-free and heat-killed culture controls. U(VI) reduction over time in the abiotic controls was shown to be insignificant (Figure 4-3). However, instantaneous U(VI) removal of 26.4% was observed in heat-killed cultures within the first 2 hours of incubation. U(VI) reduction trends observed in heat-killed cells suggested that instantaneous U(VI) reduction may be facilitated by interaction taking place on the cell surface at near neutral pH. For effective abiotic evaluation, the cells were killed by exposing them to heat (120°C) over several cycles prior inoculating them in U(VI) solution. Exposure of cells to higher temperatures in several cycles was conducted to ensure near complete cell death as it was suspected that the cultures of bacteria used in this study are capable of escaping destruction by heat. This was evident by significant U(VI) removal observed previously in heat-killed cultures which were not heated using the efficient heat-kill method (Mtimunye and Chirwa, 2013).

Live cell cultures, on the other hand, showed best performance with near complete U(VI) reduction within the first 6 hours of incubation suggesting that the observed U(VI) removal was metabolically linked. This suggests that biological U(VI) reduction by live-cell culture is facilitated by the catabolic oxidation of organic substrates which result in the production of NADH which is effective in mobilising electrons through the cytoplasmic membrane via NADH-dehydrogenase (Figure 4-3).

4.4.2 The Effect of Thioredoxin Inhibitors

In earlier studies, thioredoxin was determined to be one of the principle electron donors in the cytoplasm of living bacteria (Zeller and Klug, 2006; Li and Krumholz, 2009). In this study, deactivation of thioredoxin activity by $CdCl_2$ resulted in the discontinuation of biological U(VI) reduction (Figure 4-3). However, since uranium species were mainly detected on cell surfaces, this suggests that thioredoxin either influenced external factors responsible for U(VI) reduction or a component of thioredoxin itself is excreted into the periplasm of the

U(VI) reducing cells. The observed U(VI) removal immediately after incubating the culture with U(VI) solution was consistent with U(VI) removal by abiotic processes. Similar trends were also observed in rotenone ($C_{23}H_{22}O_6$) exposed cells. Inhibitory effects of U(VI) reduction by the thioredoxin inhibitor, $CdCl_2$, after 5-6 hours demonstrated thioredoxin is directly or indirectly involved in U(VI) reduction by live-cultures.

4.4.3 The Effect of NADH-dehydrogenase Inhibitors

The role of NADH-dehydrogenase was elucidated in this study. The objective of this component of the study was to determine whether U(VI) reduction is associated with the membrane ETR system. NADH-dehydrogenase serves as a gateway into the ETR. U(VI) reduction under NADH-dehydrogenase inhibited state could imply that U(VI) reduction in the isolated cultures is uncoupled from the ETR or that U(VI) draws electrons from other process for its reduction.

Results in Figure 4-3 showed that in the presence of $C_{23}H_{22}O_6$, immediate U(VI) reduction was observed within the first 6 hours of incubation. The immediate U(VI) removal may be attributed to physical-chemical and bisorptive processes occurring during the first few hours of incubation. However, inhibition effects were also observed after 5-6 hours of incubation, demonstrating the involvement of enzymatic U(VI) reduction process in the system. The insignificant U(VI) removal observed in the cell-free medium indicate that U(VI) reduction is a metabolically mediated biological process.

4.4.4 Biotic U(VI) Reduction

To evaluate U(VI) reduction under anaerobic conditions batch experiments were conducted at varying U(VI) concentration of 100 to 600 mg/L under near neutral pH using mixed-culture of bacteria. Experimentation under varying initial concentration using harvested and concentrated cells showed that the mixed-culture achieved near complete U(VI) reduction under initial U(VI) concentration up to 400 mg/L (Figure 4-4). Similar to heat-killed cultures instantaneous U(VI) removal was observed in all tested concentrations (100-600 mg U(VI)/L) within first few hours of incubation (1-4 hours), suggesting U(VI) removal by interactions taking place on the cell surface at near neutral pH.

At higher initial concentration of 600 mg/L complete loss of U(VI) reduction activity was observed after 6 hours of incubation. The loss or finite U(VI) reduction activity observed at

600 mg/L after 6 hours of operation was directly correlated to loss of cell viability. Viable cell concentration in the experimental run of 600 mg/L decreased from 10^9 to 10^3 cells/mL after 12 hours incubation. The deactivation of cells was attributed to toxicity effects of U(VI) to microbial cell activity at higher initial U(VI) concentration.

Figure 4-4c shows the performance of pure isolates in reducing U(VI) as individual species against the reconstituted mixed-culture. The results in Figure 4-4c show that microorganisms existing as a community, thus mixed-culture, possess significant stability and metabolic capabilities than pure isolates which can be linked to the effectiveness of synergistic interactions among members of bacterial communities (Martins *et al.*, 2010; Mtimunye and Chirwa, 2013).

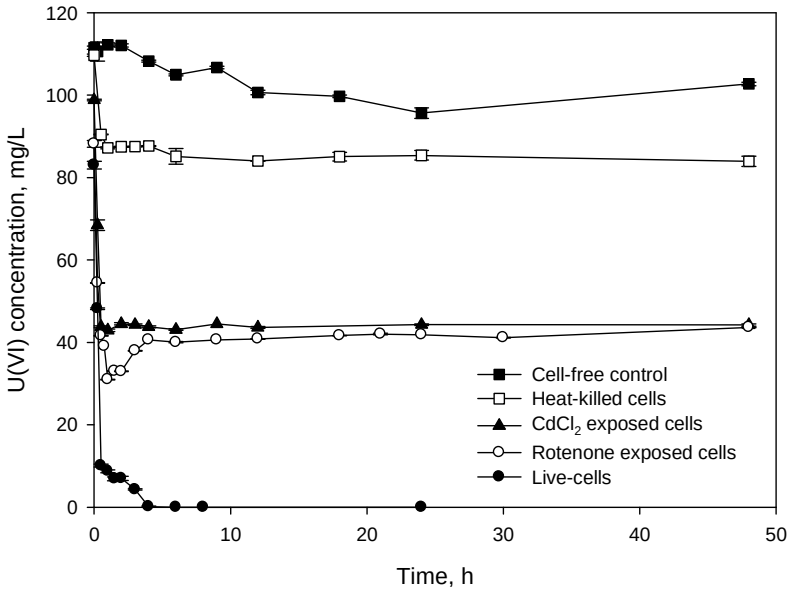

Figure 4-3: Abiotic U(VI) reduction at the initial U(VI) concentration of 100 mg/L.

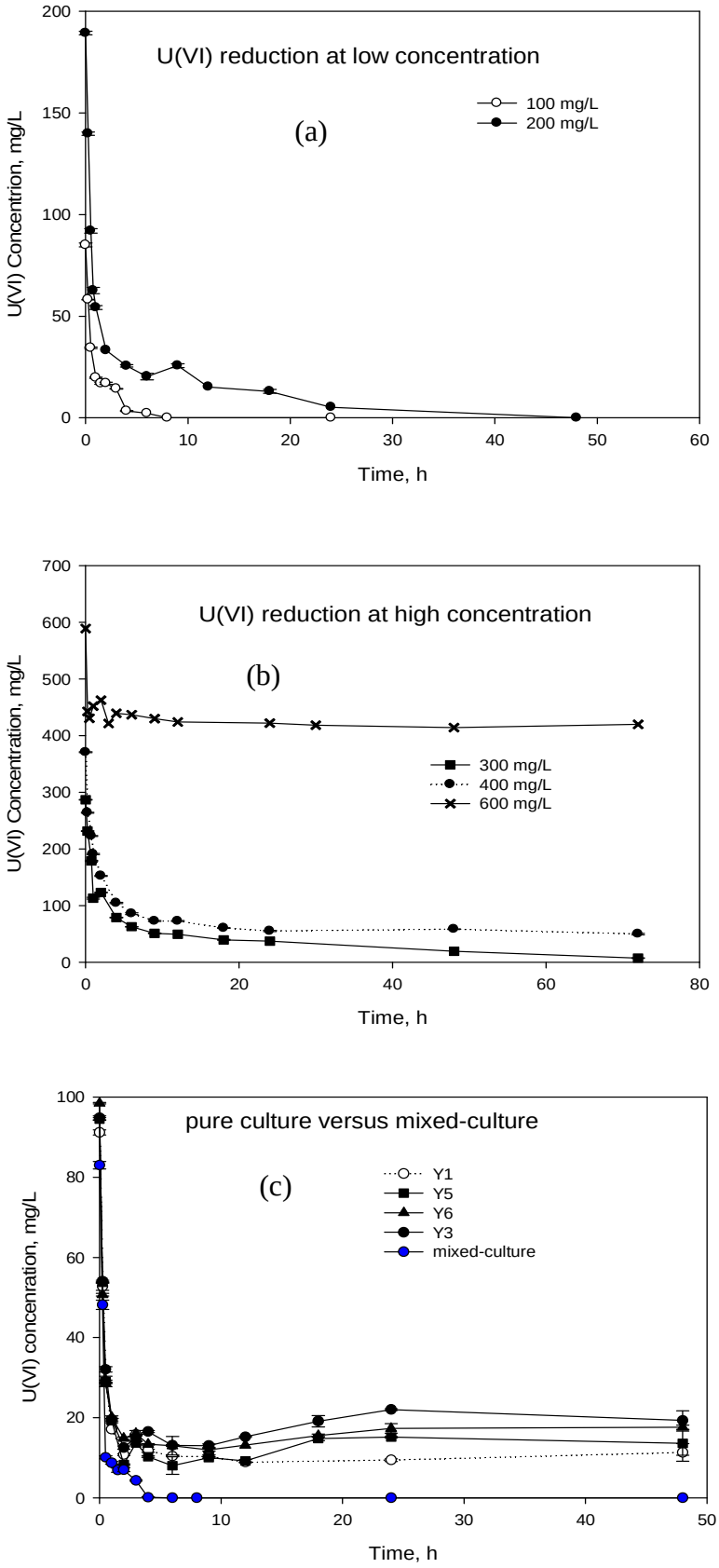

Figure 4-4: U(VI) reduction at (a) low initial U(VI) concentrations (100-200 mg/L), (b) high initial U(VI) concentrations (300-600 mg/L), and (c) pure isolates against mixed culture

4.4.5 Biomass Analysis

Viable biomass concentration was used to determine the level of cells viability during batch system operation. Figure 4-5a shows change in biomass viability after batch system operation at various initial U(VI) concentration ranging from 100-600 mg/L. Figure 4-5a shows notable decline in cell viability at higher initial U(VI) concentration (300-600 mg/L). Decrease in viable cell concentration observed at higher initial U(VI) concentrations may be attributed to U(VI) toxicity effect on cells at higher U(VI) concentration. To determine the reliability of the plate count method and to confirm the microbial activity of the viable cells in the batch systems, protein concentration analysis was also conducted (Figure 4-5b). The results from plate count method correlates with those of protein analysis, indicating the decrease in microbial activity over time.

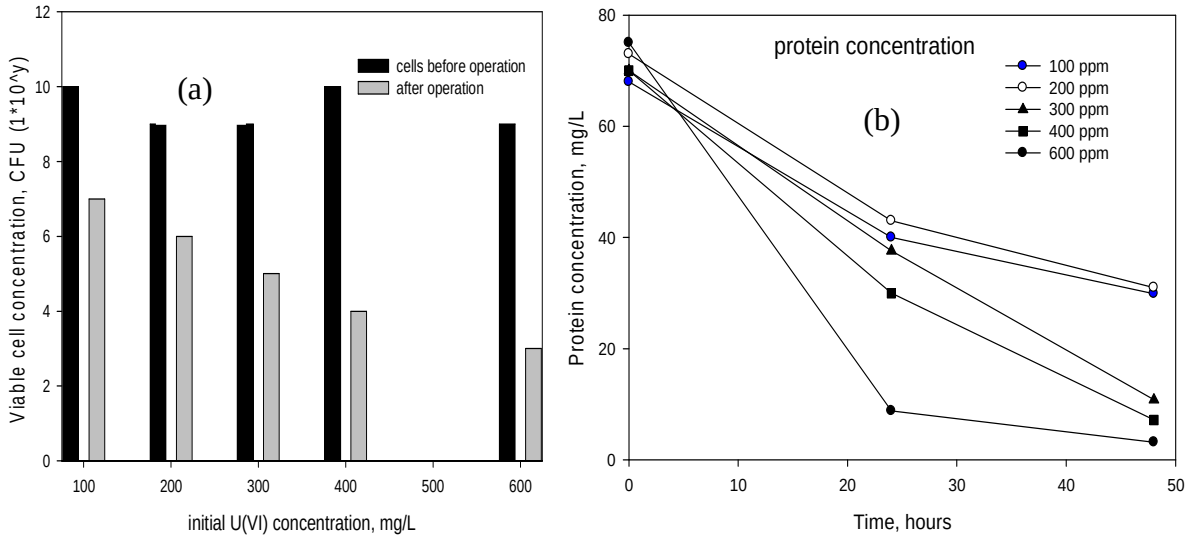

Figure 4-5: Analysis of cell concentration during batch studies operation at various initial U(VI) concentration (100-600 mg/L) (a) viable cell concentration before and after 12-24 hours of operation using plate count method, (b) protein concentration before operation and after 48 hours of operation using BSA method.

4.4.6 Fate of Reduced Uranium Species in Cells

The distribution and localization of uranium deposits in the cells was established using TEM. TEM of uranium-loaded cells revealed a dark electron opaque region extracellularly, suggesting that the metal reductase activity in the isolated species is associated with the

periplasm and outer cell membrane (Figure 4-6a). Conclusive identification of the deposited elements was achieved with EDX analysis. Using EDX coupled with TEM for conclusive identification or characterization of the deposited elements it was possible to confirm that the uranium loaded sample contained significant amount of uranium species in the precipitate as compare to the uranium-free sample which contained traces of uranium species which may be associated to the uranyl acetate dye used to stain the sample for TEM analysis (Figure 4-6b).

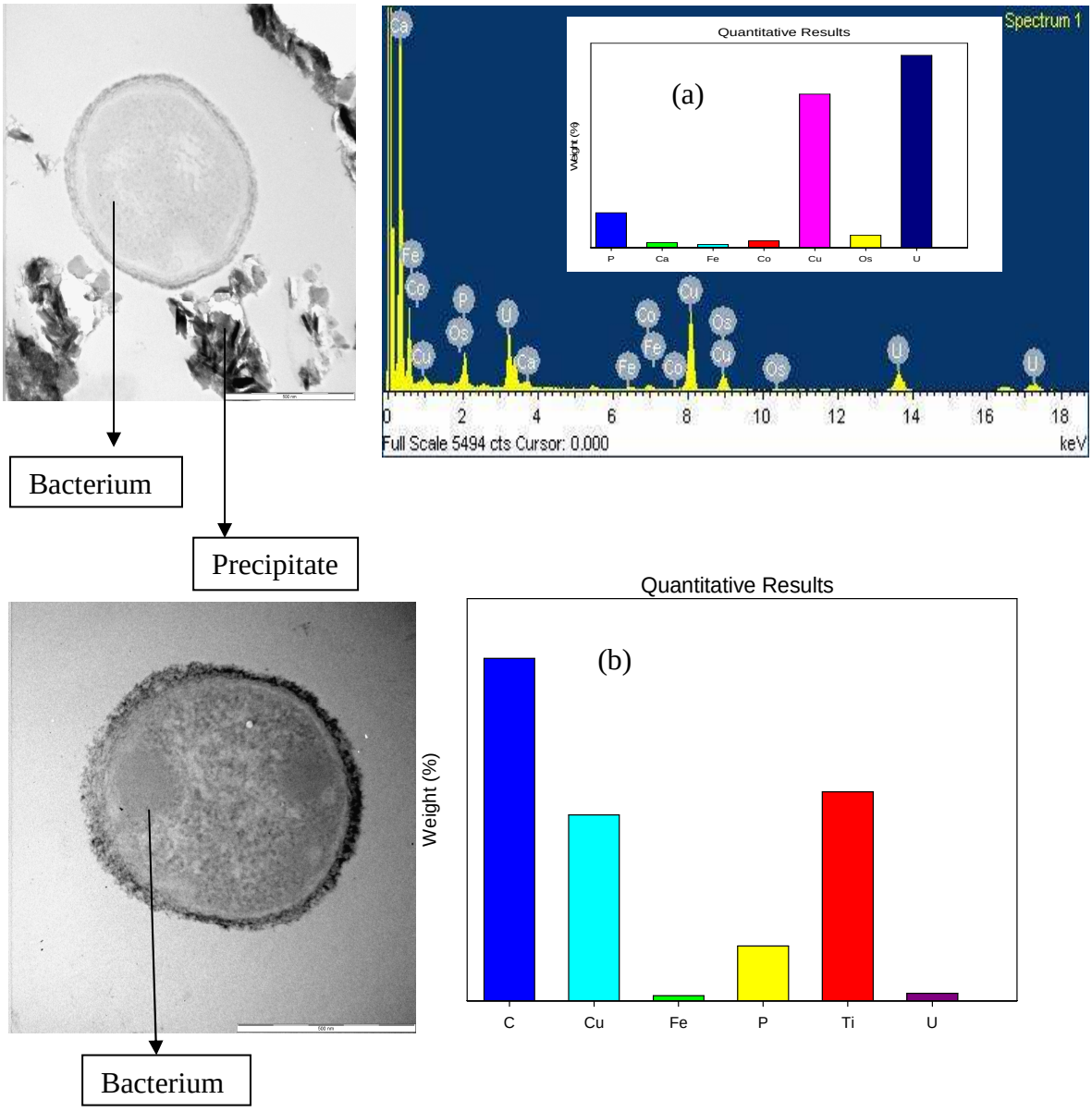

Figure 4-6: TEM scan and EDX spectrum of precipitate of (a) metal loaded biomass (Y6) indicating deposition of uranium species on cell surface and EDX spectrum of precipitate, (b) metal-free biomass.

It was observed in Figure 4-6a that the constituent percentage of uranium which was calculated from the sum of all observed peak areas dived by the peak area of uranium at a certain beam energy length was relatively higher than other associated elements identified in the precipitate such as calcium, cobalt, copper, iron, and phosphorus. Most of the elements identified in the precipitate result from the BMM which was used for U(VI) reduction kinetic studies. In addition to its presence in the precipitate, phosphorus is also a well-known important element of the bacterial cell wall (Beazley *et al*., 2007; Choudhary and Sar, 2011). The presence of copper observed in Figure 4-6a is due to the copper grid which was used to load the sample for analysis.

4.4.7 FTIR Spectroscopy

Functional groups of the bacterial cells involved in uranium binding were determined using FTIR. The FTIR spectral analysis of control (metal-free) and uranium loaded cells was applied. The FTIR spectroscopy allows certain characteristic peaks to be assigned to specific functional groups present in the bacterial cell surface. Correspondence of the IR frequencies was based on known data from the literature (Kazy *et al*., 2009; Choudhary and Sar, 2009; Martins *et al*., 2009, 2010). The FTIR spectra from (400-4000 cm-^{1}) of control cells (metal-free) and metal loaded cells are shown in Figure 4-7. The spectra of control showed a broad band from (3000-3600 cm^{-1}) with a maximum around 3300 cm-^{1}, bands corresponding to the N-H bond of amino groups along with the O-H of hydroxyl groups. In a uranium loaded sample a change in peak intensity was observed suggesting involvement of amino and hydroxyl groups in metal binding to bacterial surface (Choudhary and Sar, 2009, Martins *et al*., 2010).

The control spectra showed the presence of two peaks between (2800-3000 cm-^{1}) which can be ascribed to the asymmetric stretching C-H bond of the $–CH_2$ groups combined with that of $–CH_3$ groups. Figure 4-7 shows that both control and metal loaded cells revealed peaks of protein related bands. The C=O stretching of amide (amide I) and N-H/C=O (amide II) bands were prominent between 1500 cm^{-1} and 1700 cm^{-1}. The spectrum of control showed the bands of amide I and amide II at (1622 and 1529 cm^{-1}) respectively while the spectrum of metal loaded cells showed a shift in position of 1622 cm^{-1} to 1639 cm^{-1} and of 1529 to 1520 cm^{-1}. The intense amide bands shift in metal loaded sample presents the possible interaction of metals with cellular proteins.

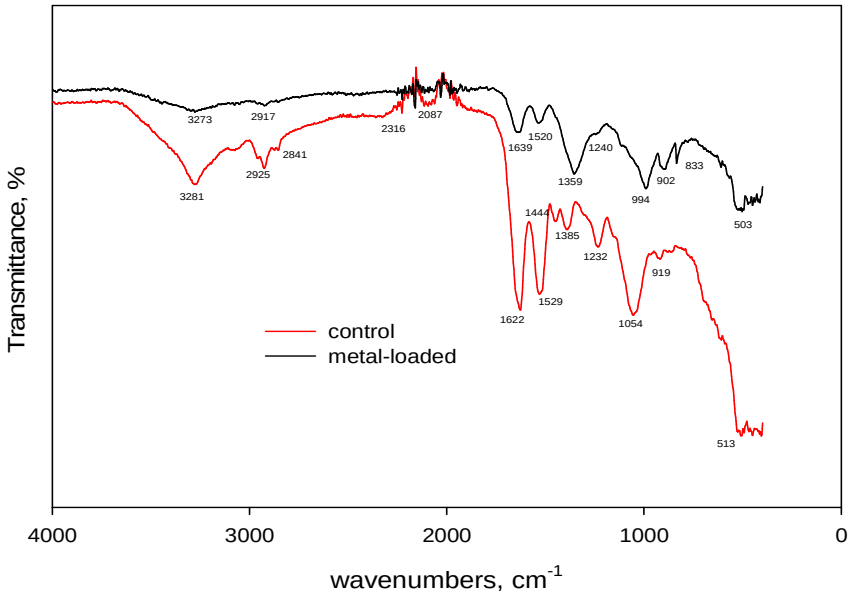

Figure 4-7: FTIR spectra of bacterial cell with and without metal.

The clear peak observed at 1444 cm^{-1} region in a control sample was attributed to the presence of carboxyl group. The role of carboxylic group in uranium binding was confirmed by decreased intensity and shift of peak observed at 1359 cm^{-1} in a metal loaded sample (Pagnanelli, *et al.*, 2000; Choudhary and Sar, 2011). Strong peaks in a control sample between (1054-1232 cm^{-1}) region are attributed to the presence of both carboxyl and phosphate group respectively. The groups mostly belong to various cellular components like, peptidoglycan, cell associated polysaccharides, phospholipids, and peptides and the groups are able to complex different metals (Martins *et al*., 2010). Following metal sorption a shift of these peaks indicates strong interaction of uranium with these functional groups. A decrease in intensity and gradual shift of the peak 1232 cm^{-1} in control sample to a lower energy in uranium loaded sample clearly indicates the weakening of P=O character as a result of uranium binding phosphate.

In both spectrums a strong absorbance between (900-1100 cm^{-1}) also ascertains the presence of carboxyl groups. The peak change position in uranium loaded sample around 900-833 cm^{-1} could be assigned to asymmetric stretching vibration of uranium species. The overall IR spectroscopic analyses suggest that carboxylic, amide, and phosphorus groups of bacteria are dominant functional groups involve in uranium interaction. For detailed sample

characterisation, Raman spectra analysis was conducted. The Raman spectrum is preferred for detailed analysis as it is not affected by the presence of water molecules in a sample and is more specific. The Raman spectra of a metal loaded sample demonstrated strong peaks in the frequency range (190-1000 cm^{-1}) as opposed to the metal-free sample (Figure 4-8). The strong vibrational bands between (191-1055 cm^{-1}) in a Raman spectrum is assigned to the symmetric stretching of O-U-O (Palacios and Taylor, 2000; Stefaniak *et al*., 2009). Similar peaks which indicate the presence of uranium mineral in the metal loaded sample were observed in the infrared spectra between (900-833 cm^{-1}). This indicates that the vibrations of uranium minerals are both IR and Raman active although strong and projective in the Raman spectra as it is less destructed.

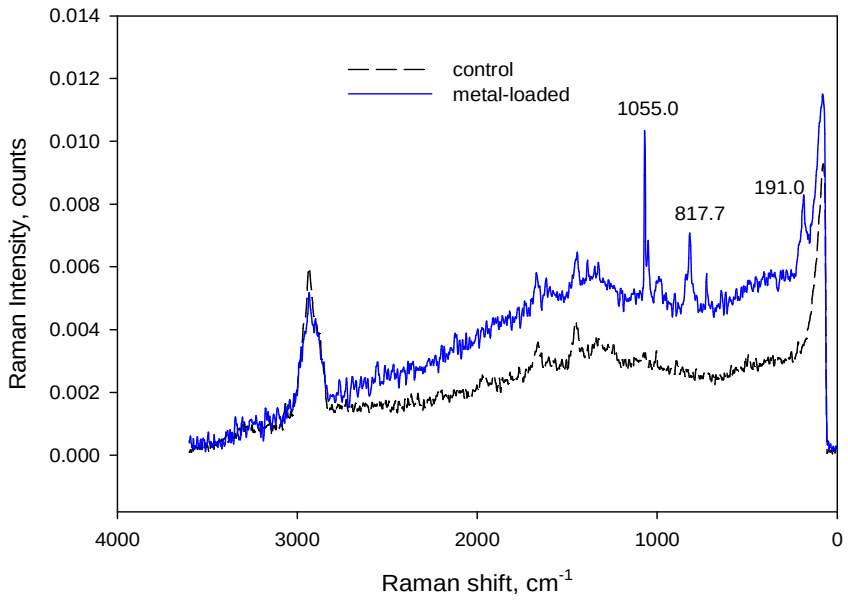

Figure 4-8: Raman spectra of a mixed culture of bacterial with uranium and without uranium.

4.4.8 X-Ray Diffraction Analysis

The chemical nature of cell bounded radionuclides was ascertained by X-ray diffraction powder spectroscopy. Characterization of the mineral phase by XRD gave a spectrum that in accordance with PDF 2 database is consistent with the presence of uranium oxide as (UO_3 and U_3O_8), and with the presence of uranium phosphate as (deuterium nitride uranyl phosphate, plutonyl hydrogen phosphate hydrate) (Figure 4-9a-d). The crystalline uranium phosphate formation following uranium accumulation indicates possible complexation of such metal with uranium facilitating metal nucleation and precipitation in crystal state.

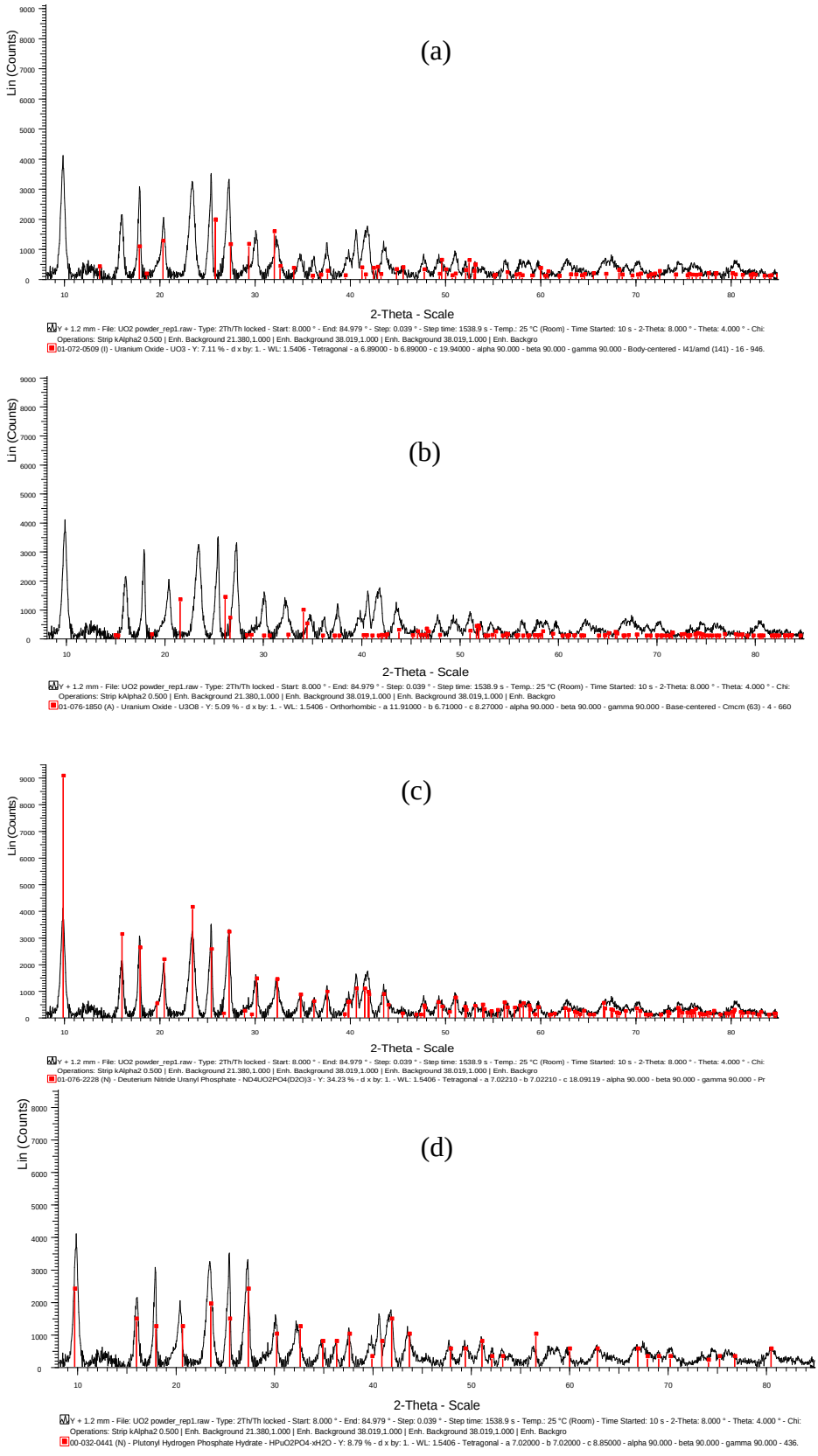

Figure 4-9: Background subtracted powder diffraction pattern of bacteria reduced uranyl nitrate powder overlaid with stick pattern of (a) UO_3, (b) U_3O_8, (c) deuterium nitride uranyl phosphate, and (d) plutonyl hydrogen phosphate hydrate.

These observations indicate the role of phosphate groups in uranium binding. Phosphate groups from intracellular phosphate or from cell membrane and wall materials may act as primary metal binding site creating negative surface charge conductive to cation binding (Merroun *et al.*, 2003; Kazy *et al.*, 2009; Choudhary and Sar 2011). The involvement of phosphate groups in uranium binding on the test biomass was also indicated by EDX and FTIR analysis. The presence of UO_3 and U_3O_8 indicates that the mineral phase was composed by a mixture of U(VI) and U(IV). The presence of U(IV) in the precipitate generated during U(VI) removal experiments using live cells, suggest a mechanism of enzymatic reduction where U(VI) is converted to insoluble U(IV). The presence of U(VI) species in the precipitate may be associated to slightly re-oxidation of U(IV) due to oxygen exposure or may be associated to U(VI) complexation with phosphate.

4.5 Modelling Theory

4.5.1 Kinetic Model Adaptation

Batch experiments on the isolated cultures were initially conducted to evaluate the rate equations of kinetic constants for processes taking place in the batch reactor system. Batch reactors are often used in the early stage for development due to their ease of operation and analysis. As a results of batch systems none-complexity batch kinetics studied were conducted to evaluate the fundamental of each process associated with biological mediated U(VI) reduction in a system. In this study high levels of U(VI) and the presence of metabolic inhibitors in a biological system inhibited both the cell microbial activity and U(VI) reduction activity in mixed culture of bacteria.

These observations led us to evaluate U(VI) reduction model based on enzymatic U(VI) reduction kinetics. To model a biological U(VI) reducing system, the reaction scheme, rate equations, and kinetic constants for the processes taking place in the batch reactor are chosen from published models on enzymatic reduction hexavalent toxic metals (Shen and Wang, 1994; Srinath *et al.*, 2002; Viamajala, 2003). Biochemical studies on U(VI) reduction suggested that U(VI) reducing mechanisms may be coupled to the membrane-electron transport system in U(VI) reducing bacteria and the rate of U(VI) reduction catalyzed by enzymes can be expressed as follows:

$$U(VI) + E \underset{k2}{\overset{k1}{\rightleftharpoons}} E^*U(VI) \xrightarrow{k3} E + U(IV) \qquad (4\text{-}1)$$

where: E = enzyme, E*U(VI) = enzyme-U(VI) complex , k_1 = rate constant for complex formulation, k_2 = rate constant for reverse complex formulation, k_3 = rate constant for U(IV) formation.

Let U(VI) = U and E*U(VI) = E*

The rate laws of formation of E* in (Equation 4-1) result in the following equation:

$$\frac{dE^*}{dt} = k_1 U(E - E^*) - k_2 E^* - k_3 E^* \qquad (4\text{-}2)$$

E* is the representative enzyme that is logically proportional to viable cell concentration, X as the only metabolic component in culture. E* can either be formed or destroyed such that $\frac{dE^*}{dt}$ is approximately zero, thus $\frac{dE}{dt} \approx 0$. Therefore the mass balance represented in (Equation 4-2) can be expressed in the form of E* as following:

$$E^* = \frac{k_1 UE}{k_1 U + k_2 + k_3} = \frac{UE}{U + \frac{k_2 + k_3}{k_1}} \qquad (4\text{-}3)$$

Then U(VI) reduction rate in (Equation 4-2) can be expressed as:

$$\frac{-dU}{dt} = \frac{k_3 UE}{U + \frac{k_2 + k_3}{k_1}}$$

Analogous to Monod kinetics, k_3 is analogous to maximum specific U(VI) reduction rate (k_u), E is analogous to biomass concentration (X) and $\frac{k_2 + k_3}{k_1}$ is analogous to half saturation constant (K_u).

$$-\frac{dU}{dt} = \frac{k_u \cdot U}{K_u + U} \cdot X \qquad (4\text{-}4)$$

where: U = U(VI) concentration at time, t (mg/L); X = concentration of active bacterial cells at time, t (mg cells/L); k_u = specific rate of U(VI) reduction (mg U(VI)/mg cells/h); and K_u = half-saturation coefficient (mg/L).

4.5.2 Toxicity Effect of U(VI)

U(VI) reduction was conducted in batch reactors using pre-concentrated and washed cells (resting cells) with very high viable cell concentration of 10^8-10^{10} cell/mL. In this case cell growth kinetics is relatively less important and may be ignored as the concentration of cells is at its maximum, indicating that future production of new cells is limited (Shen and Wang, 1993 and 1997). It was also determined from early studies (Shen and Wang, 1997, Chirwa and Wang, 2000) that the rate and the extend of U(VI) reduction in bacterial system depends on the number of active cells in the reactor, the initial U(VI) concentration, and U(VI) reduction capacity per cell (T_u). This indicates that the amount of U(VI) reduced under resting cells conditions will be proportional to the amount of cells inactivated by U(VI). Therefore, in that case the active cell concentration, X, may be assumed to decrease in proportion to the amount of U(VI) reduced due to the toxicity of U(VI) and the reduction capacity of U(VI) may be incorporate with the toxicity effect of U(VI) on active cells as follows:

$$\frac{1}{T_u} = \frac{d(X_o - X)}{d(U_o - U)} \tag{4-5}$$

Integrating Equation (4-5) and interpreting in terms of active cell concentration yield the following equation:

$$X = X_0 - \frac{U_0 - U}{T_u} \tag{4-6}$$

where: U_0 = initial U(VI) concentration (mg/L); X_0 = initial active cell concentration (mg cells/L); U = U(VI) concentration at time t; X = active cell concentration at time t; and T_u = maximum U(VI) reduction capacity of cells (mg U(VI)/mg cell). Substituting Equation 4-6 into Equation 4-4 yields the following Monod saturation equation:

$$-\frac{dU}{dt} = \frac{k_u \cdot U}{K_u + U}\left(X_0 - \frac{U_0 - U}{T_u}\right) \tag{4-7}$$

4.5.3 Parameter Estimation

The unknown kinetic parameters in the developed model were determined by performing a nonlinear regression analysis using the Computer Program for Identification and Simulation

of Aquatic Systems (AQUASIM 2.0), (Riechert, 1998). For each parameter, a search was carried out through a range of values. Trial values of the unknown parameters were initially guessed values. Constrains were also enforced to set upper and lower limits for each parameter so that nonsensical or invalid parameter values were omitted. Whenever optimization converged at/or very close to a constraint, the constraint was relaxed until the constraint no longer forced the model.

Equation 4-4 was initially used to fit the experimental data at various initial U(VI) concentrations. The results showed that the values of the specific rate of U(VI) reduction (k_u) and half-velocity constant (K_u) were not constant over a wide range of different U(VI) concentrations (Table 4-3). The enzymatic expression in Equation 4-4 which does not incorporate cell reduction capacity did not predict the data well over time. These results indicated that U(VI) reduction on live cells is affected by U(VI) toxicity on organisms as a result of its oxidising power which in turn resulted to a decrease in biomass activity over time. The results also demonstrate that the enzymatic expression in Equation 4-4 will not adequately describe the total pathway of U(VI) reduction over time.

Table 4-3: Optimum kinetic parameters obtained using Monod-kinetic model with a constant active biomass.

U(VI) concentration (mg/L)	**k_u (1/h)**	**K_u (mg/L)**	**χ^2 (Chi)**
100	9.9997554	4197.1419	415.94142
200	9.9994544	4781.2558	2606.0715
300	0.1148374	8.3211232	26928.123
400	0.14261743	8.0549127	53531.653
600	0.003259105	119.20757	184220.08

To account for U(VI) toxicity in batch cultures the kinetic model (Equation 4-7) which incorporates cell reduction capacity was evaluated. The results showed that the values of k_u, and K_u were not constant over different U(VI) concentration (Table 4-4), which indicates that the kinetic rates were directly affected by the increase in U(VI) concentration.

Table 4-4: Optimum kinetic parameters obtained using cell inhibition model incorporated with cell reduction capacity (T_u) (Equation 4-7).

U(VI) concentration (mg/L)	k_u (1/h)	K_u (mg/L)	T_u (mg/mg)	X_o (mg/L)	χ^2 (Chi)
100	9.9242689	2038.5628	1.0191318	307	338.55
200	9.8847096	2035.0568	1.0161327	339	2196.98
300	9.2528476	2319.5472	1.0002405	259	2875.30
400	9.1043222	2496.4806	1.0185975	312	1807.28
600	9.9701954	2001.5095	1.0010612	167	10528.74

Uncertainties obtained using Equation 4-7 at various U(VI) concentration did not allow accurate estimation of K_u. The values of K_u at various initial U(VI) concentrations were observed to be much greater than that of U, thus $[K_u] >> [U]$. Therefore, for such case the Monod saturation equation in Equation 4-7 was simplified to pseudo-second order kinetic equation as follows:

$$\frac{dU}{dt} = -k_u U\left(X_o - \frac{U_o - U}{T_u}\right) \tag{4-8}$$

In order to verify the validity of the model the kinetic parameters optimised using 200 mg/L data were used to simulate U(VI) concentration at a broader range and the results were plotted against the experimental data (Figure 4-10a-e). The pseudo-second order kinetic model in Equation 4-8 produced near constants kinetic parameters (k_u and T_u) (Table 4-5).

Table 4-5: Optimum kinetic parameters for pseudo-second order kinetic model incorporated with cell inactivation term (Equation 4-8).

U(VI) concentration (mg/L)	k_u (L/mg/h)	T_u (mg/mg)	X_o (mg/L)	χ^2 (Chi)
100	0.012	1.00723	140.30	211.72
200	0.012	1.00723	180.82	736.59
300	0.010	1.00723	258.36	1598.42
400	0.010	1.00723	310.54	1923.00
600	0.012	1.00723	163.09	2831.44

The model captured well the trend data under experimental conditions investigated with an R squared value of 99% and the mean square fitting error (δ^2) of 1.261. At the highest U(VI) concentration of 600 mg/L slight difficulty in fitting the parameters was observed, mainly due to excessive loss active biomass due to toxicity. The R^2 value of the model was determined as:

$$R^2 = 1 - \frac{S_{reg}}{S_{tot}} \tag{4-9}$$

Where: $S_{reg} = \left(\sum_{i=0}^{i=n} U_{i,\exp} - \sum_{i=0}^{i=n} U_{i,\,predicted} \right)^2$ and $S_{tot} = \left(\sum_{i=0}^{i=n} U_{i,\exp} - \overline{U} \right)^2$, i=1, 2, 3…n.

The mean square fitting error was estimated as:

$$\delta_u = \left(\frac{1}{(n-p)} \right) \sum \left(U_{\exp} - U_{predictate\,d} \right)^2 \tag{4-10}$$

where: n = number of data points used for curve fitting, p = number of fitting parameters, U_{exp} = experimental U(VI) concentration (ML^{-3}), $U_{predicted}$ = predicted U(VI) concentration (ML^{-3}).

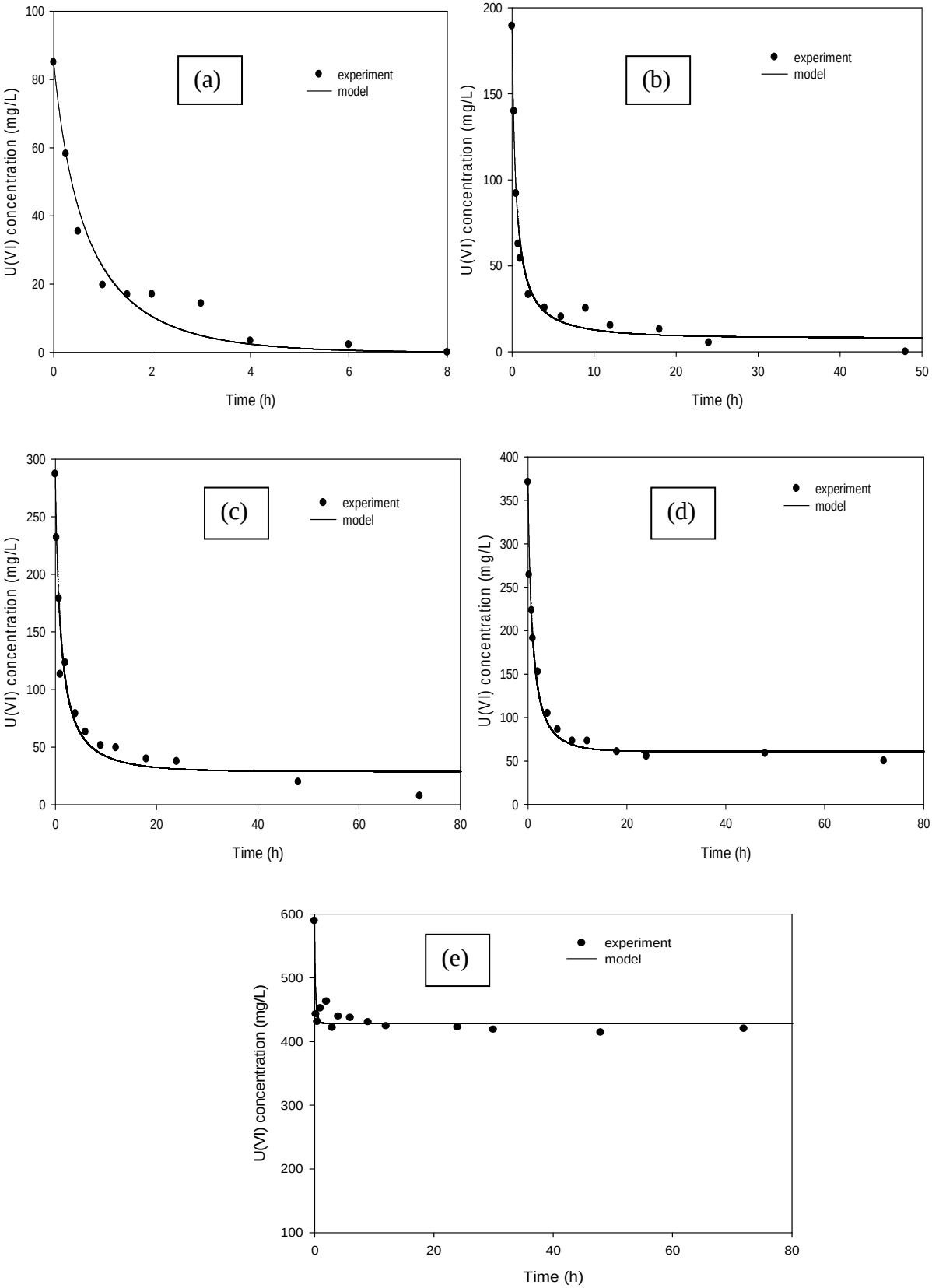

Figure 4-10: Batch culture model validation at various U(VI) initial concentration of (a) 100 mg/L, (b) 200 mg/L, (c) 300 mg/L, (d) 400 mg/L, and (e) 600 mg/L.

4.6 Sensitivity Analysis

Sensitivity analysis was evaluated to compare the effect of different kinetic parameters (k_u and T_u) on a pseudo-second order model. Figure 4-11 illustrates the dependence of sensitivity response curve of each optimized kinetic parameter. The results show that the model in Equation 4-8 was highly sensitive to minor adjustment in (k_u and T_u) within the first 10 hours of incubation indicating the period of activity. The kinetic parameter T_u was observed to be significantly sensitive, than that of k_u this demonstrated the effectiveness of cell U(VI) reduction capacity over time.

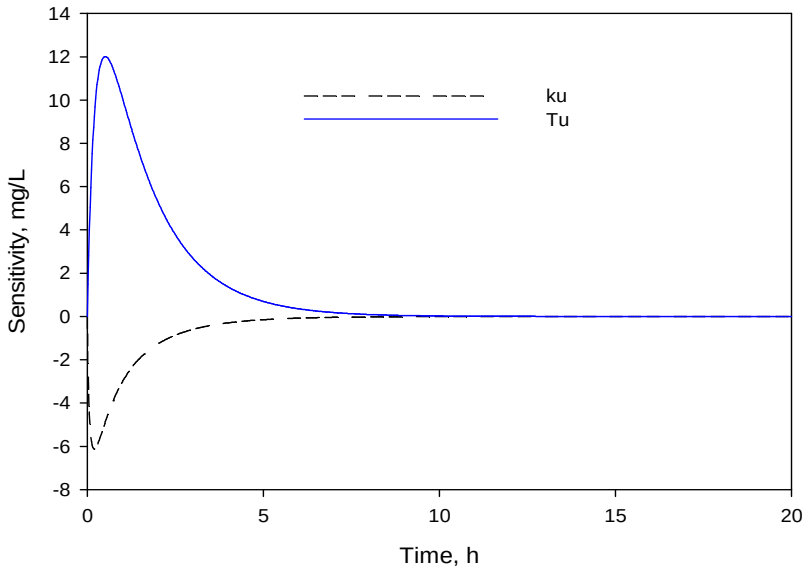

Figure 4-11: Sensitivity test for the initial U(VI) concentration of 100 mg/L with respect to optimized parameters in anaerobic batch system.

4.7 Summary

It is demonstrated in this chapter that, for successful design and operation of suspended growth biological system in wastewater treatment, it is essential to understand the types of microorganisms involved. The mechanisms of radionuclide-bacteria interaction was elucidated by employing several analytic techniques such as TEM, EDX, FTIR spectroscopy, XRD, and RAMAN spectroscopy. The analysis from these techniques indicated U(VI) removal by means of more than one mechanism. TEM analysis demonstrated extracellular U(VI) reduction by the culture. Additionally, EDX did not only identify uranium in the precipitate, but also the phosphorus which is an essential element in the bacterial cell wall. FIR analysis demonstrated the involvement cell functional groups such as phosphate,

carboxylic, and amide group in U(VI) removal in a solution. The XRD analysis indicated the presence of U(IV) in the precipitate indicating enzymatic reduction, where U(VI) is converted to U(IV). The involvement of enzymatic U(VI) reduction was also confirmed by complete prohibition of U(VI) reduction observed in this study in the presence of NADH-dehydrogenase inhibitor.

The phosphate observed in the EDX analysis, FTIR analysis, and XRD analysis indicated that the phosphate groups from intracellular phosphate or from cell membrane and wall materials may act as primary metal binding site creating negative surface charge conductive to cation binding. The results from this chapter demonstrated that U(VI) reduction by live cells can be carried out by two mechanisms: biosorption, and enzymatic reduction. The results also suggest that the process of U(VI) reduction in live cells can be divided into two steps: in the first step U(VI) is adsorbed to the cell surface by interaction between metals and functional groups displayed on the cell surface. The interaction taking place on the cell surface includes ion exchange, micro-precipitation, complexation, and nucleation. The second step involves enzymatic reduction of adsorbed U(VI) species on the cell surface to U(IV) (Nilanjana *et al*., 2008).

Biosorption using live-cells offers a potential for biological process improvement through genetic engineering of metabolizing cells. The species used in this study offers a potential of instantaneously removing the dissolved species of U(VI) from the solution through biosorption and then enzymatically reducing the adsorbed U(VI) species to U(IV). Extracellular U(VI) reduction observed in this study present an opportunity to recover uranium for further use.

A kinetic model for describing microbial U(VI) reduction by incorporating the toxicity effect of U(VI) was evaluated. The kinetic parameters (k_u, and T_u) were adequately described by pseudo-second order model and were capable of predicting U(VI) reduction for a broad range of initial U(VI) concentrations or cell densities with smaller uncertainties. The sensitivity of each kinetic parameter (k_u, and T_u) in the model was shown be significant indicating that the two kinetic parameters are very essential for the scale up of the reactor. This model offers quantitative insights of kinetics of microbial U(VI) reduction and may be useful for evaluating reactor designs and improved for advance reactive transport modelling.

CHAPTER 5

KINETIC STUDIES OF CONTINOUS-FLOW SYSTEMS

5.1 Background

Continuous-flow systems have the potential of treating large volumes of wastewater continuously under shock loading conditions at relatively lower cost. Additionally, where *in situ* bioremediation is planned continuous-flow systems may be effective in simulating the effects of diffusion, clogging of pores, and advection rates in the actual system. Results from continuous-flow systems may be sufficient to understand kinetic process taking place in the system with respect to hydrodynamic issues. Generally, the success of biological treatment of contaminated environments is prominently determined by fundamental knowledge and understanding of microbial processes taking place in the system at the laboratory level and the ability to replicate those processes at the actual system. This study evaluates the performance of the bench-scale continuous-flow systems, i.e. suspended-growth system and attached-growth system in reducing U(VI) in the environment with respect to abrupt changes in U(VI) concentration.

5.2 Conceptual Basis of Suspended Growth System

Experiments on suspended growth system were conducted to quantify the capacity of the mixed-culture of bacteria in reducing U(VI) under shock loading conditions. In a suspended growth system the mixed-culture of bacteria, *Bacilli*, *Microbacterieceae*, *Anthrobacteriae*, and *Acinetobater* species responsible for U(VI) reduction were grown as a bio-floc and then suspended in a system. The suspended culture was maintained in liquid suspension by appropriate mixing methods. The system was operated under anaerobic conditions at low velocities for quiescent mixing of U(VI) and biomass. U(VI) feed solution amended with BMM and glucose as a sole added carbon source was continuously fed into the reactor.

Nutrients and carbon source were continuously added in a suspended growth system to stimulate the growth of suspended culture as the system was operated without re-inoculation. The system was not overloaded with higher U(VI) concentration until a near constant U(VI) effluent concentration of the operated feed was achieved. To evaluate the performance of the system the influent and effluent U(VI) concentration were measured regularly under

sustained hydraulic loading. Factors affecting U(VI) removal in the system such as the effect of nitrate, the change in microbial activity, oxidation-reduction potential, and pH were also continuously evaluated in the system.

5.3 Suspended Growth System Kinetic Studies

5.3.1 U(VI) Removal Efficiency

Time series data in a reactor (Figure 5-1) shows near complete U(VI) removal in all treatment at initial U(VI) feed concentration ranging from (100-400 mg/L). It is observed in Figure 5-1 that the response of the bioreactor to the increase in U(VI) feed concentration of 150 mg/L, 200 mg/L, and 400 mg/L was achieved after 9 hours, 38 hours, and 165 hours of operation, respectively. The delayed response of the reactor to the feed concentration was attributed to the effectiveness of the mixed-culture in stabilizing U(VI) in the bioreactor. Consequently, the response of the reactor to near feed concentration observed thereafter may be associated to insufficient residence time of the feed at higher concentration in the reactor as the reactor was operated without re-circulation. However, although the response of the reactor to the feed concentration was detected over time, subsequent recovery of the system was attained in all operated U(VI) feed concentrations. This demonstrates the effectiveness of the mixed-culture used in this study in reducing U(VI).

Figure 5-1 also demonstrates that the flexibility of the reactor in accommodating sudden fluctuation in U(VI) feed concentration improved with time when certain favourable conditions were sustained. This was evident by the improvement of the reactor performance after shock loading treatment of 150 mg/L. Removal efficiency of 65% was observed after shock loading treatment of 150 mg U(VI)/L, while on the other hand near complete U(VI) reduction was achieved at higher U(VI) feed concentration of 200 and 400 mg/L. Throughout the entire period of system operation, the new feed concentration was not introduced into the reactor until a near constant concentration of the previously feed U(VI) concentration was achieved.

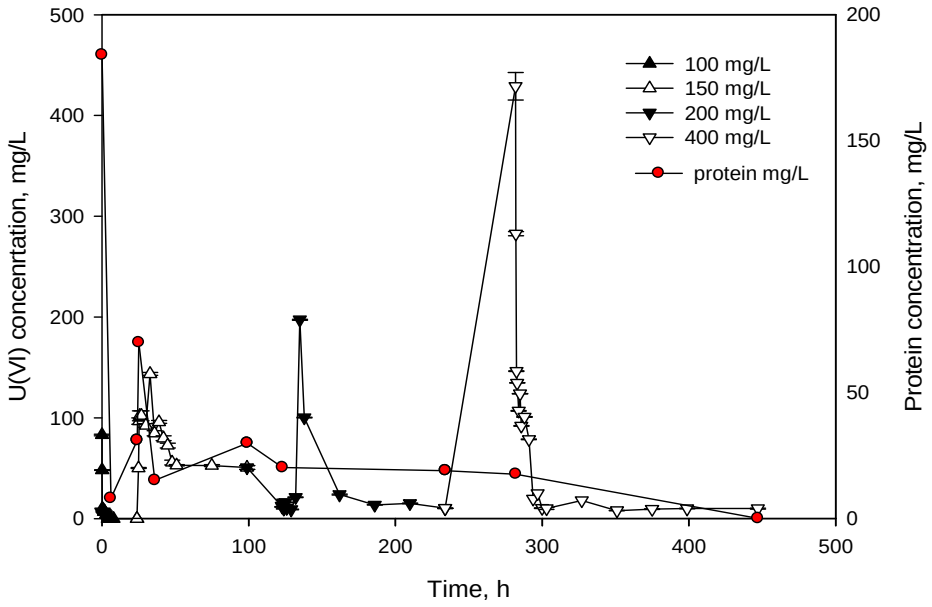

Figure 5-1: Evaluation of U(VI) reduction in at the initial U(VI) concentration of 100, 150, 200, and 400 mg/L and initial protein concentration of 184 mg/L.

5.3.2 Microbial Activity

Protein concentration, which served as surrogate parameter for microbial activity in a suspended culture system was analysed over time. The steep decline of protein concentration observed in Figure 5-1 within the first 6-12 hours of operation may be attributed to initial exposure to high uranium concentration. Microbial activity entered a log growth phase between 28 and 35 hours of incubation followed by the stationery phase after 100 hours of operation. The increase in protein concentration observed between 28 and 35 hours of operation may be associated to the adaptation of a mixed-culture of bacteria to U(VI) exposure. At this stage the presence of U(VI), glucose, and nutrients in the reactor was assumed to be beneficial for the cell activity. The stabilisation of the cell activity observed between 100-300 hours of operation demonstrates that during this period cells were able to reduce uranium via a respiratory process that does not conserve energy to support anaerobic growth. After operating the system at highest U(VI) feed concentration of 400 mg/L excessive loss of microbial activity was observed. The excessive loss of microbial activity observed after shock loading treatment of 400 mg/L demonstrated that at higher influent loadings, U(VI) was reduced at the expense of metabolic activity in suspended cells.

5.3.3 The Effect of Nitrate

The capability of the isolated species in reducing uranium in the presence of nitrate which is a common pollutant co-existing with uranium in the nuclear waste was evaluated. Since nitrate has the high reduction potential than uranium it was expected that the presence of NO_3^- in the system will inhibit U(VI) reduction. The results from this study showed that the presence of nitrate in the system at the concentration of 62 mg/L, background nitrate concentration at the study site did not have any inhibition effect on U(VI) reduction. These results are in agreement with those reported by Madden and co-workers (2007) and Boonchayaanant and co-workers (2009) evaluated at nitrate concentration of 6 mg/L. In this study near complete U(VI) reduction was achieved with very little loss of nitrate at near neutral pH using glucose as a sole added carbon source (Figure 5-2). It was therefore suggested from this observation that nitrate at the initial concentration of 62 mg/L was not acting inhibitor in U(VI) reduction process.

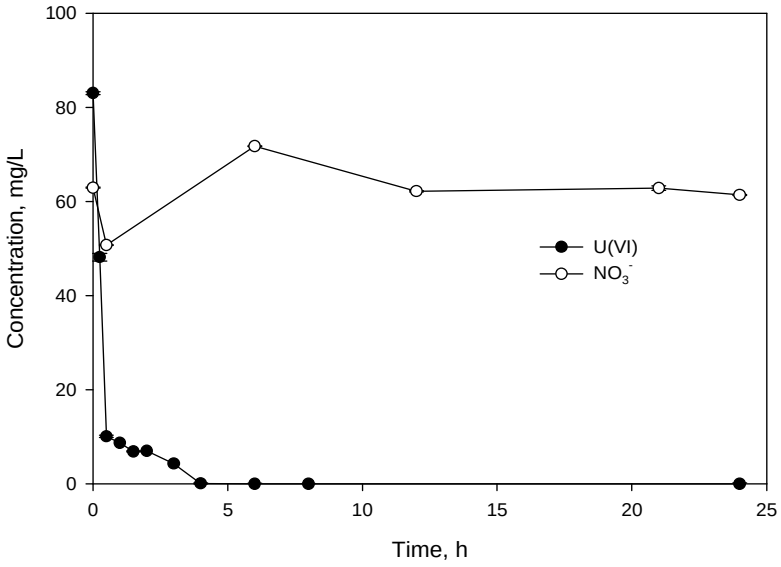

Figure 5-2: Simultaneous evaluation of nitrate (62 mg/L) and U(VI) (100 mg/L) reduction.

5.3.4 Impact of Redox and pH Conditions

The reactivity and mobility of radionuclides in biological system depends upon the ambient pH and redox reaction. The U(VI) reduction profile observed in Figure 5-3 at the initial U(VI) feed concentration of 100 mg/L showed a good correlation with the ORP of the solution. The negative ORP observed in the system during the first 6 hours of incubation reflected the reducing conditions when the culture was still highly anaerobic after purging

with N_2 gas. After 6 hours of operation the ORP increased to a positive value due to the removal of electrons from the system during U(VI) reduction to a lower oxidation state (Figure 5-3). The pH in the continuous flow system was near constant ranging from pH (6.5-6) mainly because the feed solution was buffered by potassium phosphate which was introduced into the system as part of the BMM medium.

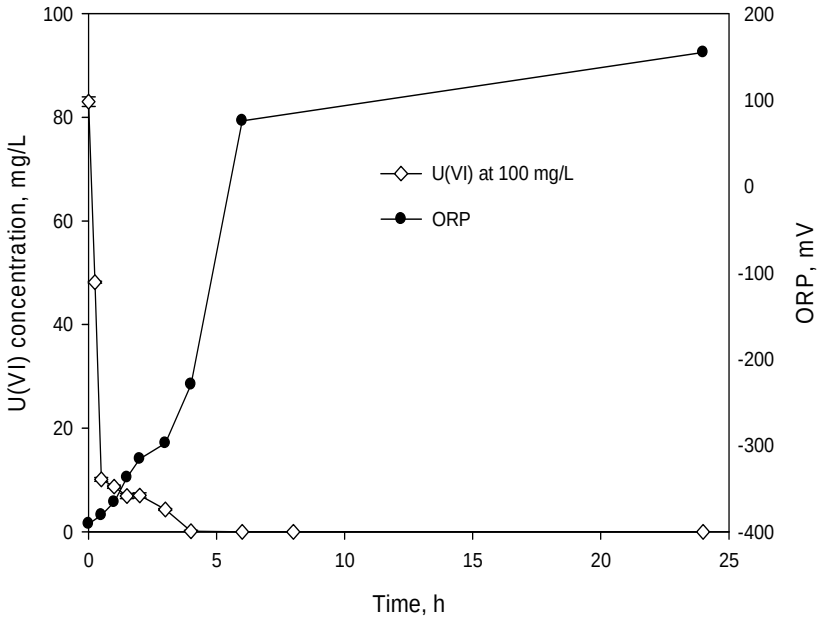

Figure 5-3: Evaluation of U(VI) reduction, and oxidation reduction potential (ORP) at the initial U(VI) concentration of 100 mg/L in a suspended-growth biological reactor system within the first 24 hours of operation.

5.3.5 Performance Evaluation of the Suspended Growth System

The overall performance of the suspended culture in reducing U(VI) in a reactor under shock loading conditions is summarized in Table 5-1. The results shows that the suspended culture effectively reduced U(VI) at various shock loading treatment over time under near neutral pH (6-7.5) in the presence of glucose as a sole added carbon source. In addition to reducing U(VI) effectively, high percentage uranium recovery was also achieved in the tested culture at various U(VI) concentration ranging from (100-400 mg/L). Since U(VI) and U(IV) are the predominant forms of uranium in the environment, it was assumed using results from batch kinetic studies that U(VI) is completely reduced to U(IV). U(IV) was determined as a difference of total uranium and U(VI).

Table 5-1: Performance evaluation of U(VI) reduction in suspended growth system at near neutral pH

U(VI) feed concentration, (mg/L)	Initial Protein concentration, (mg/L)	Protein concentration after operation, (mg/L)	HRT (h)	U(VI) removal efficiency after operation, (%)	Total uranium recovered after operation, (%)
100	184.3	31	24	100	88
150	31	29.9	75	65	91
200	29.9	19	136	95	95
400	19	0	213	98	96

5.4 General Principles of Bioremediation Technologies

The distribution and biodiversity of microorganisms inhabiting contaminated sites with genes that facilitate metal-microbe interactions is crucial for *in situ* bioremediation of metal contaminated environments (Ngwenya, 2011). Studies on *in situ* immobilisation of metals such as uranium, chromium, and other harmful metals using microbial barriers have been widely attempted at the laboratory level. The lack of specific application of *in situ* uranium bioremediation to the actual sites has mainly been due to the unavailability of microorganisms capable of growing under nutrient deficient or oligotrophic conditions, and also due to the lack of information on the faith of the reduced metal species in the environment.

Recently, experiments at a field site in Rifle, Colorado were conducted to determine if results obtained from the laboratory sediment inoculated with pure culture of *Geobacter sp*. could be extrapolated to *in situ* uranium bioremediation at the actual site (Anderson *et al*., 2003; Wu *et al*., 2006). In the later study, *in situ* bioremediation was facilitated by the addition of an external carbon source, acetate to stimulate the growth of *Geobacter* species. The growth of these species was targeted due to their known ability in coupling acetate oxidation with U(VI) reduction (Brodie *et al*., 2006; Nyman *et al*., 2006; Chirwa, 2011). Results from the previous study showed that continuous injection of acetate at the site over time yielded conditions that were less favourable for the growth of *Geobacter* species and more favourable for the growth

of SRB. Consequently, the predominance of SRB in the system over time resulted in reduced activity of *Geobacter* species and decrease in U(VI) removal rates.

In this study a mixed-culture of bacteria from the soil samples of the abounded uranium mine in Phalaborwa, Limpopo, South Africa was evaluated for its potential in reducing U(VI) in the organic source free environment without introducing external nutrients. Results from this study could serve as the initial step towards possible development of *in situ* U(VI) bioremediation process for the target site.

5.4.1 Conceptual Basis of Biofilm System

The mixed-culture of uranium reducing bacteria in this study was grown on a support media as a biofilm. The bio-cell filters used as biofilm support media possess large specific surface area and high porosity. The experiments on the treatment of U(VI) containing water were conducted in bench-scale fixed-film bioreactor system. The performance of the fixed-film bioreactor system in treating U(VI) containing plume water was evaluated under oxygen stressed and nutrient deficient conditions. This was done to evaluate the ability of the mixed-culture of bacteria in reducing continual influx of U(VI) under natural aquifer conditions characterized by large specific surface area, high pore volume, and low nutrient concentration. The bio-cell filters used as support growth media were plastic material with geometric shape representative of fractured and porous aquifer system expected at the study site due to excessive mining.

The column inoculated with a mixed-culture of U(VI) reducing bacteria (R1), and the cell-free, control column (R2) were installed in the laboratory as previously discussed and demonstrated in Figure 3-4 and operated as packed-bed continuous-flow reactor. To ensure completely submerged conditions the reactors were operated in an up flow mode at the flow rate of 0.33 L/h and actual hydraulic retention time of approximately 24 hours. The entire packed-bed reactor had a total surface area of 0.33 m^2 for biomass attachment and a clean bed pore volume of 7.5 L. The biofilm reactor (R1) was operated without any external nutrients and organic carbon source. This is of great environmental importance as the addition of external organic carbon source may not effectively predict the potential risks of uranium migration within tailings and depository sites. Furthermore, addition of external organic carbon source may yield conditions that encourage the potential growth of foreign species at site and in turn decrease U(VI) removal rates.

The performance of each column was evaluated based on the influent and effluent U(VI) concentration under sustained hydraulic loading. The shift in microbial community was evaluated using 16S rRNA gene sequencing for microbial culture. This analysis was done after column operation to determine the shift in species to the original inoculum. A conceptual representation of the permeable reactive barrier constructed by inoculating specialized cultures of bacteria in a selected barrier zone is presented in Figure 5-4.

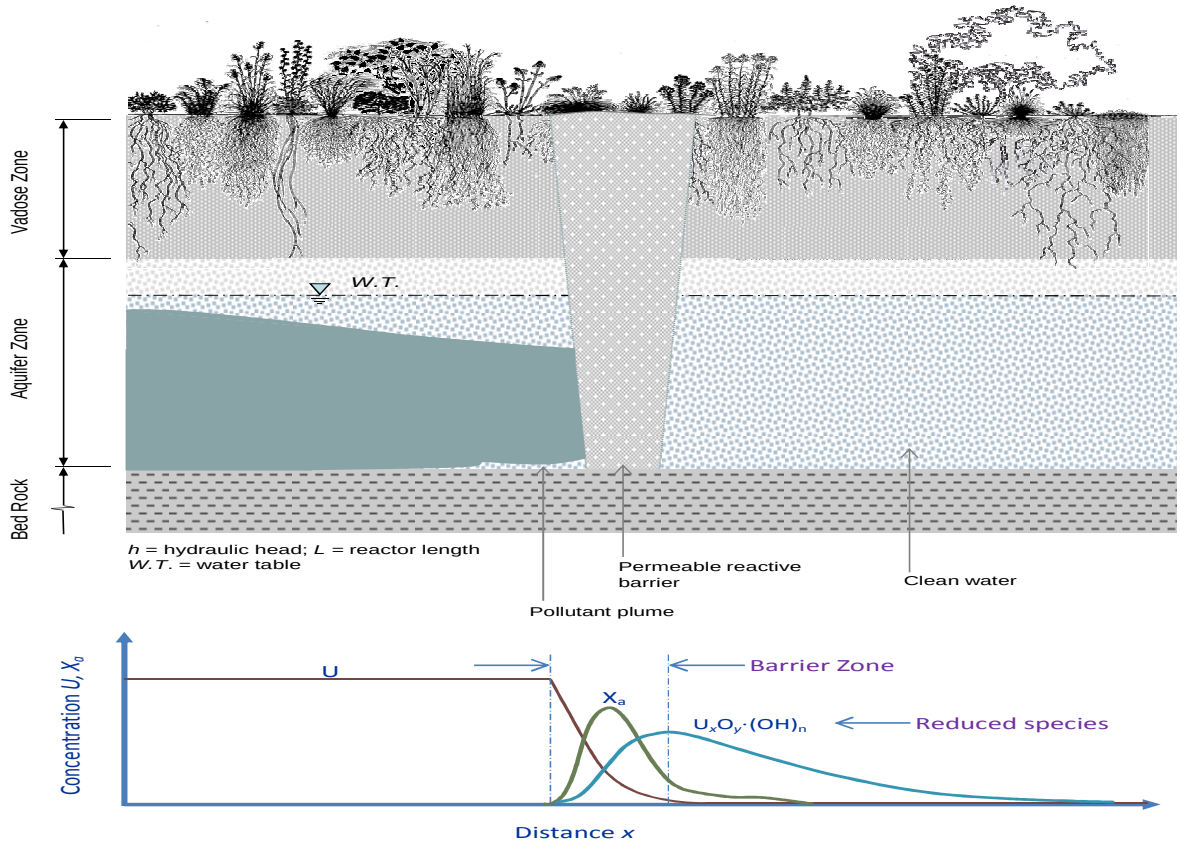

Figure 5-4: Theoretical representation of the microbial permeable reactive barrier system as an intervention for U(VI) pollution in an unconfined aquifer system. The graph shows the U(VI) concentration and biomass propagation under optimum operation conditions. U = hydroxide precipitates of reduction products. The number of complexed hydroxyl ions, *n*, will depend on the charge on the uraninite group $U_xO_y^{n+}$ (Mtimunye and Chirwa, 2013).

Theoretically, the decreasing concentration of U(VI) across the barrier is envisioned if barrier is inoculated with U(VI) reducing bacterial species. In the case of U(VI) reduction across a barrier system, we expect to utilise U(VI) as an electron acceptor in a dissimilatory respiration process in which the organisms introduced in the barrier (X_a) will require U(VI) at

optimum concentration to optimise their growth. If the organisms require U(VI) as a growth limiting electron sink, their survival away from the barrier zone will be limited. This will prevent increased microbial counts in the aquifer water if the aquifer downstream of the direction of flow is utilised as a drinking water supply source.

5.5 Attached Growth System Kinetic Studies

5.5.1 Evaluation of the Abiotic Process

Operation of the reactor without added biomass (R2) showed characteristics of exponential rise following effluent tracer line for clean-bed reactor (Figure 5-5). Low effluent U(VI) concentration observed in (R2) within the first few days of operation may be attributed to the presence of water in the reactor which was initially fed in the reactor to saturate pores and to adjust flow rates to the required reactor hydraulic retention time. Exponential rise of U(VI) effluent in the control reactor suggest that the adsorption processes were insignificant over time, i.e., the reactor reached equilibrium with respect to adsorption during operation. The data in Figure 5-5 also indicates that U(VI) was not retained in the column as effluent levels always approached the influent levels over time. This data demonstrates that the control reactor which was used in tracer analysis approached flow characteristics of mixed reactor over time with respect to physical properties such as clean- bed mean hydraulic residence time, advection, and porosity.

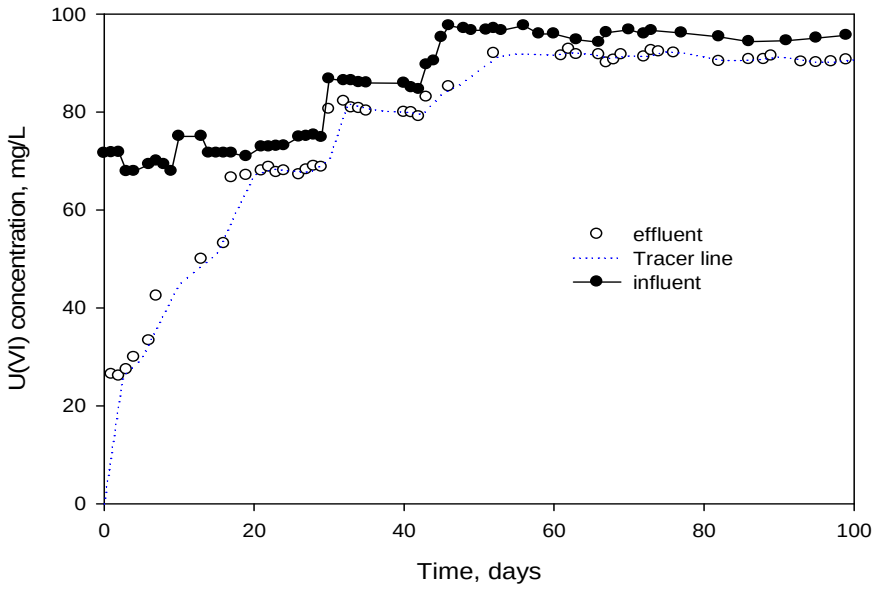

Figure 5-5: Performance of cell-free control reactor (R2) showing characteristics of exponential rise in the effluent U(VI) as compared to the tracer.

5.5.2 Temporal Variation

The performance of fixed-film bioreactor system in treating U(VI) contaminated plume water was evaluated over time. Figure 5-6 demonstrates near complete U(VI) removal after 29 days of operation at the initial U(VI) feed concentration of 75 mg/L. Increasing U(VI) feed concentration to 85 mg/L, near complete U(VI) removal was achieved 13 days after the feed was increased. Near complete U(VI) removal achieved at loading treatment of 75 and 85 mg/L may be associated to various active processes taking place within the biofilm reactor at the initial stage. Moreover, enhanced or improved U(VI) reduction rates observed at the loading treatment of 85 mg/L may be attributed to the improvement of the biofilm system over time when certain favourable conditions were sustained. Similar trends of reactor improvement after the treatment of initial U(VI) feed concentration were also observed in a continuous-flow suspended growth system.

After complete U(VI) removal was observed at 85 mg/L the system was challenged by increasing the U(VI) feed concentration to 100 mg/L. Increasing U(VI) concentration up to 100 mg/L the biofilm system achieved U(VI) removal efficiency of 60%. The insignificant U(VI) removal observed in the bioreactor after 66 days of operation at the loading treatment of 100 mg/L may be attributed to limited diffusion of dissolved U(VI) species across the biofilm layer. The limited metal-microbe interactions achieved in the bioreactor over time may be associated to uranium precipitate [$U(OH_4)_{(s)}$] observed around the biofilm layer after complete U(VI) reduction of up to 85 mg/L was achieved. These results demonstrate the potential of accumulated reduced metal precipitates in changing groundwater hydrodynamics and physically plugging critical aquifers features. Figure 5-6 shows that in all loading treatments, U(VI) concentration in the biofilm system did not rise up to the actual added U(VI) feed concentration, demonstrating the ability of the bioreactor system in stabilizing U(VI) under a range of influent U(VI) concentrations.

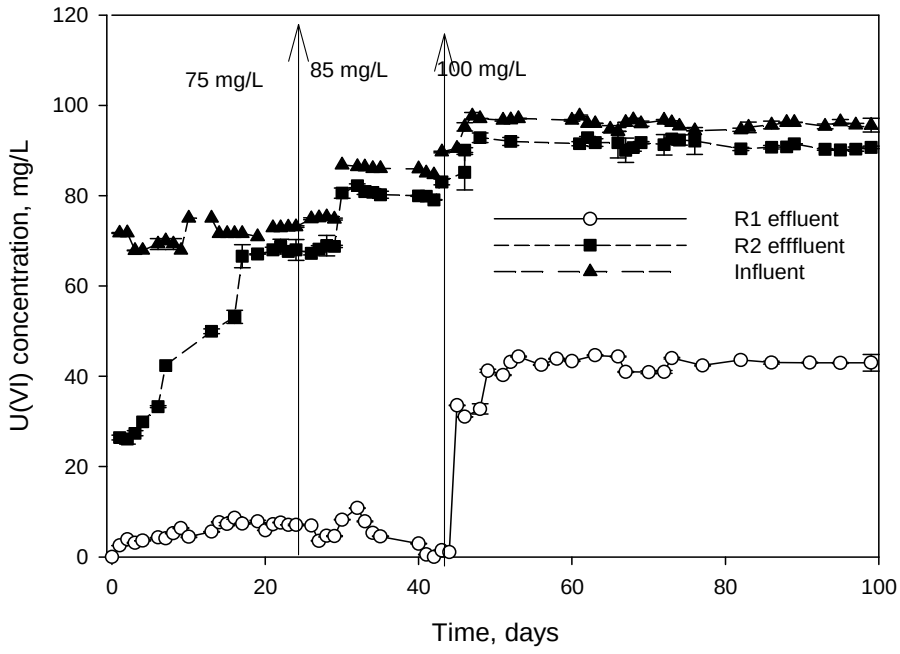

Figure 5-6: Performance of attached growth system (R1) and cell-free control system (R2) in stabilizing U(VI) under oxygen stressed conditions. Biomass reactor (R1) effluent represents average experimental data from the last port.

5.5.3 U(VI) Concentration Profiles

U(VI) removal across the biofilm system (R1) was evaluated over the entire period of operation using data collected from equally spaced longitudinal sampling ports. Figure 5-7a demonstrate that at the initial U(VI) feed concentration of 75 mg/L under non-steady conditions, U(VI) removal was notably higher at the first sampling port from the bottom of the reactor (port 1, h= 0.2 m) than in (port 2, h= 0.4 m). Higher U(VI) removal observed in port 1 may be due to (i) the possibility of high accumulation of biomass at the bottom part of the reactor as the cells were inoculated in the reactor in the up-flow mode, and/or (ii) delayed response of the reactor to the feed concentration. Operating the biofilm reactor at the higher U(VI) feed concentration of 85 mg/L and 100 mg/L, respectively, Figure 5-7 b and Figure 5-7c shows near constant U(VI) removal across the column over time.

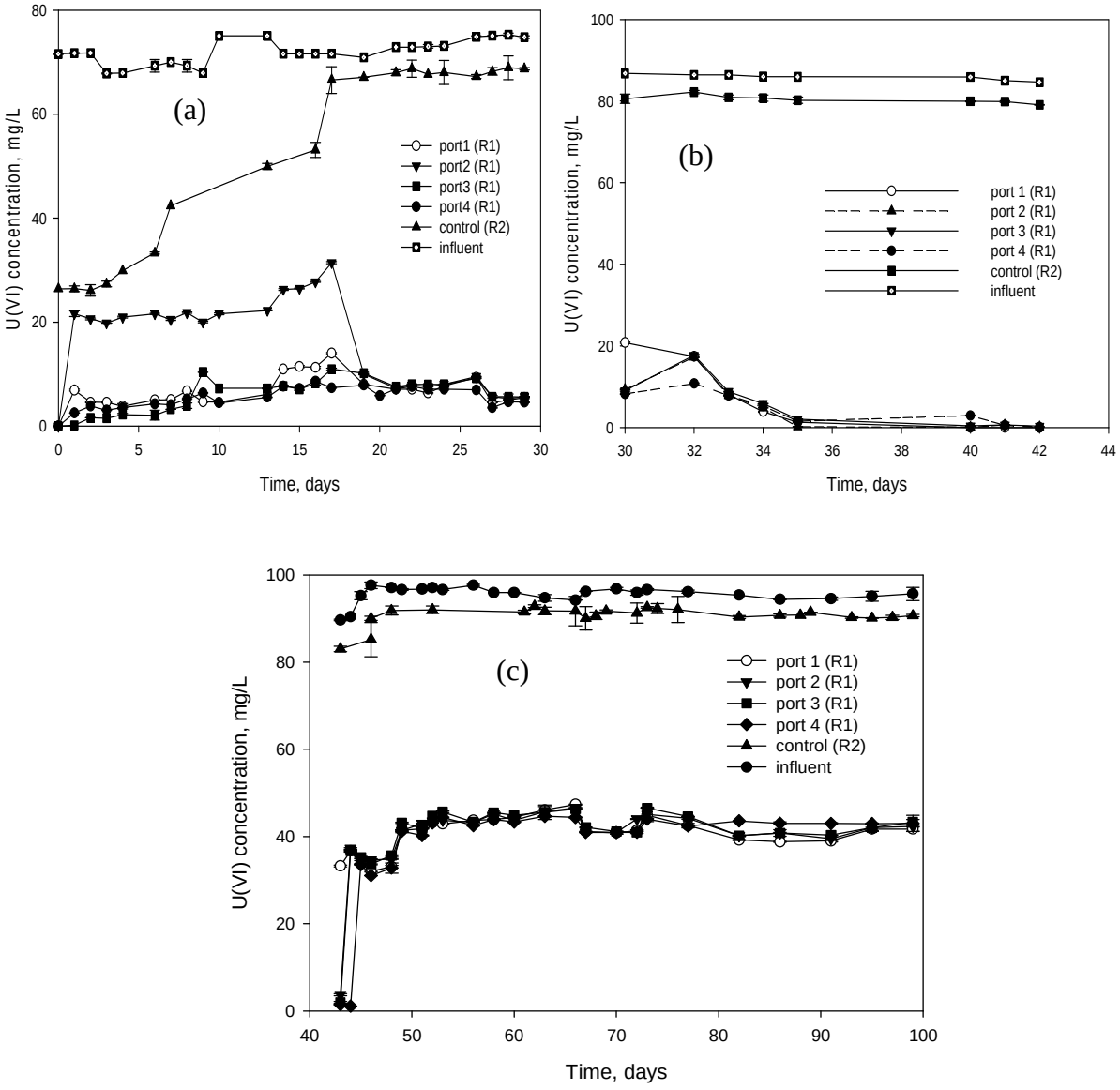

Figure 5- 7: Evaluation of U(VI) removal across the biofilm reactor over time at initial feed concentration of (a) 75 mg/L, (b) 85 mg/L, and (c) 100 mg/L.

Spatial Variation at Discreet Times

To determine or depict when near constant U(VI) removal was achieved across the reactor, data collected from equally spaced longitudinal sampling ports at discreet times was analysed. The results in Figure 5-8a show that at the initial U(VI) feed concentration of 75 mg/L the rate of U(VI) removal from the first 17 days of operation varied significantly over length. Figure 5-8a also demonstrate near constant U(VI) removal across the reactor after 20 days of operation. These results are in agreement with tracer analysis results whereby

significant increase in effluent concentration to the influent level was observed after 20 days of operation.

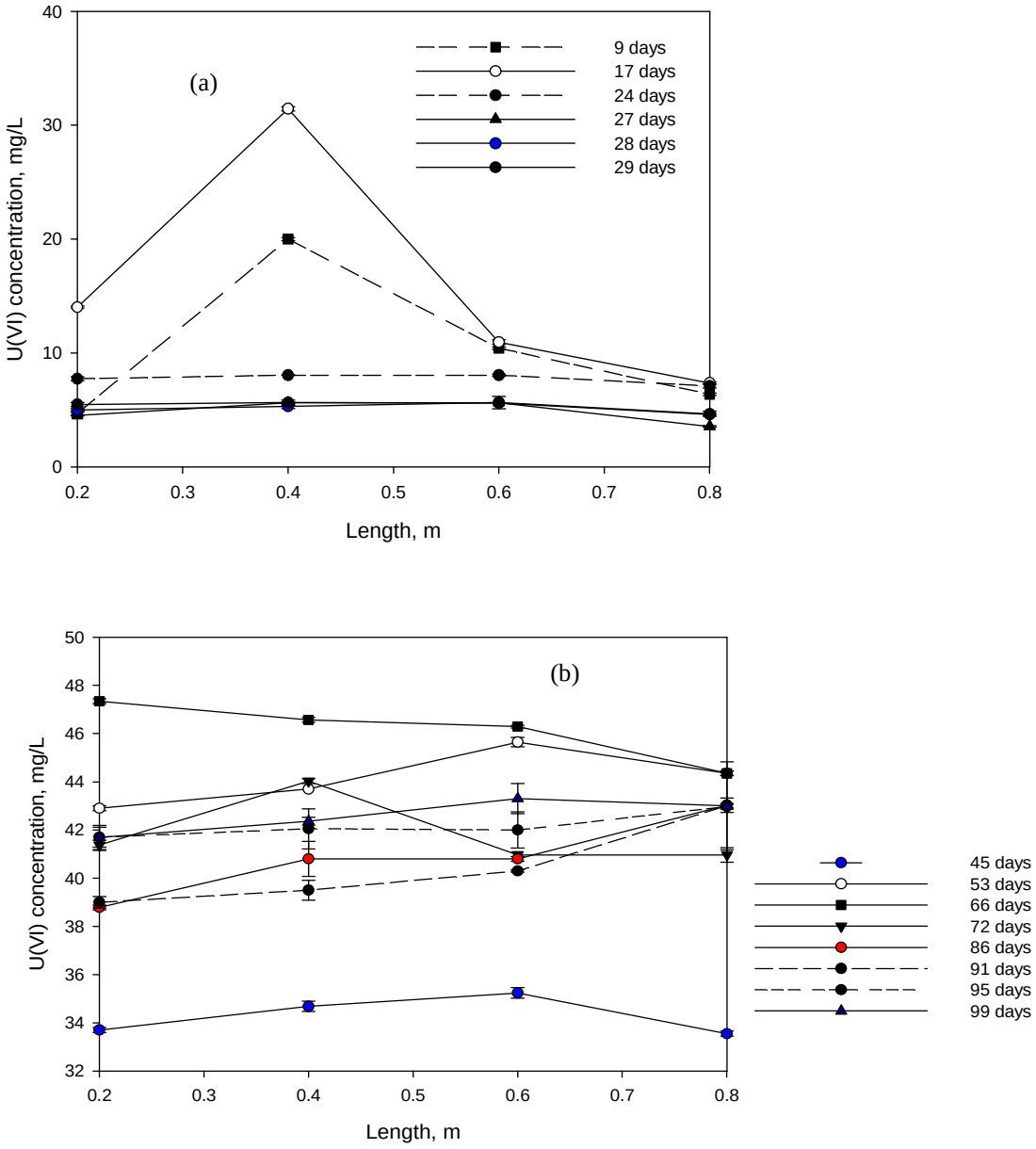

Figure 5- 8: Evaluation of U(VI) effluent across the reactor at initial feed concentration of (a) 75 mg/L and (b) 100 mg/L.

On the other hand data in Figure 5-8b show immediate increase of effluent U(VI) concentration to about 40 mg/L, when influent U(VI) concentration was increased to 100 mg/L. Thereafter, near constant U(VI) effluent concentration was observed across the column over time. The near constant U(VI) effluent concentration (with variance of about 5%)

observed along the four intermediate sampling ports may be attributed to distribution of fluid residence times across the porous system which may cause a degree of fluid mixing in axial direction. However, although near constant U(VI) effluent concentration was observed across the reactor, higher U(VI) removal rates were consistently achieved at first sampling (port 1, h= 0.2 m) and the last sampling point (port 4, h= 0.8 m) over time.

5.5.4 Biomass Analysis

The growth curve in Figure 5-9 shows insignificant change in attached cells population number per surface area within the first 7 days of operation which may be attributed to initial exposure of cells to U(VI). The biomass population exponentially increased after 15 days of operation. After about 18 days of operation, the biofilm was assumed to be at the mature stage generating processes that contributes to the life of the biofilm, and play role in biofilm survival, and biofilm spread. The increase in viable attached biomass population between 15-43 days of operation may be attributed to cell defence mechanism such as cell acclimation to the U(VI) toxicity.

The near constant growth of biomass observed between 50 and 90 days operation. Near constant attached cell growth may be attributed to maximum attainable cell growth on the surface of the biofilm due to the accumulated uranium precipitate. A slight increase in viable cells observed after 90 days of operation may be attributed to change in community. Scanning electron microscopy (SEM) was used to determine the surface morphology of the culture attached to the growth support material (Figure 5-10). Figure 5-10b shows the evidence of biofilm and crystals on the support material.

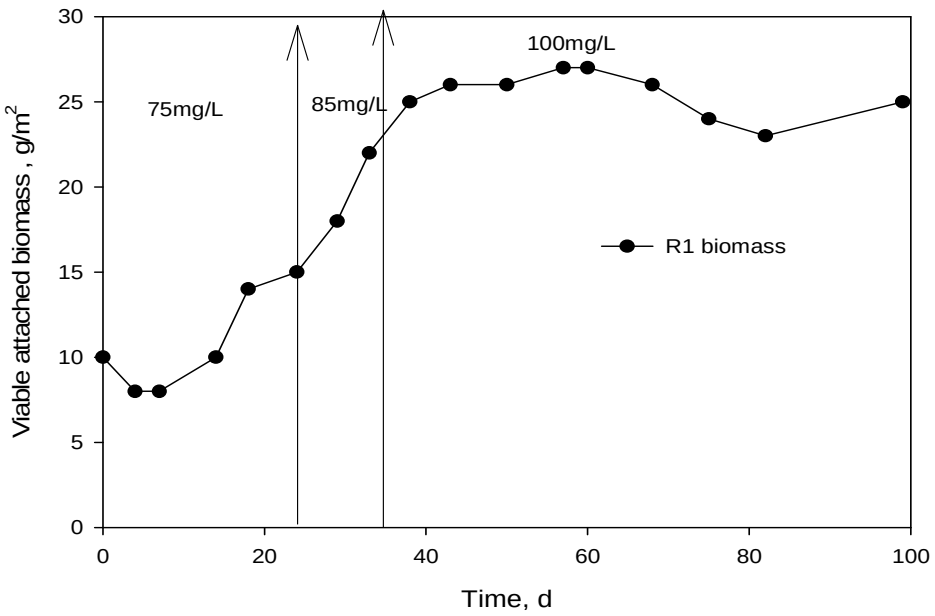

Figure 5- 9: Evaluation of biomass in the biofilm reactor showing rise to the viable attached biomass density.

5.6 Microbial Shift Dynamics

5.6.1 Characterization of Initial Inoculated Culture

The mixed-culture of bacteria isolated from the uranium contaminated soil samples was grown under micro-aerobic conditions and inoculated in the column containing support medium as a start-up culture. The start-up culture of U(VI) reducing bacteria was identified from the 16S rRNA gene analysis as phenotypes of *Bacillius*, *Microbacterieceae*, *Anthrobacteriae*, and *Acinetobater*. After operating the reactor for 99 days under oxygen stressed and nutrient deficient conditions, the presence and the absence of U(VI) reducers initially inoculated in the reactor was monitored by 16S rRNA fingerprinting method. Results show the predominance of *Acinotobacter spp.*, *Bacillus spp.*, *Rhodococcus spp.*, *Cellulosimicrobium spp.*, and *Curtobacterium spp.*, after column operation (Figure 5-11). These species are characteristic of bacterial communities commonly found in the soil and are closely related to the original inoculum.

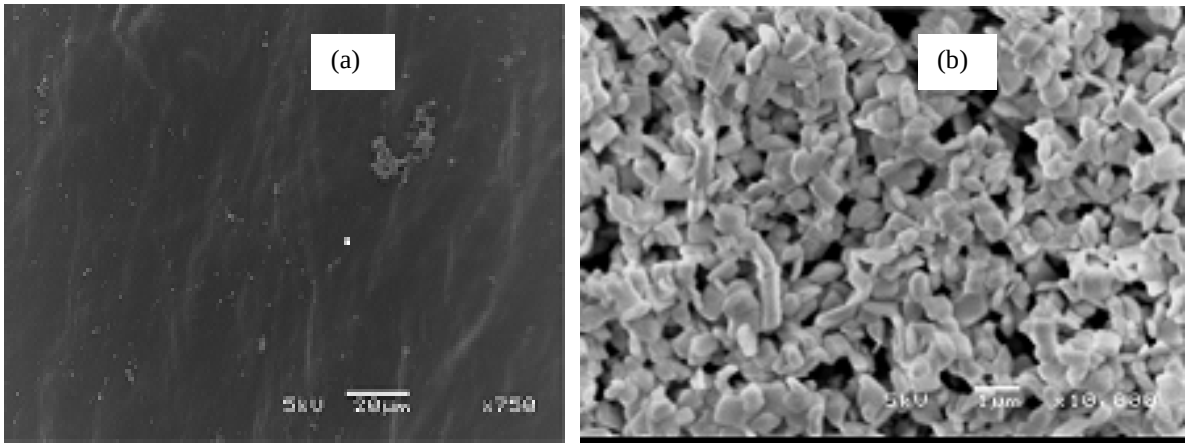

Figure 5- 10: SEM analyses of a support material (a) without cells, control, (b) with cells attached on it as a biofilm.

The *Cellulosimicrobium spp*., *Rhodococcus spp*., and *Curtobacterium spp*., are known species of bacteria belonging to the family *Microbacterieceae* within the order of *Actinomycetales*. These species are Gram-positive, facultative anaerobes that are also related to *Bacilli* but differ in the DNA encoding of the 16S rRNA. These species are known to have extensive metabolic capabilities under aerobic to micro-aerobic conditions. Elwakeel and co-workers (2012) showed the effectiveness of *Cellulosimicrobium spp*., isolated from the radioactive waste in treating thorium contaminated aqueous solutions. The presence of these bacterial species which are closely related to the initially inoculated culture after column operation under oxygen stressed and nutrient deficient conditions demonstrate the effectiveness of these phenotypes in reducing and tolerating U(VI) under shock loading conditions. No foreign bacterial species were identified in the reactor after operation. The insignificant change of the microbial community in the reactor after operation may be attributed to the operation of the reactor without external carbon source as it is well known from the literature that the addition of such may effectively result in the change of the microbial community in the system (Wall and Krumholz, 2006; Chirwa, 2011).

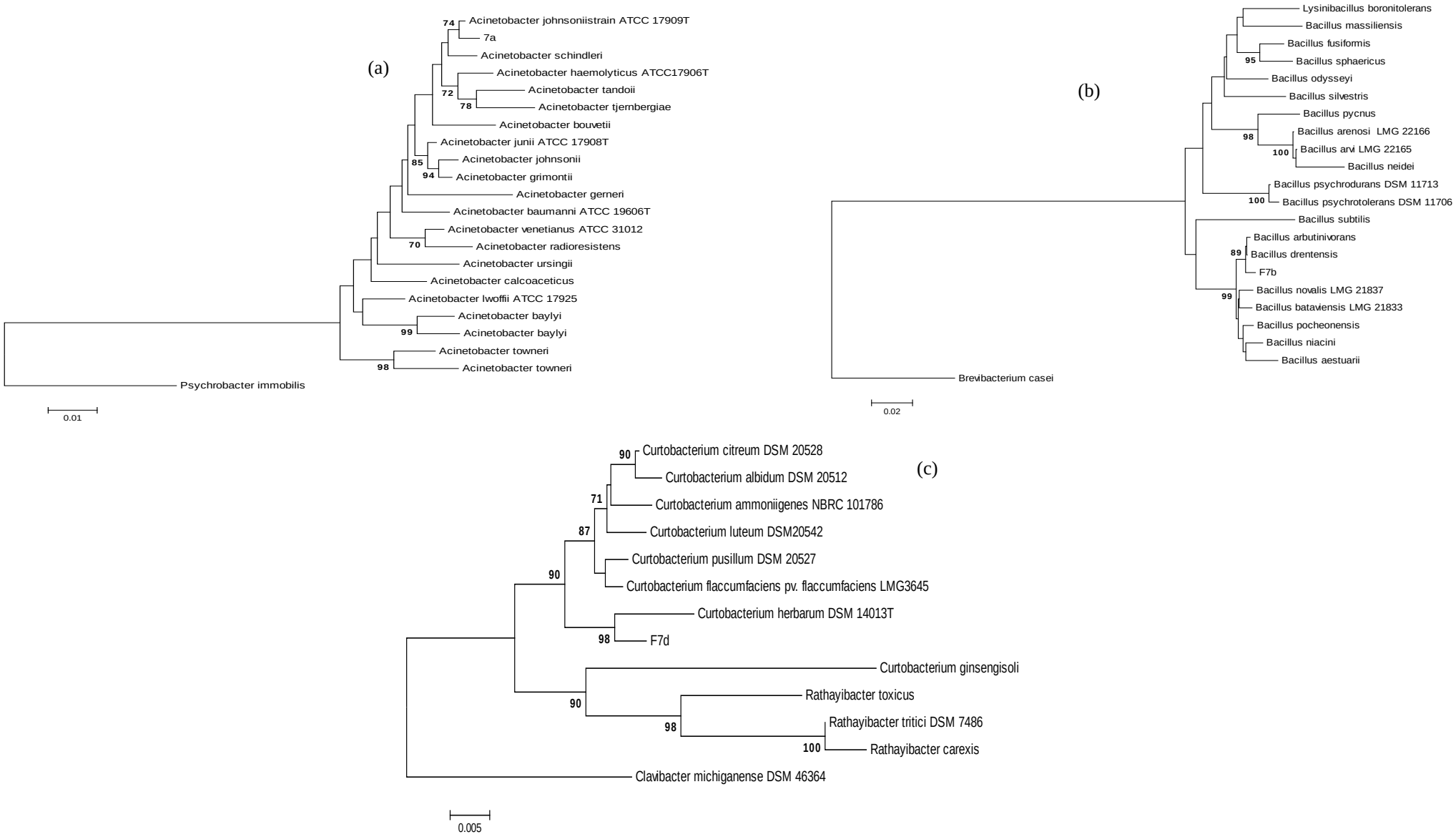

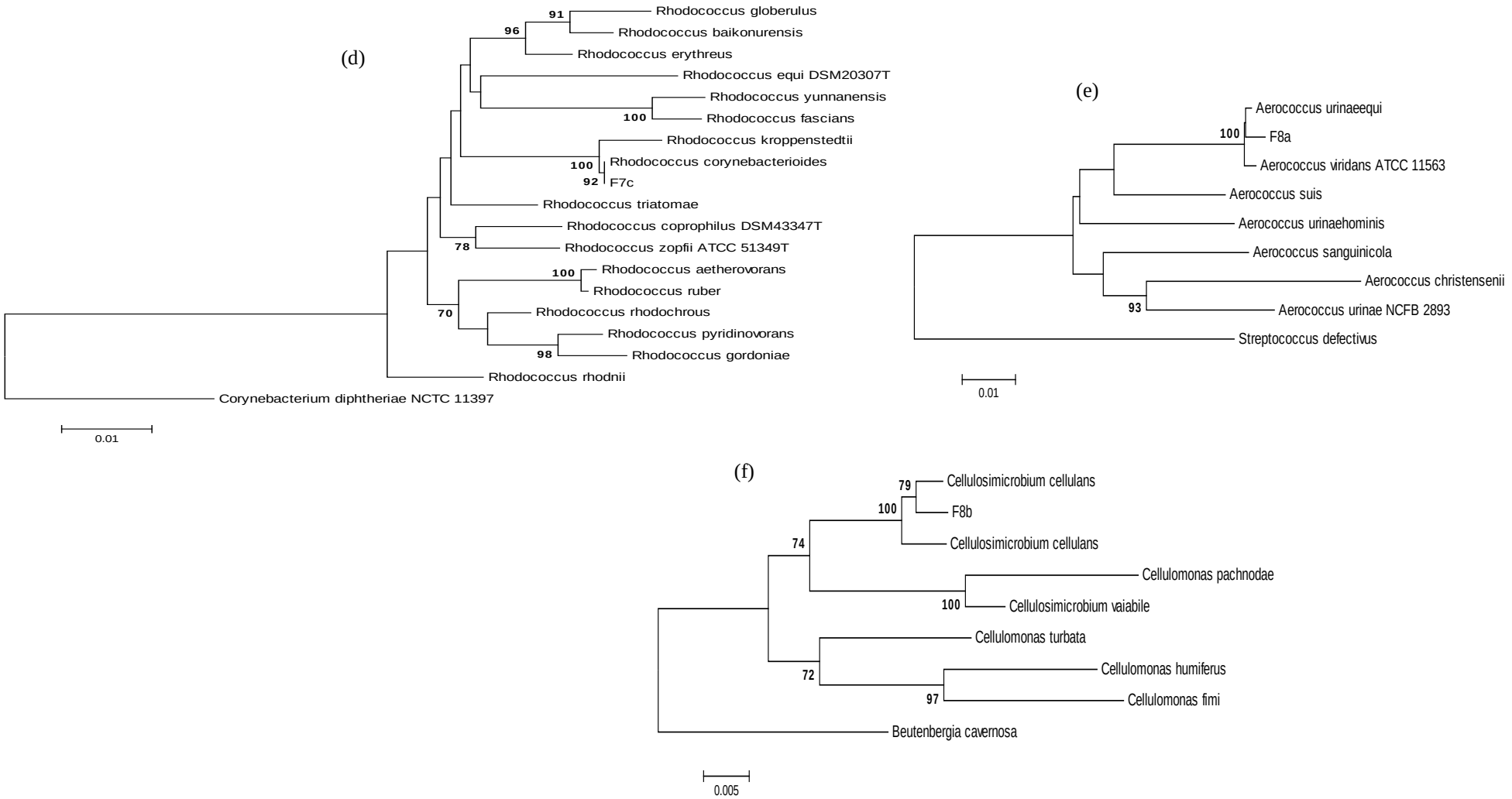

Figure 5- 11: Phylogenetic analysis results showing the predominance of the Gram-positive bacteria (a-f) belonging to *Microbacterieceae*, *Anthrobacteriae*, *Bacilli* group after shock loading treatment of U(VI).

5.7 Summary

Continuous-flow bioreactor systems have the potential of treating shock loadings of U(VI) in both suspended growth and attached growth system. The mixed-culture of bacteria in the suspended growth system was observed to be effective in reducing U(VI) in the solution at relatively higher initial U(VI) feed concentration ranging from (100-400 mg/L). The suspended culture was able to reduce or stabilize U(VI) in the system at concentrations up to 400 mg/L. Higher U(VI) removal rates observed in the suspended culture system which was operated without re-inoculation with fresh cells may be attributed to continuous addition of concentrated nutrients and glucose solution in the system. These demonstrates the effectiveness of nutrients and glucose in enhancing U(VI) removal in the system by stimulating the activity of viable URB.

The fixed-bed bioreactor was operated under oxygen and nutrient deficient conditions without addition of external organic carbon source. The results from this study showed that the biofilm system was able to stabilize U(VI) up to the initial feed concentration of 100 mg/L, which is much higher than the background uranium concentration at the study site. Higher U(VI) removal rates observed in biofilm system under shock loading treatment without biostimulation may be attributed to the effectiveness of the mixed-culture and interrelationships that occur within the biofilm structure.

Results presented here have strong implications of *ex situ* biological reduction of U(VI) through the use of the bioreactor systems. Moreover, operation of the biofilm system under oxygen stressed and nutrient deficient conditions with continual influx of the contaminant also demonstrated the ability of indigenous culture in reducing U(VI) *in situ*. These results could be effective towards successful development and proper design of biological containment barrier technologies at U(VI) contaminated aquifers. The complex nature of the biofilm which is attributed to complex processes within the attached growth biofilm system such as mass transport resistance, cell and substrate diffusion, and biofilm detachment often pose difficulty in analysing biofilm system experimentally. Therefore, for effective analysis of a complex biofilm system a mathematical model that effectively approximates or simulates the observed process behaviour should be developed.

CHAPTER 6

MODELLING OF CONTIONOUS-FLOW SYSTEM

6.1 Biofilm Systems Background

The second component of the study utilising the continuous flow process capitalises on the improved performance observed in attached growth biofilm systems. Attached growth technologies such as trickle-bed reactor systems, rotating biological contactors (RBCs), membrane bioreactors (MBRs), and anaerobic sludge blanket reactors (ASBR) have been widely used for treatment of both municipal and industrial wastewater. Biofilm system have been observed to provide better treatment efficiency of wastewater streams due the high volumetric density of microorganisms accumulated in the presence of large surface area inducing biofilm resistance to environmental changes (Rittman and McCarthy, 2001; Kermani *et al*., 2008). However, the efficiency of biofilm systems in treating contaminated water is not only dependent on the capability of the microbial culture to degrade or transform pollutants but is also dependent on the microbial interactions within the biofilm matrix. These interactions include (i) community level interdependencies, (ii) substrate concentration profiles with varying biofilm depth, (iii) and biofilm loss rates influenced by surface shear created by hydrodynamic loading.

The biofilm system is very complex in structure and heterogeneous in composition. Model performance of the biofilm is therefore achieved by approximations and space averaged values (Rao *et al*., 2010). Generally, mathematical models that resemble real system and phenomena taking place within it are very rare. This is due to the complexity associated with hydrodynamic regime and mass transfer characteristics within the biofilm system. In practice, mathematical models are primarily developed to provide adequate and critical information required for conceptual understanding and optimum design and operation of biofilm system at the actual site.

Biofilm models previously presented by Wanner et al. (1995), Chirwa and Wang (2005), and Rittman and Davantzis (1983) were developed under the assumption of the two-dimensional propagation of biomass and substrate removal constrained within the biofilm space. Each of the above models oversimplified the internal structure of the biofilm into a homogeneous

matrix with a singular diffusion and reaction rate property. The results from the previous models were observed to be effective for routine reactor design. The problem associated with the application of such models to real practical problems is that they could not generate sufficient information required for optimum operation of microbial barrier system at actual site. Therefore, there is a need to develop a mathematical model that could simulate near real system situation under shock loading conditions.

This study is one of the few efforts to develop a fixed-film mathematical model that predict the fate of U(VI) across the biofilm system under oxygen stressed and nutrient deficient conditions. The model in this study takes into consideration the physical properties of the system and the microbial growth kinetics of the bacteria composing the biofilm. Numerical solutions of this model is essential for fundamental understanding of a complex biofilm system from hydrological, chemical, and biological point of view under natural aquatic system conditions.

6.2 Basic Biofilm Model Assumptions

- Biofilm is treated as a continuum: variables are described by average quantities such as concentrations and volume fraction
- Gradients of system properties $\left(\frac{\Delta U}{\Delta t}\right)$ are in orders of magnitude greater perpendicular to substratum than in other direction, thus the flow in the column is considered to be one-dimensional for biofilm modelling.
- The flow has no radial gradient in velocity: perfectly mixed in radial direction
- The reactor approached mixed reactor flow characteristics over time with respect to hydraulic residence times, porosity, and advection.
- The porous medium is homogeneous
- Since the biofilm consisted of 95 % water, the porosity was assumed to be constant
- Biofilm consist of one liquid phase and one solid phase, whereby each phase consists of mass of particulate matter.

- The flow is saturated, which means that all available pores space are filled with fluid, this is exclusive of dead end pores where water is trapped.
- Liquid phase consist of both dissolved components and particulate components
- Assume complete reduction of U(VI) to U(IV)
- U(IV) generated due to biotransformation is either precipitated and retained or adsorbed onto the media almost immediately
- Change in temperature and pH is insignificant

6.3 Model Approach

Generally there are three predominant mechanisms influencing transport and removal of dissolved species in a porous media, i.e, (i) advection, (ii) molecular diffusion, and (iii) kinematic (mechanical) dispersion. Within the biofilm itself, the rate of removal is influenced by adsorption processes at the liquid-biofilm interface and conversion rate within the biofilm matrix. For the purpose of discussing the mass transport dynamics in the biofilm, the biofilm is divided into two parts: away from the biofilm surface (bulk solution) and approximately on the biofilm surface. The model developed for the biofilm system is based on the mass balances which describe in mathematical terms the (i) transportation of the substance in the bulk liquid solution which is controlled by advection, (ii) the transportation of the dissolved substances towards the biofilm surface which is controlled by diffusion, (ii) the microbial processes causing population dynamics (thus microbial growth, cell attachment and detachment). To simulate the fate of U(VI) across the biofilm system under oxygen stressed conditions, the general mathematical expression of diffusion-reaction equation that describe the transport of dissolved species from the bulk phase into the biofilm and vice-versa and, is evaluated in this study. Figure 6-1 below shows the conceptual biofilm model in the biofilm reactor:

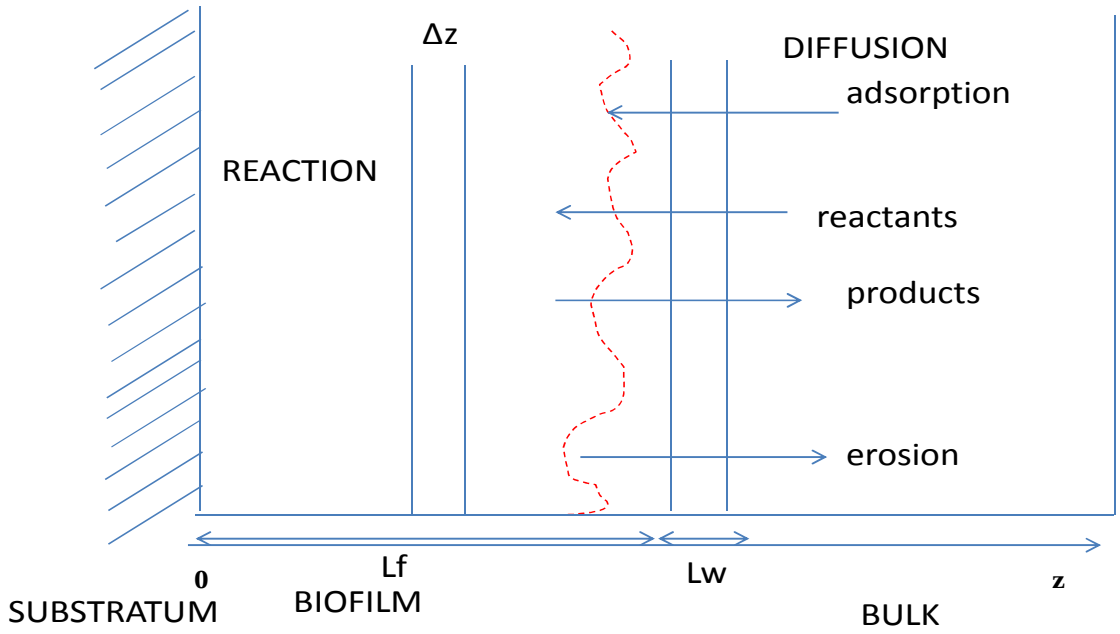

Figure 6-1: Conceptual biofilm model

6.3.2 Analytical Methods of Biofilm Measurements

For effective model development parameters, A_f, X_f, and L_f were initially calculated using the experimental data as following:

$$A_f = Va_v \tag{6-2}$$

$$L_f = \frac{W_w}{A_f \rho_f} \tag{6-3}$$

$$X_f = \frac{W_d}{A_f \alpha L_f} \tag{6-4}$$

where: A_f = available biofilm surface area (L^2), V= volume of the reactor (L), a_v = specific surface area of the particles (L^2L^{-3}), ρ_f = wet biofilm density (ML^{-3}), W_w = wet weight of attached biomass (M), W_d = dry weight of attached biomass (M), X_f = biofilm density (ML^{-3}), L_f = thickness of biofilm layer (L), and α= biofilm density factor. Values of α are in the range of 0.9-1.0 by (Moller *et al.*, 1998). In this study $\alpha = 0.95$ was used. The surface area of the biofilm is expected to be less than the total surface area of the filter material due to incomplete biofilm coverage.

6.3.3 Hydraulic Characteristics

The cross-sectional area of the reactor $A(t)$ affects the interfacial fluid velocity v (LT^1) and the stagnant liquid layer (L_w) around the support media. This is because the void (pore)

volume available for free flow of water in microbial barrier column decreased as biomass grows around the support media. This resulted in decrease in the available cross-sectional area of the reactor [$A(t)$] and constrained flow with increasing time. The initial value of cross-sectional area of the reactor [$A(t)$] before biomass attachment is computed as a function of pore volume as follows:

$$A(0) = \frac{\pi(\mathrm{ID})^2}{4} \cdot \left(\frac{V_s}{V_T}\right) \tag{6-5}$$

where: $V_T = \pi(\mathrm{ID})^2 \cdot h/4$, the empty-column volume (L^3), V_s = volume of void space occupied by water (L^3), ID = internal diameter of the reactor column (L), and h = the height of the packed-bed reactor (L).

6.3.4 Liquid Layer Effect

In order to estimate the stagnant liquid boundary layer (L_w) in the fixed film reactor the parameters: Q (inflow rate); A (cross sectional area of a reactor); d_p (diameter of the filter media); D_{uw} (diffusion coefficient of U species in water); and υ (kinematic viscosity of water) are required. Empirical correlations by (Frosslings, 1938; Wilke and Chang, 1955; Sherwood *et al*., 1975; Cussler, 2003; Basmadjiaan, 2004; Incropera *et al*., 2011) are used to calculate (L_w) using Schmidt number (Sc), Sherwood number (Sh), Reynolds number (Re) as follows:

$$\mathrm{Sh} = \frac{K_{LU} d_p}{D_{uw}} \tag{6-6}$$

The Sherwood number is often expressed as a function of non-dimensional Reynolds number Schmidt number (Sc) as follows:

$$R_e = \frac{v d_p}{\upsilon} \tag{6-7}$$

$$Sc = \frac{\upsilon}{D_{uw}} \tag{6-8}$$

where: d_p = average particle size (L), D_{uw} = diffusion coefficient of dissolved uranium species in water (L^2T^{-1}); υ = kinematic viscosity; K_{LU} = mass transfer coefficient (LT^{-1}).

$$L_w = N + B\,\mathrm{Re}^m\, Sc^n \tag{6-9}$$

where: N (depends on geometry of biofilm and it runs from 0, 1, 2, and 3); B= 0.6; m=1/2; n =1/3

Therefore the equation (6-9) above can be represented as:

$$L_w = \left[0.6 \cdot \left(\frac{1}{D_{uw}^{1/3} \upsilon^{1/6}} \right) \cdot \left(\frac{\nu^{1/2}}{d_p^{1/2}} \right) \right]^{-1} \quad (6\text{-}10)$$

where: D_{uw} = diffusion coefficient of dissolved species of U(VI) in water (L^2T^{-1}), $\nu = Q/\varepsilon A(t)$ is the interfacial velocity (LT^{-1}), Q = flow rate across the bulk liquid zone (L^3T^{-1}), d_p = average particle size (diameter) (L), υ = kinematic viscosity (L^2T^{-1}), and $A(t)$ = effective cross sectional area of the reactor column (L^2). The diffusion coefficient of U(VI) in water D_{uw} = 6×10^{-6} m^2/d, determined from standard 1M of uranyl nitrate at (25°C, dynamic viscosity =1.01 centipoises= 1.01 g/cm/s, and kinematic viscosity of ($\upsilon = \frac{\mu}{\rho}$ =4.2 cm^2/s) was used in this study (Ondrejcin, 1961).

6.4 Reactor Mass Balance

6.4.1 Mass Balance of Dissolved Species

In general terms the mass balance of dissolved species across the bulk liquid zone of the packed-bed reactor at a transient state can be represent by various physico-chemical and biological processes described below:

Advection

The transport of dissolved U(VI) species from one point to another governed by bulk motion of fluid as follows:

$$\frac{-dU_B}{dt} V_B = Q(U_{in} - U_B) \quad (6\text{-}11)$$

where: U_B = U(VI) concentration at the bulk liquid zone at time, t (ML^{-3}), V_B = bulk liquid volume (L^3), U_{in} = influent U(VI) concentration (ML^{-3}), Q = influent flow rate (L^3T^{-1}), and t = time (T).

Molecular Diffusion

The transport of all dissolved species across the boundary layer (L_w) into the biofilm is caused by random molecular motions and collusions of particles themselves. Molecular diffusion is the only means of mass transport mechanism within the biofilm that follows Fick's law and can be defined as a function of external mass transfer resistance (K_{LU}) across the biofilm surface area and bulk U(VI) concentration as follows:

$$\frac{-dU_B}{dt}V_B = K_{LU}A_f\left(U_B - U_{sf}\right) = \frac{D_{uw}}{L_w}A_f\left(U_B - U_{sf}\right) = j_u A_f \qquad (6\text{-}12)$$

where: A_f = total biofilm surface area (L^2), D_{uw} = diffusion coefficient of dissolved uranium species in water (L^2T^{-1}), L_w = the thickness of the stagnant liquid layer, which may decrease the flux of dissolved particles into the biofilm (L), U_B = U(VI) concentration at the bulk zone at time, t (ML^{-3}), U_{sf} = liquid-biofilm interface U(VI) concentration (ML^{-3}). In most mass transfer limited reactions $U_B >> U_{sf}$, thus U_{sf} is negligible and may therefore be omitted in the equation above. The external mass transfer resistance, K_{LU}, (LT^{-1}) can be visualized by introducing a boundary layer (L_w) as follows:

$$K_{LU} = \frac{D_{uw}}{L_w} \qquad (6\text{-}13)$$

Adsorption

The rate at which U(VI) is removed across the reactor is dependent on the rate at which U(VI) is transported across the liquid layer by diffusion and adsorbed within the biofilm matrix. The rate at which U(VI) can be reduced on the surface area of the biofilm is defines as:

$$\frac{-dU_B}{dt} = k_{ad}\left(U_{eq} - U_B\right) = q_u \qquad (6\text{-}14)$$

where: k_{ad} = U(VI) adsorption rate coefficient (T^{-1}), U_{eq}= equilibrium bulk liquid U(VI) concentration (ML^{-3}), U_{sf} = liquid-biofilm interface U(VI) concentration (ML^{-3}).

Microbial-Reduction

The rate of U(VI) reduction in the biological system is highly dependent on the number of active cells present in the reactor, and the capacity of cells to produce enzymes that can reduce U(VI) under various loading concentrations. A fraction of cells leaving the biofilm and exiting the reactor after time equivalent to HRT of the reactor are assumed to be at resting conditions. It has been shown in batch kinetic studies that resting cells may reduce U(VI) without the accompanying cell growth. It is suggested therefore that the amount of U(VI) reduced under resting cells conditions will be proportional to the amount of cells inactivated by U(VI) (Chirwa and Wang, 2005).

The inhibitory effects observed in the reactor over time at higher initial U(VI) concentration of 100 mg/L under oxygen stressed conditions suggested incorporation of U(VI) toxicity

threshold concentration, U_r, and deactivation coefficient of cells in the system. Therefore, a mathematical model incorporating U(VI) toxicity threshold concentration, U_r, and deactivation coefficient of cells in the system was used during simulation of U(VI) effluent concentration:

$$\frac{-dU_B}{dt} = \frac{k_u U_B}{K_u + U_B\left(K^{\left(1-\frac{U_B}{U_r}\right)}\right)}\left(X_B - \frac{U_{in} - U_B}{T_u X_B}\right) = r_{uB} \qquad (6\text{-}15)$$

where: k_u= specific rate of U(VI) reduction ($L^3M^{-1}T^{-1}$), K_u = half-velocity coefficient (ML^{-3}), X_{0B} = initial cell concentration at the bulk zone (ML^{-3}), U_{in} = influent U(VI) concentration (ML^{-3}), K = dimensionless U(VI) inhibition factor (MM^{-1}), U_r = inhibition threshold concentration (ML^{-3}), T_u= maximum U(VI) reduction capacity of cells [g U(VI) reduced/g cells] (MM^{-1})].

The overall non-linier equations from Equation 6-11 to Equation 6-15 governing the liquid phase at transient state yield the following mass balance equation of the dissolved species across the bulk liquid zone of the reactor:

$$\frac{dU_B}{dt}V_B = Q(U_{in} - U_B) - r_{uB}V_B - q_u V_B - j_u A_f \qquad (6\text{-}16)$$

where: U_B = U(VI) concentration at the bulk liquid zone at time, t (ML^{-3}), V_B = bulk liquid volume (L^3), U_{in} = influent U(VI) concentration (ML^{-3}), Q = influent flow rate (L^3T^{-1}), r_{uB}=U(VI) reduction rate coefficient at the bulk phase ($ML^{-3}T^{-1}$), q_u= rate of U(VI) removal by adsorption (T^{-1}), j_u= U(VI) flux rate (ML^2T^{-1}), A_f = surface area in the biofilm reactor (L^2), t = time (T), and r_u = dissolved species removal rate ($ML^{-3}T^{-1}$),

The terms $\boldsymbol{q}_u$, $\boldsymbol{j}_u$, $\boldsymbol{r}_u$ in the above equations represent adsorption, diffusion processes, and reaction by suspended or inert cells in the bulk liquid respectively. The term $\boldsymbol{q}_u$ in the above equation can approach equilibrium easily whereas the terms $\boldsymbol{r}_u$ and $\boldsymbol{j}_u$ depend on the active biomass. The term j_u in Equation 6-16 applies across the stagnant liquid layer and the entire biofilm depth.

6.4.2 Biofilm Zone Mass Balance

The flow of dissolved species across the biofilm layer was expected to decrease over time due to the thickness of the mass transfer boundary layer by reduced uranium precipitate. Therefore, as a result of these the transport of dissolved uranium species across the surface of the biofilm over time was based on molecular diffusion which follows Fick's law as follows:

$$j_u = D_{uw}\frac{dU_f}{dz} \qquad \text{at } 0 < z < L \qquad (6\text{-}17)$$

A mass balance of the dissolved species over an infinitesimal film segment δz gives:

$$\frac{d}{dz} j_u = r_{uf} \qquad (6\text{-}18)$$

Therefore, the partial differential equation describing molecular diffusion of a particulate matter in water inside the biofilm is represented as follows:

$$\frac{dU_f}{dt} = \frac{d}{dz} j_u + r_{u\,f} \qquad (6\text{-}19)$$

$$= \frac{dU_f}{dt} = \frac{d}{dz}\left(D_{uw}\frac{dU_f}{dz}\right) + r_{uf} \qquad (6\text{-}20)$$

Because the diffusion of species across biofilm is influenced by the volume fraction (porosity) the diffusion-reaction biofilm equation for U(VI) removal rate and biomass growth rate within the biofilm is computed as a function of porosity as follows:

$$\varepsilon\frac{dU_f}{dt} = \varepsilon D_{uw}\frac{d^2U_f}{dz^2} + r_{uf} \qquad (6\text{-}21)$$

$$\frac{dU_f}{dt} = \frac{dj_u}{dz} + \frac{r_{uf}}{\varepsilon} \qquad (6\text{-}22)$$

where: $j_u = D_{uw}(dU/dz)$ flux rate of dissolved species ($ML^{-2}T^{-1}$), U_f = U(VI) concentration at biofilm zone (ML^{-3}), r_{uf} = removal rate of dissolve uranium species in the biofilm ($ML^{-3}T^{-1}$), δz = infinitesimal region across the biofilm (L), ε= biofilm porosity constant. The reaction rate is defined as follows:

$$r_{uf} = -\frac{k_u U_f X_f}{K_u + U\left(K^{\left(1-\frac{U_f}{U_r}\right)}\right)} \qquad (6\text{-}23)$$

where: where: k_u= specific rate of U(VI) reduction ($L^3M^{-1}T^{-1}$), K_u = saturation coefficient (ML^{-3}), X_f = biomass concentration at the biofilm zone (ML^{-3}), U_{in} = influent U(VI)

concentration (ML^{-3}), K = dimensionless U(VI) inhibition factor ($M^{-1}M^{-1}$), U_r = inhibition threshold concentration (ML^{-3}), r_{uf} = removal rate of dissolved uranium species in biofilm ($ML^{-3}T^{-1}$). The boundary conditions for dissolved species at the liquid-biofilm interface are defined as:

$$j_u = K_{LU}\left(U_B(t) - U_{f,s}(t, L_f)\right) \qquad \text{at } z = L_f \qquad [\text{inner boundary}] \qquad (6\text{-}24)$$

$$j_u = 0 \qquad \text{at } z = 0 \qquad [\text{outer boundary}] \qquad (6\text{-}25)$$

6.4.3 Biomass Mass Balance at Liquid Zone

Various kinetic models can be used to represent the various biological processes in a system. In the bulk-liquid zone of the biofilm the accumulation of cells in the zone is related to the cell detachment from the biofilm, bulk phase net cell growth, as well as cell death rate. The mass balance of cells across the bulk liquid zone and in the actual biofilm zone of the reactor is generally represented as:

$$\frac{dX_B}{dt}V_B = Q(X_{in} - X_B) + r_{XB}V_B + \Phi(\nu).X_f L_f A_f \qquad (6\text{-}26)$$

$$\Phi(\nu) = k_d A_f \rho_f \left(\frac{\nu^2}{2}\right) \qquad (6\text{-}27)$$

$$\frac{dX_f}{dt} = \frac{dj_x}{dz} + \frac{r_{xf}}{\varepsilon} \qquad (6\text{-}28)$$

where: X_B = viable cell concentration in the bulk liquid zone at time, t (ML^{-3}), b_x = cell death rate coefficient (L^3T^{-1}), $\Phi(\nu)$ = cell detachment rate (T^{-1})_a function of the interfacial velocity ν (LT^{-1}), k_d = cell detachment rate coefficient ($TM^{-1}L^{-1}$), A_f = surface area in the biofilm (L^2), ν = interfacial velocity (LT^{-1}), $j_x = D_{xw}(dX/dt)$ mass flux rate of biomass ($ML^{-2}T^{-1}$), r_{xf} = biomass production rate in the biofilm ($ML^{-3}T^{-1}$), ε= biofilm porosity (LL^{-1}) . Since there was no continuous addition of biomass over time the term QX_{in} in Equation (6-26) is equal to zero.

Due to bio-cell filters rougher surface and limited shear forces of liquid across the biofilm layer limited cell detachment was expected. Moreover, due to the dependence of cell attachment on metabolism most of the cells present in the bulk liquid through detachment which is minimal in this system were expected to be more susceptible to U(VI) toxicity than attached cells. Thus, the viable cell concentration in the bulk liquid zone was expected to be either less than or equivalent to the inert cell concentration. In this study we assume that the

viable suspended cell concentration (X_B) is equal to suspended inert biomass (X_{iB}), thus $X_B = X_{iB}$, at $X_{iB} >> 0$.

The reaction rate is defined as follows:

$$r_{xf} = \mu_{max}\left(\frac{U_f}{K_u + U_f}\right)\left(X_f - \frac{U_{in} - U_f}{T_u}\right) - b_x X_f - k_d A_f \rho_f \left(\frac{\nu^2}{2}\right) X_f L_f \frac{A_f}{V_f} \qquad (6\text{-}29)$$

where: K_u = saturation coefficient (ML^{-3}), X_f = biomass concentration at the biofilm zone (ML^{-3}), U_{in} = influent U(VI) concentration (ML^{-3}), T_u= maximum U(VI) reduction capacity of cells [g U(VI) reduced/g cells] (MM^{-1})], μ_{max} = maximum attainable cell growth rate (T^{-1}). Because the transport of cells across the biofilm is by physical displacement and that of dissolved substance is by molecular diffusion, j_x is expected to be lower than j_u. The boundary conditions for biomass at the liquid-biofilm interface are defined as:

$$j_x = k_d A_f \rho_f \left(\frac{\nu^2}{2}\right) . X_f L_f \qquad \text{at z} = L_f \qquad [\text{ inner boundary }] \qquad (6\text{-}30)$$

$$j_x = 0 \qquad \text{at z} = 0 \qquad [\text{ outer boundary }] \qquad (6\text{-}31)$$

6.5 Initialization and Simulation

The application of the biofilm model was initially evaluated in the cell-free reactor which resulted in the characteristic of exponential curve showing saturation of absorption process in the system. This indicates that the predominant processes across the biofilm over time are limited to mass transport by diffusion, reduction, and cell growth. The biofilm model was used in combination with U(VI) reduction rate kinetic parameters adapted from the anaerobic batch culture system. However, adjustments of these reduction rate kinetic parameters were allowed in the continuous flow biofilm system due to different culture sensitivity in the two systems. Physical parameters were determined from known literature values (Ondrejcin, 1961). Mass transport and adsorption parameters were estimated from continuous-flow reactor data. Since the accuracy of simulation of performance also depends on the prediction of viable biomass in the rector, the viable cell concentration in this study was predicted based on direct measurement of viable cells using the plate count method.

6.6 Parameter Optimization

The model defined by a set of partial differential equations was very stiff in nature. Solution without practical constraints resulted in convergence to false optima for several parameters.

To avoid convergence to nonsensical values, upper and lower constraints upper and lower constrains were set for each parameter to allow the omission of invalid parameter values. Whenever optimization converged at or very close to a constraint, the constraint was relaxed until the constraint no longer forced the model. This process was repeated until unique values lying away from the constraints, but between the set limits were found for each parameter. The inverse of the mean residual sum of squares computed as the global variance was used as a fitness function during parameter optimization. Based on the optimised values and other operating parameters, the model calculated the time series data of U(VI) concentration within the reactor. The simulated U(VI) concentration using the model was then compared with the measured experimental data and the deviations between the two are used determine the accuracy of the model using Equation 4-10 defined in Chapter 4.

6.7 U(VI) Removal Kinetics

6.7.1 Bulk Liquid Phase Kinetics

Equation 6-16 and Equation 6-26 were solved numerically using the computer programme for evaluating numerical methods Octave 3.0. Appendix B shows the code used to solve the equation in the bulk liquid zone. Figure 6-2a shows the simulation of effluent concentration at the bulk liquid zone, and data in Figure 6-2b shows the simulated biomass growth at the bulk liquid zone. The model predicted well the change in U(VI) concentration at the bulk liquid zone with respect to biomass growth. The inhibitory conditions observed in the simulated effluent at bulk liquid zone at higher initial U(VI) concentration corresponded well to the decreased growth rate of viable biomass observed over in the bulk zone.

6.7.2 Biofilm Zone Kinetics

Equation 6-22 and Equation 6-28 were solved numerically using the computer programme for evaluating numerical methods Octave 3.0. The model for biofilm reactor at the biofilm surface was initially tested with the experimental data of 75 mg/L. The kinetic parameters obtained at 75 mg/L were then used to simulate U(VI) effluent concentration under various loading conditions of 85 mg/L and 100 mg/L respectively.

Figure 6-3a and Figure 6-3b shows simulation of effluent concentration and biomass growth at the biofilm zone. The kinetic parameters summarized in Table 6-1 shows that the kinetic parameters obtained at the experimental run of 75 mg/L were maintained at various initial

concentrations with only minor adjustment on the half saturation concentration (K_u) at initial higher concentrations. The adjustment of the kinetic parameter (K_u) may be associated to the breakthrough characteristics observed in the packed-bed reactor at 85 mg/L with moderate dispersion depicting an exponential rise up to maximum point and then followed by reduction in effluent as U(VI) reducing culture become more established.

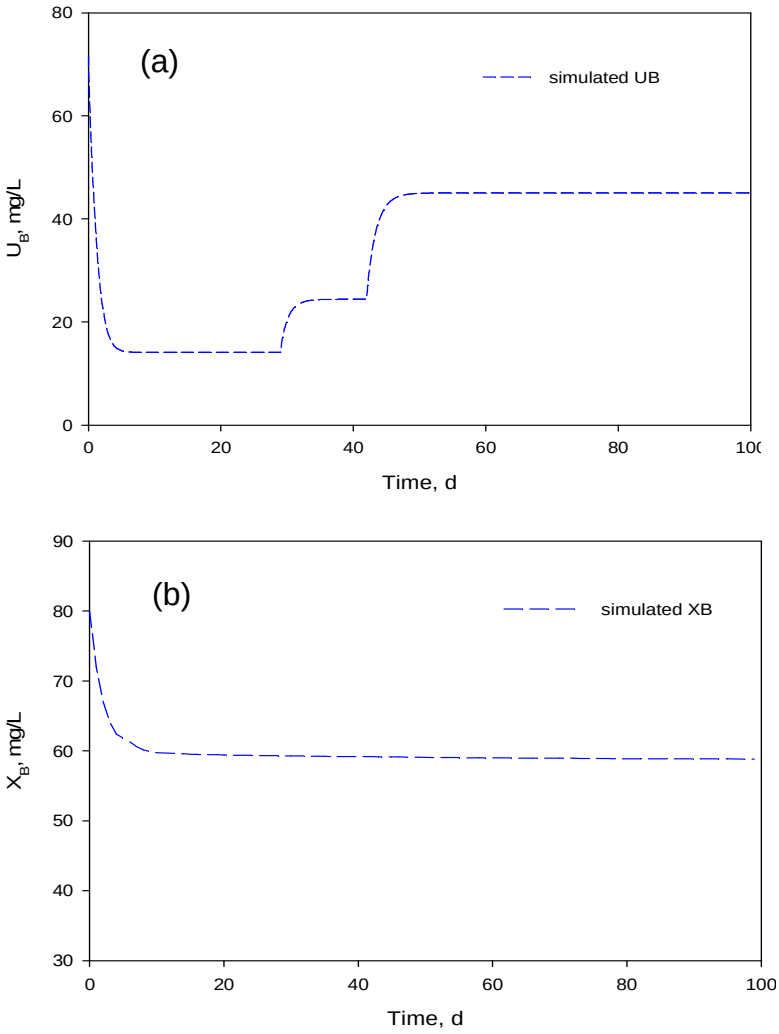

Figure 6-2: Model simulation at the liquid phase of (a) U(VI) effluent (b) biomass activity in the reactor inoculated with live culture from the local environment.

For numerical simulation the attached viable cell concentration was initialised by values ($X_{f,\ init}$ = 60 mg/L) determined using analytic methods. It is observed in Figure 6-3a and Figure 6-3b that regardless of the lower initial biomass concentration in the biofilm reactor high bioconversion rates were observed in the continuous flow biofilm system than in the batch reactor system. The reaction rate coefficients obtained from the continuous flow attached growth system (k_u= 0.75) is much higher than the one previously observed in batch cultures

in this study (k_u=0.012). It is also observed that the reaction rate (k_u= 0.75) at the biofilm zone is much higher than the one observed at the bulk liquid zone (k_u= 0.5). This may be attributed to the shielding effect or mass transport resistance against toxic effects on cell towards biofilm.

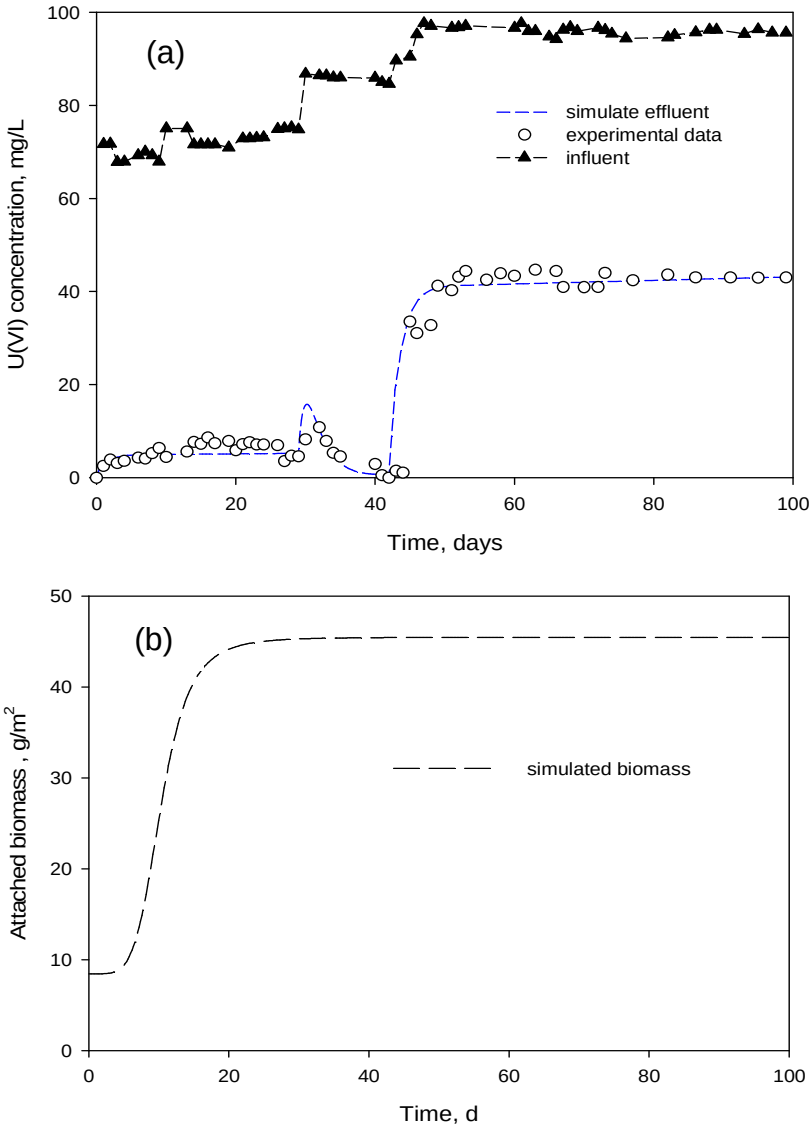

Figure 6-3: Model simulation at the solid phase of (a) U(VI) effluent (b) biomass activity in the reactor inoculated with live culture from the local environment.

Table 6-1: Summary of kinetic parameters optimized in the biofilm system and applied constraints.

Parameter Symbol	Definition	Constrains [lower, upper]	Optimum value [output]
U_{in} (mg/L)	Influent uranium concentration	--	75-100
K_u (mg/L)	Half velocity concentration	[0, 2]	0.5 1.5@ 100 mg/L
k_u (L/mg/d)	Specific reduction rate	[0, 1]	0.75
X_{fin} (mg/L)	Initial biofilm cell concentration	[40-80]	80
k_d (d/mg/m)	Cell detachment coefficient	[0-1000]	0.006
b_x (d^{-1})	Cell death rate	[0- 5]	0.0005
T_u(mg/mg)	U(VI) reduction capacity	[0- 5]	1.00
U_r (mg/L)	U(VI) toxicity threshold	--	100
Theta (%)	Porosity	--	95
rho_s (kg/m^3)	biofilm density	--	2300
Q_{in} (L/d)	Influent flow rate	--	0.00792
D_{uw} (m^2/s)	Dispersion coefficient	--	6×10^{-6}
D_{xw} (m^2/s)	Cell diffusion coefficient	--	1.108×10^{-6}
A (m^2)	Cross sectional area	--	Column properties
A_f (m^2)	Available surface area	--	Column properties

--- Constant values

6.8 Model Validation

The developed mathematical model incorporated with inhibitory conditions was evaluated for its effectiveness in simulating the fate of U(VI) in the biofilm system over time under various loading conditions. Kinetic parameters of the mathematical model were obtained by solving Equation 6-16, 6-22, 6-26, and 6-28 using a Computer Program for Solving Numerical

Problems (Octave 3.0). The validity of the developed model was tested using broader range of measured experimental data. This is known as the inverse problem approach. Table 6-1 indicates good fit between the model in Equation 6-26 and experimental data for different initial U(VI) levels with an $R^2 > 95\%$.

6.9 Biofilm Thickness Kinetics

The rate of biofilm thickness propagation is correlated to the rate at which cells and particles suspended in the bulk fluid are attached to the biofilm surface and the rate by which cells are detached from the biofilm surface area as follows:

$$\frac{dL_f}{dt} = U_L \tag{6-32}$$

where: U_L = velocity by which particular components are attached and detached from biofilm surface.

$$\frac{dL_f}{dt} = \left(\frac{1}{1-\varepsilon}\right)\frac{1}{\rho_f}\left(X_f b_x L_f\right) - \frac{1}{\rho_f}\left(\Phi(v) X_f L_f \frac{A_f}{V_f}\right) \tag{6-33}$$

$$\Phi(v) = k_d A_f \rho_f \left(\frac{v^2}{2}\right)$$

where: ρ_f = biofilm density (ML^{-3}), A_f = available biofilm surface area (L^2); V_f = volume of the biofilm (L^3), X_f = biomass density (ML^{-3}), and L_f = thickness of biofilm layer (L).

Equation 6-33 was simulated using a fourth-order Runge-Kutta routine for solution of ordinary and partial differential equations in A Computer Program for Solving Numerical Problems (Octave 3.0) (Appendix B). For numerical simulation the initial biofilm thickness was determined from the literature. Figure 6-4 shows that the thickness of the biofilm was increasing over time until a near constant growth rate was achieved in the reactor between 60-99 days. The increase in biofilm thickness is associated with the increase in cell growth/attachment while near constant biofilm thickness observed was associated to steady state conditions whereby attachment and detachment of cells occurs simultaneously in the system and roughly assumed to be equal.

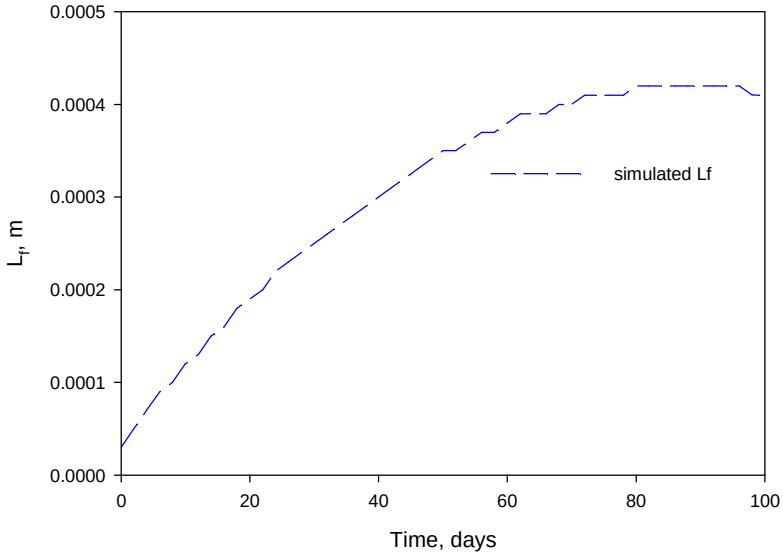

Figure 6-4: Simulation of biofilm thickness over time in the biofilm reactor

6.10 Steady-state Analysis

6.10.1 Model Formulation

To facilitate the spatial modelling of U(VI) across the column, samples were collected from equally spaced longitudinal sampling ports. The stable state condition of each experiment was observed with regard to minimal variation of U(VI) concentration in the reactor. An average effluent data from the last three sampling times with a deviation of 5% was considered as a data point for each experimental run. Generally, biological reactor systems operate under either mass transport limited or reaction rate limited kinetics. This implies that the removal of dissolved species in the biofilm is not only determined by the total amount of biomass in the reactor, but by the available surface area and the flux of the dissolved species across the mass transfer boundary layer into the biofilm. In one dimensional model where the U(VI) concentration varies only in the axial direction, the rate of mass transfer is considered to be proportional to the concentration difference between the interface and the bulk fluid. Under steady state there can be no accumulation of the component at the interface. The mass transported from the bulk liquid to the film interface moves from interface to the solid surface.

The mass balance of the dissolved species in the reactor at steady-state between segment, z+Δz, may be represented as follows:

$$F_{uz}|_{z} - F_{uz}|_{z+\Delta z} + r_u a_v (A\Delta Z) = 0 \qquad (6\text{-}34)$$

Dividing equation by AΔZ and taking the limit as AΔZ→0 we get the following:

$$\frac{1}{A}\frac{dF_{uz}}{dz} + r_u a_v = 0 \qquad (6\text{-}35)$$

Expressing F_{uz} (molar flow rate of U(VI)) in terms of concentration, thus $F_{uz} = vAU$ the equation above can be represented as follows:

$$v\frac{dU}{dz} + r_u a_v = 0 \qquad (6\text{-}36)$$

For reactions at steady state the disappearance of the dissolved species U on the surface is equal to flux of the species to the particle surface, thus $r_u = W_{ru}$

The boundary condition at external surface is:

$$r_u = W_{ru} = K_{LU}(U_B - U_{fs}) \qquad (6\text{-}37)$$

Therefore the differential equation governing the dissolved species in a biofilm system is given as:

$$v\frac{dU}{dz} = K_{LU} a_v (U_B - U_{fs}) \qquad (6\text{-}38)$$

where: K_{LU} = mass transfer coefficient (LT^{-1}), a_v = specific surface area of particle (L^2L^{-3}), v= superficial velocity (LT^{-1}).

With boundary conditions:

$U_B = U_{in}$ at z =0 (6-39)

The interfacial concentration of U(VI) across the reactor can be computed from the total mass flux term and bulk liquid concentration as follows:

$$U_{sf} = U_B - \frac{j_u}{K_{LU}} \qquad (6\text{-}40)$$

Equation 6-38 was simulated using a fourth-order Runge-Kutta routine for solution of ordinary and partial differential equations in A Computer Program for Solving Numerical Problems (Octave 3.0). Figure 6-5a-c shows that the model depicted the near constant U(VI) removal over time across the reactor at various U(VI) concentration. The near constant U(VI) concentration observed across the porous biofilm system over time at the initial concentration of 100 mg/L was mainly attributed to mass transport limitation across the biofilm layer which resulted in the system being reaction rate limited. The model simulated well the experimental data at last three sampling times under various loading conditions with an R^2 value of 96 %.

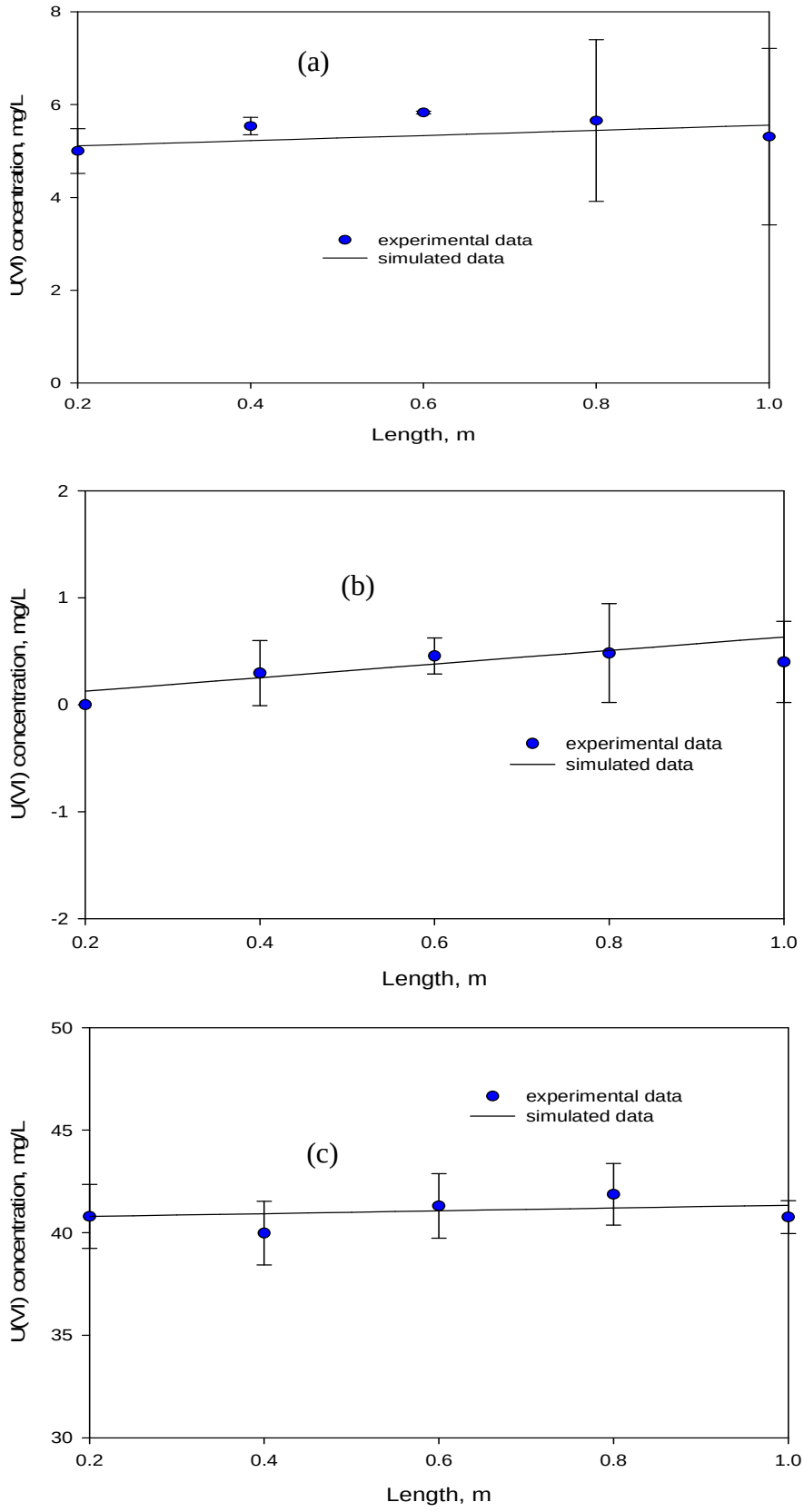

Figure 6-5: Model simulation of effluent U(VI) across the biofilm at (a) 75 mg/L, (b) 85 mg/L, and (c) 100 mg/L. Experimental data is the average effluent U(VI) concentration of the last three sampling times where near constant U(VI) removal was observed over time.

6.11 Summary of Kinetic Parameters

The diffusion-reduction equation was used to model the biofilm system under various loading conditions at transient state. Kinetic parameters initially optimised in batch systems were adjusted and applied to continuous flow system. Minor adjustments were applied to inhibition parameters due to the low level of biomass in continuous flow biofilm system. Other parameters such as the mass transport kinetic parameters were determined from physical-chemical properties related to the continuous flow column. Table 6-2 below shows the direct comparison of optimum kinetic parameters in the bulk liquid phase and the solid phase of the reactor.

Table 6-2: Comparison of kinetic parameters at the bulk and solid phase

Parameters	**Description**	**Units**	**Bulk phase [output]**	**Solid phase [output]**
b_x	Death rate coefficient	1/d	0.05	0.0005
k_u	Reaction rate coefficient	mg/L/h	0.5	0.75
K_u	Saturation coefficient	mg/L	2.5	[0.5-1.5]
T_u	Finite cell reduction capacity	mg/mg	2.5	1

Data in Table 6-2 above shows higher biological activity in the biofilm zone than in the bulk liquid zone, indicating higher bioconversion rates in the biofilm zone due to the shielding effects of transport resistance against toxic effects on cells inside the biofilm. This finding is also confirmed by the higher biomass death rate observed in the bulk zone than that observed in the biofilm zone.

The model output of biomass represents the biomass/density for each category, thus the total biomass for each category or section. Because in this study the sample for viable attached biomass was taken from only one sampling point due to oxygen stressed condition required in an operated close system, direct comparison of measured data with model data output $X_{fn}L_F$ was difficult. The model for saturated column at the steady state was determined by an ordinary differential equation as shown in Equation 6-38 which incorporated the mass transport kinetic parameters.

6.12 Summary

The numerical methods for describing bio-kinetics in an anaerobic fixed-media bioreactor were determined and validated using experimental data. Results show that the mathematical model developed in this study was capable of simulating or predicting the fate of U(VI) in the biofilm reactor under oxygen stressed and nutrient deficient conditions without any added organic carbon source. Mass transport kinetics and U(VI) removal kinetics in the biofilm reactor were represented by diffusion-reduction model. The model showed that uranium (VI) removal efficiency in the biofilm reactor was limited by mass transfer processes across the biofilm layer. The developed model predicted well U(VI) effluent concentration under various influent U(VI) concentrations in the biofilm zone with 97% confidence. Moreover, kinetics obtained from continuous flow biofilm reactor showed higher biological activity than those observed previously in batch cultures. Although the model tracked successful trends in effluent U(VI) concentration in the biofilm reactor modification of the model is still required to take into consideration the change available biofilm surface area, change in mean residence time distribution, and working volume which may occur due to accumulated precipitate in the reactor or due to biomass growth. The modification of the model could result into a proper model that can in detail predict field scale system that can aid in defective design and operation of site for clean-up.

CHAPTER 7

SUMMARY AND CONCLUSIONS

Industrial activities such as uranium ore mining and milling, nuclear power generation, radioisotope manufacturing, and other activities has resulted into a huge amount of radiotoxic waste into the environment. Because uranium and its fission products are known to be radiotoxic on living organisms treatment of U(VI) contaminated surface and sub-surface water is required. As an initiation towards addressing the problem of U(VI) contamination in the environment, experimental studies were conducted in this study in batch and continuous flow bioreactor systems using indigenous cultures from the local environment. Experimental studies on batch and suspended growth bioreactor system demonstrated U(VI) reduction efficiency under oxygen stressed conditions in the presence of glucose as sole added carbon source.

For bioremediation of subsurface water, a more practical system was demonstrated by operating an attached growth biofilm system under oxygen stressed and nutrient deficient conditions. The fate of U(VI) in the attached growth system was simulated by a developed mathematical model which was validated using the experimental data, thus inverse proportion. The following is a summary of the conclusions on both batch and continuous-flow bioreactor systems (suspended growth and attached growth system):

1. The rapid rate of U(VI) removal observed within the first few hours of incubation in both batch reactors inoculated with heat-killed cells and live-cells at initial U(VI) concentration of 100 mg/L demonstrated U(VI) removal by interaction taking place on the cell surface at near neutral pH, thus physico-chemical processes.

2. The decreased rate of U(VI) removal observed thereafter when physico-chemical processes were saturated demonstrated U(VI) reduction by enzymatic processes. This was confirmed by the insignificant U(VI) removal observed in heat-killed cultures over time.

3. The inhibitory effects observed in rotenone ($C_{23}H_{22}O_6$), and thioredoxin exposed cells further confirmed the involvement of enzymatic process in U(VI) reduction.

4. Near complete U(VI) removal was observed in batch kinetic studies at concentration up to 400 mg/L. Inhibitory effects observed at higher initial concentration of 600 mg/L after removal efficiency of 30% was achieved was associated to U(VI) toxicity to cells at higher initial U(VI) concentration.

5. The presence of nitrate which a common co-pollutant existing with uranium in the nuclear waste did not inhibit U(VI) removal efficiency in the system and also insignificant nitrate removal observed over time in the system indicated that nitrate was not a competitive electron acceptor under operating conditions of this study.

6. Mass balance analysis of uranium species aided by TEM coupled with EDX suggest that most U(VI) reduction occurred on the cell surface of the isolated species. This finding indicates the possibility of easy uranium recovery for beneficial use.

7. The performance of the cultures in reducing U(VI) in batch system at various U(VI) concentrations was well represented by pseudo-second order kinetic model with the cell deactivation term. The pseudo-second order model (Equation 4-8) fitted well the batch experimental data at various initial U(VI) concentration [100-600] with an R^2 value of 99%.

8. The continuous-flow suspended growth system demonstrated high removal efficiency than both batch and attached growth system. Higher performance of suspended growth system in effectively reducing U(VI) at higher initial concentration up to 400 mg/L was attributed to (i) high initial protein concentration, (ii) continuous purging of the reactor with N_2 which increased the anaerobic conditions in the systems and hence favour reducing conditions, and (iii) continuous addition of BMM amended with glucose which greatly enhanced U(VI) removal in the system.

9. Near complete U(VI) removal under high influent U(VI) loading of 400 mg/L in the suspended growth system was observed under low biological activity, indicating that U(VI) was not used as an electron acceptor to generate energy for cell growth, thus U(VI) was reduced at the expense of metabolic activity in cells.

10. Near complete U(VI) removal was observed in attached growth system at highest U(VI) feed concentration of 85 mg/L which is higher than the current background uranium concentration at the study site.

11. The continuous-flow suspended bioreactor system did not stabilize in various feed concentration until a quasi-steady state was achieved.

12. Mass transport kinetics and U(VI) removal kinetics in the biofilm reactor was represented by diffusion-reduction model formulated using a set of differential equations which were solved using a computer programme for solving numerical problems, Octave 3.0. The diffusion-reduction model predicted well U(VI) effluent concentrations with 97% confidence.

14. The steady state model (Equation 6-38) predicted mass transport limitation and reaction rate limitation on the biofilm surface layer over time.

CHAPTER 8

ENGINEERING SIGNIFICANCE AND RECOMMENDATIONS

8.1 Significance of the Biofilm Reactor

Biological treatment processes for U(VI) contaminated groundwater systems offer a great advantage over the currently used physical-chemical processes due to their cost effectiveness and environmentally compatibility. Among the proposed biological systems, attached growth systems are markedly known for their higher pollutant removal efficiency. U(VI) is removed from the wastewater under oxygen stressed and nutrient deficient conditions by quantitatively transforming it to U(IV), which is easily precipitated from water as an insoluble hydroxide [$UOH_{4(s)}$].

In-situ treatment of uranium contaminated groundwater may be accomplished by introducing the U(VI) reducing bacteria into aquifers through injection wells. This technology has been attempted at a field site in Rifle, Colorado using pure isolates (Anderson *et al*., 2003). Although, this study was effective for fundamental understanding of interaction taking place between the cells and the metals, the problem at this site was the need to introduce an external carbon source which stimulated the growth of non-essential species that could compete with target species for space an micronutrients and increases the risk of increasing background COD and therefore polluting the groundwater environment.

The biological treatment technology proposed in this study can be utilized for treatment of process water effluent streams and in remediation of U(VI) contaminated sites as part of a pump-and-treat bioremediation process. A model is developed to aid in the evaluation of reactor performance and to establish loading limits. The model parameters determined from the batch and continuous flow processes may be useful during scale up to the pilot stage of the study.

8.2 Future Research and Recommendations

This work represents an effort at using fixed-film bioreactors to reduce U(VI) under nutrient deficient conditions without biostimulation. Although the biological reduction processes have been considered for removal of metals in wastewater streams, the application in packed bed media and underground *in situ* barriers has been hampered by lack of means of removal of precipitated metals in the medium. During U(VI) reduction process, the U(IV) formed

hydrolyses easily into $[U(OH)_4]_{(s)}$ which tends to accumulate in the reactor or barrier system. Therefore, in order to achieve optimum application of this technology, future studies for mobilizing the uranium precipitate in the reactor by flushing the reactor with the weak organic acid such as citric acid must be conducted. Organic acids are preferred to use than inorganic acids as they produce biodegradable organic waste product which are less harmful to the environment (Gavrilescu *et al*., 2009; Huang *et al*., 1998; Joshi-Tope *et al*., 1995; Francis *et al*., 1993). Moreover, since in the actual system environmental contamination is not only limited to single element, it is important to understand how bacteria can interact with other radionuclides that co-exist with uranium in nature. Results from such studies would provide sufficient knowledge to make decisions about how to manage or remove radionuclides from the environment.

In this study the provision was made to analyse the attached microbial growth per surface area at only one end of the reactor. This was due to the difficulty or rather the impossibility of sampling for at various locations in a closed reactor system which was operated under oxygen stressed conditions. These results on attached biomass do not provide a clear indication of the overall change in attached microbial growth across the reactor for the entire reactor. Therefore, in order to circumvent such limitations in the close biofilm system, advanced experimental techniques such as micro sensors and gene probes must be applied directly within the biofilm for effective measurements of many soluble compounds such as nitrate, oxygen, and others within the biofilm and total biofilm accumulation. Experimental results from such advanced techniques will provide more details especially on biomass analysis and could be effective for validation of the developed biofilm model in a continuous flow closed system.

REFERENCES

Ajlouni, A.M.S., 2007. Health consequences of nuclear fission products. J. Appl. Sci. Environ. Manag, 11: 11-14.

Akob, D.M., Mills, H.J., Gihring, T.M., Kerkhof, L., Stucki, J.W., Anastacio, A.S., 2008. Functional diversity and electron donor dependence of microbial populations capable of U(VI) reduction in radionuclide-contaminated subsurface sediments. Appl. Environ. Microbiol, 74: 3159-3170.

Anderson, C., Pedersen, K., 2003. In situ growth of Gallionella biofilms and partitioning of lanthanides and actinides between biological material and ferric oxyhydroxides. Geobiol, 1: 169-178.

Anderson, R.T., Vrionis, H.A., Ortiz-Bernad, I., Resch, C.T., Long, P.E., Dayvault, R., Karp, K., Marutzky, S., Metzler, D.R., Peacock, A., White, D.C., Lowe, M., Lovley, D.R., 2003. Stimulating the in situ activity of Geobacter species to remove uranium from groundwater of uranium contaminated aquifer. Appl. Environ. Microbiol, 69: 5884-5891.

ATSDR (Agency for Toxic Substances and Disease Registry), 1999. US Public Health Service, Department of Health &Human Services. Toxicological Profile for Uranium, Atlanta, GA.

Aubert, C., Brugna, M., Dolla, A., Bruschi, M., Giudici-Orticoni, M.T., 2000. A sequential electron transfer from hydrogenases to cytochromes in sulphate-reducing bacteria. Biochim. Biophys. Acta, 146: 85-92.

Basmadjian, D., 2004. Mass Transfer: Principle and Applications London: CRC Press.

Beazley, M.J., Martinez, R.J., Sobecky, P.A., Webb, S.M., Taillefert, M., 2007. Uranium bioremineralization as a result of bacterial phosphate activity: Insights from bacterial isolates from a contaminated subsurface. Environ. Sci. Technol, 41: 5701-5707.

Bencheikh-Latmani, R., Williams, S.M., Haucke, L., Criddle, C.S., Wu, L., 2005. Global transcriptional profiling of *Shewanella oneidensis* MR-1 during Cr(VI) and U(VI) reduction. Appl. Environ. Microbiol, 71: 7453-7460.

Bhatti, T.M., Mateen, A., Amin, M., Malik, K.A., Khalid, A.M., 1991. Spectrophotometric determination of uranium (VI) in bacterial leach liquors using arsenazo-III. Chem. Technol. Biotech, 52: 331-341.

Bleise, A., Danesi, P.R., Burkart, W., 2003. Properties, use and health effects of depleted uranium (DU): A general overview. Environ. Radio, 64: 93-112.

Boonchayaanant, B., Nayak, D., Du, X., Criddle, C.S., 2009. Uranium reduction and resistance to re-oxidation under iron reducing and sulfate-reducing conditions. Water Research, 43: 4652-4664.

Brodie, E.L., DeSantis, T.Z., Joyner, D.C., Baek, S.M., Larsen, J.J., Andersen, G.L., Hazen, T.C., Richardson, P.M., Herman, D.J., Tukunaga, T.K., Wan, J.M., Firestone, M.K., 2006. Application of high-density oligonucleotide microarray approach to study bacterial population dynamics during uranium reduction and reoxidation. Appl. Envir. Microbiol, 72: 6288-6298.

Bush, M.B., 2003. Ecology of a Changing Planet, third ed. Prentice Hall, New Jersey, USA.

Chabalala, S., Chirwa, E.M.N., 2010. Uranium(VI) reduction and removal by high performing purified anaerobic cultures from mine soil. Chemosphere, 78(1): 52-55.

Chabalala, S., Chirwa, E.M.N., 2011. Uranium (VI) reduction under facultative anaerobic conditions. Proc. 84th Annual Water Environment Federation Technical Exhibition and Conference (WEFTEC), Los Angeles, California, USA, pp. 6565-6573.

Chen, J.P., 1997. Batch and continuous adsorption of strontium by plant root tissues. Bioresource Technol, 60: 185-189.

Chirwa, E.M.N., Wang, Y.T., 2005. Modeling Cr(VI) reduction and phenol degradation in a coculture biofilm reactor. ASCE J. of Environ. Eng, 131(11): 1495-1506.

Chirwa, E.M.N., 2011. Developments in bioremediation for separation/recovery, in: Nash, K.L., Lumetta, G.J. (Eds.), In Advanced Separation Techniques for Nuclear Fuel Reprocessing and Radioactive Waste Treatment. Woodhead Publishing, Cambridge, UK, pp. 436-472.

Chirwa, E.M.N., Wang, Y.T., 2000. Simultaneous Cr(VI) reduction and phenol degradation in an anaerobic consortium of bacteria. Water Research, 34(8): 2376-2384.

Choudhary, S., Sar, P., 2009. Characterization of a metal resistant *Pseudomonas* sp. isolated from uranium mine for its potential in heavy metal (Ni^{2+}, Co^{2+}, Cu^{2+}, and Cd^{2+}) sequestration. Bioresource Technol, 100(9): 2482-2492.

Choudhary, S., Sar, P., 2011. Uranium biominerilization by resistant *Pseudomonas aeruginosa* strain isolated from contaminated mine waste. J. Hazard. Mater, 186: 336–343.

Choy, C.C., Korfiatis, G.P., Meng, X., 2006. Removal of depleted uranium from contaminated soils. J. Hazard. Mater, 136: 53–60.

Coates, J.D., Bhupathiraju, V.K., Achenbach, L.A., McInerney, M.J., Lovley, D.R., 2001. *Geobacter hydrogenophilus* and *Geobacter chapellei* and *Geobacter grbiciae*, three new, strictly anaerobic, dissimilatrory Fe(III)-reducers. International Journal of Systematic and Evolutionary Microbiology, 51(2): 581-588.

Comte, S., Guidbaud, G., Baudu, M., 2008. Biosorption properties of extracellular polymeric substances (EPS) towards Cd, Cu, and Pb for different pH values. J. Hazard. Mater, 151: 185-193.

Craig, D.K., 2001. Chemical and Radiological Toxicity of Uranium and its Compounds, Report WSRC-TR-2001-00331, Contract No. DE-AC09-96SR18500, Westinghouse Savannah River Company, Aiken/U.S. Department of Energy.

Cussler, E.L., 2003. Diffusion: Mass Transfer in fluid systems, 2nd ed. Cambridge University, Press.

DiChristina, T.J., Fredrickson, J.M., Zachara, J.M., 2005. Enzymology of Electron Transport: Energy Generation with Geochemical Consequences. Rev. Mineral. and Geochem, 59: 27-52.

DiChristina, T.J., 1992. Effects of nitrate and nitrite on dissimilatory iron reduction by *Shewanella putrefaciens* 200. J. Bacteriol, 174: 1891-1896.

Doherty, R., Phillips, D.H., McGeough, K.L., Walsh, K.P., Kalin, R.M., 2006. Development of modified flyash as a permeable reactive barrier medium for a former manufactured gas plant site. Northern Ireland. Environ. Geol, 50: 37-46.

Elias, D.A, Suflita, J.M., McInerney, M.J., Krumholz, L.R., 2004. Periplasmic cytochrome c3 of *Desulfovibrio vulgaris* is directly involved in H_2-mediated metal but not sulfate reduction. Appl. Environ. Microbiol, 70(1): 413-420.

Elwakeel, K.Z., El-Sadik, H.A., Abdel-Razek , A.S., Beheary, M.S., 2011. Environmental remediation of thorium(IV) from aqueous medium onto *Cellulosimicrobium cellulans* isolated from radioactive wastewater. Desalination and Water Treatment, 46: 1-9.

Fowle, D.A., Fein, J.B., Martin, A.M., 2000. Experimental study of uranyl adsorption onto *Bacillus subtilis*. Environ. Sci. Technol, 34: 3737-3741.

Francis, A.J., Dodge, C.J., Gillow, J.B., Halada, G.P., Honeyman, B.D., 2004. Reductive precipitation and stabilization of uranium complexed with organic ligands by anaerobic bacteria. DOE-NABIR PI Workshop, 12 (Abstr.)

Francis, A.J., 1998. Biotransformation of uranium and other actinides in radioactive wastes. J. Alloys and Compounds, 271-273: 78-84.

Francis, A.J., Dodge, C.J., Lu, F., Halada, G.P., Clayton, C.R., 1994. XPS and XANES studies of uranium reduction by Clostridium sp. Environ. Sci. Technol, 28: 636-639.

Francis, C.W., Mattus, A.J, Elless, M.P.,Timpson, M.E., 1993. Carbonate and citrate based selective leaching of uranium from uranium-contaminated soils, in: Removal of Uranium from Uranium-Contaminated Soils, Phase I: Bench-Scale Testing, ORNL-6762, Oak Ridge National Laboratory, Oak Ridge, TN.

Frossling, N., 1938. Of [Over] the volatilization of falling drops. (German). Gerlands Beitréage Geophysik, 52: 170-216.

Gavrilescu, M., 2006. Overview of in situ remediation technologies for sites and groundwater. J. Environ. Eng. Manag, 5(1): 79-114.

Gavrilescu, M., Pavel, L.V., Cretescu, I., 2009. Characterization and remediation of soils contaminated with uranium. J. Hazard. Mater, 163: 475-510.

Geissler, A., Selenska-Pobells, S., Morris, K., Burke, I.T., Livens, F.R., Lloyd, J.R., 2010. The microbial ecology of land and water contaminated with radioactive waste: towards the development of bioremediation options for the nuclear industry, in: Batty, L.C., Hallberg, K.B. (Eds.), Ecology of Industrial Pollution. Cambridge University Press, British Ecological Society, pp. 226.

Ginder-Vogel, M., Fendorf, S., 2008. Biogeochemical uranium redox transformation: Potential oxidants of uraninite. In *Adsorption of Metals by Geomedia II: Variables, Mechanisms, and Model Applications*; Barnett, M.O., Kent, D.B., (Eds.) Elsevier: Amsterdam, The Netherlands,Vol. 7, pp. 293-320.

Glauert, A.M., 1975. Fixation, dehydration and embedding of biological specimens, in: Glauert, A.M. (Ed.), Practical Methods in Electron Microscopy. North-Holland Biomedical Press, Amsterdam, pp.1-201.

Gorby, Y.A., Lovley, D.R., 1992. Enzymatic uranium precipitation. Environ. Sci. Technol, 26(1): 205-207.

Gramss, G., Voight, K.D., Bergmann, H., 2004. Plant availability and leaching of heavy metals from ammonium-calcium, carbohydrate, and citric acid-treated uranium-mine-dump soil. J. Plant Nutrition and Soil Sci, 167: 417-427.

Hayat, M.A., 1981. Principles and techniques of electron microscopy. Biological Applications, Vol 1. University Park Press, Baltimore.

Huang, F.Y.C., Brady, P.V., Lindgren, E.R., Guerra, P., 1998. Biodegradation of uranium citrate complexes: implications for extraction of uranium from soils. Environ. Sci. Technol, 32: 379-382.

IAEA, 2011. International Status and Prospects of Nuclear Power, Report by the Director General, Board of Governors General Conference, 2010 Edition, IAEA, Vienna, Austria.

IAEA, 2009. Nuclear Technology Review. International Atomic Energy Agency Scientific and Technical Publication Series, Vienna, Austria.

IAEA, 2002. Status of design concepts of nuclear desalination plants, IAEA-TEC DOC-1326.

Incropera, F.P., 2011. Fundamentals of heat and mass transfer, Wiley.

Istok, J.D., Senko, J.M., Krumholz, L.R., Watson, D., Bogle, M.A., Peacock, A., Chang, Y.J., White, D.C., 2004. In situ bioreduction of Technetium and Uranium in a nitrate-contaminated Aquifer. Environ. Sci. and Technol, 38(2): 468–475.

Joeng, B.C., Hawes, C., Bonthrone, K.M., Macaskie, L.E., 1997. Localization of enzymatically enhanced heavy metal accumulation by *Citrobacter sp*. and metal accumulation in vitro by liposome containing entrapped enzyme. Microbiol, 143: 2497-2507.

Joshi-Tope, G., Francis, A.J., 1995. Mechanism of biodegradation of metal–citrate complexes by *Pseudomonas fluorescens*. J. Bacteriol, 177: 1989-1993.

Jroundi, F., Merroun, M.L., Arias, J.M., Rossberg, A., Selenska-Pobell, S., González-Muñoz, M.T., 2007. Spectroscopic and microscopic characterization of uranium biomineralization in *Myxococcus xanthus*. J. Geomicrobiol, 24(5): 441-449.

Jukes, T.H., Cantor, C.R., 1969. Evolution of protein molecules, in: Munro, H.N. (Ed.), Mammalian Protein Metabolism. Academic Press, New York, pp. 21-123.

Kantar, B., Honeyman, B.D., 2006. Citric acid enhanced remediation of soil contaminated with uranium by soil flushing and soil washing. J. Environ. Eng, 132(2): 247-255.

Kazy, S.K., D'Souza, S.F., Sar, P., 2009. Uranium and Thorium sequestration by Pseudomonas sp.: mechanism and chemical characterization. J. Hazard. Mater, 163: 65-72.

Kennedy, D.W., Marshall, M.J., Dohnalkova, A.C., Saffarini, D.A., Culley, D.E., 2004. Role of *Shewanella oneidensis c*-type cytochromes in uranium reduction and localization. ASM 105th Gen. Meet. Q-389 (Abstr.).

Kermani, M., Bira, B., Movahedian, H., Amin, M.M., 2008. Application of moving bed biofilm process for biological organics and nutrients removal from municipal wastewater. American J of Environ. Sci, 4: 675-682.

Khijniak, T.V., Slobodkin, A.I., Coker, V., Renshaw, J.C., Livens, F.R., 2005. Reduction of uranium(VI) phosphate during growth of the thermophilic bacterium *Thermoterrabacterium ferrireducens*. Appl. Environ. Microbiol, 71: 6423–6426.

Khripunov, V.I., Kurbatov, D.K., Subbotin, M.L., 2006. C-14 Production in CTR Materials and Blankets. Proceedings of the 21st Fusion Energy Conference (FEC2006), 16-21 October 2006, Chengdu, China. SE/p2-3. Available online at *http://www-pub.iaea.org/MTCD/Meetings/FEC2006/se_ p2-3.pdf*. Last accessed on 28/04/15, 22:00.

Kjelleberg, S., Hermanson, M., 1984. Starvation-induced effects on bacterial surface characteristics. Appl. Environ. Microbiol, 48 (3): 497-503.

Koster, A., Matzner, H.D., Nicholsi, D.R., 2003. PBMR design for the future. Nuclear Engineering and Design, 222(2-3): 231-245.

Kratochvil, D., Volesky, B., 1998. Advances in the biosorption of heavy metals. Trends in Biotechnol, 16(7): 291-300.

Li, X., Krumholz, L.R., 2009. Thioredoxin is involved in U(VI) and Cr(VI) reduction in *Desulfovibrio desulfuricans* G20. J. Bacteriol, 191: 4924-4933.

Lior, N., 2008. Energy resources and use: The present situation and possible paths to the future. Energy, 33(6): 842-857.

Liu, C., Zachara, J.M., Fredrickson, J.K., Kennedy, D.W., Dohnalkova, A., 2002. Modeling the inhibition of the bacterial reduction of U(VI) by MnO_2(s). Environ. Sci. Technol, 36: 1452–1459.

Lloyd, J.R., Leang, C., Hodges-Myerson, A.L., Coppi, M.V., Cuifo, S., 2003. Biochemical and genetic characterization of PpcA, a periplasmic *c*-type cytochrome in *Geobacter sulfurreducens*. J. Biochem, 369(1): 153-161.

Lloyd, J.R., 2003. Microbial reduction of metals and radionuclides. FEMS Microbiol. Rev, 27: 411-425.

Lloyd, J.R., Chesnes, J., Glasauer, S., Bunker, D.J., Livens, F.R., Lovley, D.R., 2002. Reduction of actinides and fission products by Fe(III)-reducing bacteria. J. Geomicrobiol, 19: 103-120.

Lopez, C.V.G., Garcia, M.delC.C, Fernandez, F.G.A., Bustos, C.S., Chisti, Y., Sevilla, J.M.F., 2010. Protein measurements of microalgal and cyanobacterial biomass. Bioresource Tech, 101(19): 7587-7591

Lovley, D.R., Phillips, E.J.P., Gorby, Y.A., Landa, E.R., 1991. Microbial reduction of uranium. Nature (London), 350: 413-416.

Lovley, D.R., Phillips, E.J.P., 1992. Reduction of uranium by *Desulfovibrio desulfuricans*. Appl. Environ. Microbiol, 58: 850-856.

Lovley, D.R., Widman, P.K., Woodward, J.C., Phillips, E.J.P., 1993. Reduction of uranium by cytochrome c3 of *Desulfovibrio vulgaris*. Appl. Environ. Microbiol, 59: 3572-3576.

Luo, J., Weber, F., Cirpka, O.A., Wu, W., Nyman, J.L., Carley, J., Jardine, P.M., Criddle, C.S., Kitanidis, P.K., 2007. Modeling in-situ uranium(VI) bioreduction by sulfate-reducing bacteria. J. contam. hydrol, 92(1–2): 129-148.

Macaskie, L.E., Bonthrone, K.M., Yong, P., Goddard, D.T., 2000. Enzymically mediated bioprecipitation of uranium by a Citrobacter *sp*.: a concerted role for extracellular lipopolysaccharide and associated phosphatase in biomineral formation. Microbiol, 146: 1855-1867.

Macaskie, L.E., Jeong, B.C., Tolley, M.R., 1994. Enzymatically accelerated biomineralization of heavy-metals: application to the removal of americium and plutonium from aqueous flows. FEMS Microbiol. Rev, 14: 351–367.

Macaskie, L.E., Empson, R.M., Cheetham, A.K., Grey, C.P., Skarnulis, A.J., 1992. Uranium accumulation by a *Citrobacter* sp. As a result of enzyme mediated growth of polycrystalline HUO_2PO_4. Science, 257: 782-784.

Madden, A.S., Smith, A.C., Balkwill, D.L., Fagan, L.A., Phelps, T.J., 2007. Microbial uranium immobilization independent of nitrate reduction. Environ. Microbiol, 9(9): 2321-2330.

Martins, M., Faleiro, M.L., Rosa da Costa, A.M., Chaves, S., Tenreiro, R., Matos, A.P., Costa,.M.C., 2010. Mechanism of U(VI) removal by two anaerobic bacterial communities. J. Hazard Mater, 184: 89-96.

Martins, M., Faleiro, M.L., Barros, R.J., Verıssimo, A.R., Barreiros, M.A., Costa,.M.C., 2009. Characterization and activity studies of highly heavy metal resistant sulphate-reducing bacteria to be used in acid mine drainage treatment. J. Hazard. Mater, 166: 706-713.

Mathews, E.P., 1986. Biological techniques for electron microscopy: a lab manual. Stockton, California.

McConnell, M.W., 2012. “Enhancement of NRC station blackout requirements for nuclear power plants”, Int. Congress on Advances in Nuclear Power Plants 2012, ICAPP 2012, 2, 1438-1442.International Atomic Energy Agency, 2002, “Status of design concepts of nuclear desalination plants”, IAEA-TECDOC-1326.

McLean, J., Beveridge, T.J., 2001. Chromate reduction by a pseudomonad isolated from a site contaminated with chromated copper arsenate. Appl. Environ. Microbiol, 67: 1076-1084.

Meadows, P. S., 1971. The attachment of bacteria to solid surfaces. *Archiv fur Mikrobiologie*, 75(4): 374-381.

Merroun, L.M., Selenska-Pobell, S., 2008. Bacterial interactions with uranium: An environmental perspective. J. Contam. Hydrol, 102: 285-295.

Merroun, M.L., Nedelkova, M., Rossberg, A., Henning, C., Solenska-Pobell, 2006. Interaction mechanisms of bacterial strains isolated from extreme habitats with uranium. Radiochim. Acta, 94: 723-729.

Merroun, M.L., Henning, C., Rossberg, A., Rech, T., Selenska-Pobell, S., 2003. Characterization of U(VI)-Acidithiobacillus ferrooxidans complexes by using EXAFS, transmission electron microscopy and energy-dispersive X-ray analysis. Radiochim Acta, 91: 583-591.

Moller, S., Sternberg, C., Andersen, J.B., 1998. In situ *g*ene expression in mixed-culture biofilms: *evidence of metabolic interactions between community members*. Appl. Environ. Microbiol, 64: 721–732.

Mtimunye, P.J., Chirwa, E.M.N., 2013. Bioremediation of radiotoxic elements under natural environmental conditions. In: Patil, Y.B. and Rao, P., (Eds). *Applied Bioremediation-Active and Passive Approaches*, InTech Open Publishers Chapter 8, pp. 177-206.

Mtimunye P.J., Chirwa, E.M.N., 2014. Characterization of the Biochemical Pathways of Uranium (VI) Reduction in Facultative Cultures. Chemosphere, 113:22-29.

Mtimunye P.J., Chirwa E.M.N., 2014. Finite difference simulation of biological chromium (VI) reduction in aquifer media columns. Water SA, 40(2): 359-368.

Musango, J.K., Brent, A.C., Bassi, A., 2009. South African Energy Model: a systems dynamics approach. Conference Proceedings of the 27th International Conference of the System Dynamics Society, July 26-30, 2009, New Mexico, USA.

Myers, C.R., Myers, J.M., 1992. Localization of cytochromes to the outer membrane of anaerobically grown Shewanella putrefaciens MR-1. J. Bacteriol, 174: 3429-38.

Nakajima, A., Tsuruta, T., 2004. Competitive biosorption of thorium and uranium by *Micrococcus luteus*. J. of Radioanalytical and Nuclear Chemistry, 260(1): 13-18.

Nancharaiah, Y.V., Joshi, H.M., Mohan, T.V.K., Venugopalan, V.P., Narasimhan, S.V., 2006. Aerobic granular biomass: a novel biomaterial for efficient uranium removal. Curr. Sci, 91: 503-509.

Nealson, K.H., 1999. Post-Viking microbiology: new approaches, new data, new insights. Origins of life and evolution of the biosphere. Journal of the International Society for the Study of the Origin of Life, 29(1): 73-93.

Nedelkova, M., Merroun, M.L., Rossberg, A., Hennig, C., Selenska-Pobell, S., 2007. Microbacterium isolates from the vicinity of a radioactive waste depository and their interactions with uranium. FEMS Microbiol. Ecol, 59(3): 694-705.

Nilanjana, D., Vimala, R., Karthika, P., 2008. Biosorption of heavy metals- An Overview. Indian J. Biotech, 7: 159-169.

Ngwenya, N., 2011. Bioremediation of metallic fission products in nuclear waste: biosorption and bio-recovery, PhD thesis, University of Pretoria, URL:http://upetd.up.ac.za/thesis/available/etd-10-122011-151728.

Nkalambayausi-Chirwa, E.M.,Wang, Y.T., 2001, Simultaneous chromium(VI) reduction and phenol degradation in a fixed-film coculture bioreactor: reactor performance. Water Research, 35(8): 1921-1932.

Nyman, J.L., Marsh, T.L., Ginder-Vogel, M.A., Gentile, M., Fendorf, S., Criddle, C.S., 2006. Heterogeneous response to biostimulation for U(VI) reduction in replicated sediment microcosms. Biodegradation, 17: 303-316.

Obuekwe, C., Westlake, D.W., 1982. Effects of medium composition on cell pigmentation, cytochrome content and ferric iron reduction in a Pseudomonas sp. isolated from crude oil. Canadian J. of Microbiol, 28: 989-992.

Olexsey, R.A., Parker, R.A., 2006. Current and future *in situ* treatment techniques for the remediation of hazardous substances in soil, sediments, and groundwater I. Twardowska, H.E. Allen, M.M. Häggblom, S. Stefaniak (Eds.), Soil and Water Pollution Monitoring, Protection and Remediation, NATO Science Series, IV. Earth and Environmental Science, Springer, Netherlands, 69, 211-219.

Ondrejcin, R.S., Garrett, JR., T.P., 1961. The thermal decomposition of anhydrous uranyl nitrate and uranyl nitrate dihydrate. Savannah River Laboratory, E. I. du Pont de Nemours & Go., Aiken, South Carolin,Vol. 65, pp 470-473.

Pabby, A.K., Rizvi, S.S.H., Sastre, A.M., 2008. Membrane techniques for treatment in nuclear waste processing, a global experience. Membrane Technology, 11: 9-13.

Pagnanelli, F., Peterangelipapin, M., Toro, I.L., Trifoni, M., Veglio, F., 2000. Biosorption of Metal Ions on Anthrobacter sp.: biomass characterization and biosorption modeling. Environ. Sci. Tech, 34: 2773-2778.

Palacious, M.L., Taylor, S.H., Stuart, H., 2000. Characterization of uranium oxides using in situ micro-Raman spectroscopy. Appl. Spectrosc, 54: 1372-1378.

Paul, J.H., 1984. Effects of antimetabolites on the adhesion of an estuarine Vibrio sp. to polystyrene. Appl. Environ. Microbiol, 48 (5): 924-929.

Phillips, E.J.P., Landa, E.R., Lovley, D.R., 1995. Remediation of uranium contaminated soils with bicarbonate extraction and microbial U(VI) reduction. J. of Ind. Microbiol, 14(3-4): 203-207.

Poullikkas, A., 2013. An overview of Future Sustainable Nuclear Power Reactors. International J of Energy and Envir, 4(5): 743-776

Qiu, G., Li, Q., Yu, R., Sun, Z., Liu, Y., Chen, M., Yin, H., Zhang, Y., Liang, Y., Xu, L., Sun, L., Liu, X., 2011. Column bioleaching of uranium embedded in granite porphyry by a mesophilic acidophilic consortium. Bioresour, 102: 4697-4702.

Rao, KM., Srinivasan, T, Venkateswarlu, Ch., 2010. Mathematical and kinetic modelling of biofilm reactor based on ant colony optimization. Proc. Biochem, 45: 961-972.

Reed, D.T., Pepper, S.E., Richmann, M.K., Smith, G., Deo, R., Rittmann, B.E., 2007. Subsurface bio-mediated reduction of higher valent uranium and plutonium. J. Alloys Comp, 444-445: 376-382.

Reichert, P., 1998. Swiss Federal Institute for Environmental Science and Technology (EAWAG), Switzerland, ISBN: 3-906484-16-5.

Renshaw, J.C., Lloyd, J.R., Livens, F.R., 2007. Microbial interactions with actinides and long-lived fission products. Comptes Rendus Chimie, 10:1067–1077.

Renshaw, J.C., Butchins, L.J.C., Livens, F.R., May, I., Charnock, J.M., Lloyd, J.R., 2005. Bioreduction of uranium: environmental implications of a pentavalent intermediate. Environ. Sci. Technol, 39: 5657–5660.

Rittman, B.E., McCarty, P.L., 2001. Environmental biotechnology: Principles and applications. New York: McGraw Hill, pp. 754.

Rittman, B.E., Davantzis, 1983. Dual limitation of biofilm kinetics. Water Reseach, 17(12): 1721-1724.

Roh, Y., Liu, S.V., Li, G., Huang, H., Phelps, T.J., Zhou, J., 2002. Isolation and characterization of metal-reducing *Thermoanaerobacter* strains from deep subsurface environments of the Piceance Basin, Colorado. Appl. Environ. Microbiol, 68: 6013–6020.

Rollin-Genetet, F., Berthomieu, C., Davin, A.H., Quemeneur, E., 2004. *Escherichia coli* thioredoxin inhibition by cadmium: two mutually exclusive binding sites involving Cys32 and Asp26. Eur. J. Biochem, 271:1299-1309.

Roslev, P., Madsen, P.L., Thyme, J.B., Henriksen, K., 1998. Degradation of phthalate and di-(2-ethylhexyl) phthalate by indigenous and inoculated microorganisms in sludge-amended soil. Appl. Environ. Microbiol, 64: 4711-4719.

Sani, R.K., Peyton, B.M., Dohnalkova, A., 2004. Effect of uranium (VI) on *Desulfovibrio desulfuricans* G20: influence of soil minerals. ASM 104th Gen. Meet. Q-007 (Abstr.).

Sar, P., D'Souza, S.F., 2002. Biosorption of thorium (IV) by a Pseudomonas strain. Biotechnology Letters, 24(3): 239-243.

Sawyer, C.N., McCarthy, P.L., Parkin, G.F., 2003. Chemistry for Environmental Engineering, fifth edition, McGraw-Hill, New York, NY, 410-451.

Senanayake, R., Rousseau, D., Colegrave, H., Idriss, H., 2005. The reaction of water on polycrystalline UO2: Pathways to surface and bulk oxidation. J. Nucl. Mater, 342: 179-187.

Shelobolina, E.S., Sullivan, S.A., O'Neill, K.R., Nevin, K.P., Lovley, D.R., 2004. Isolation, characterization, and U(VI)-reducing potential of a facultative anaerobic, acid-resistant bacterium from low-pH, nitrate- and U(VI)-contaminated subsurface sediment and description of *Salmonella subterranea sp*. nov. Appl. Environ. Microbiol, 70: 2959-2965.

Shen, H., Wang, Y.T., 1993. Characterization of enzymatic reduction of hexavalent chromium by Escherichia coli ATCC 33456. Appl. Environ. Microbiol, 59: 3771-3777.

Shen, H., Wang, Y. T., 1994. Modeling hexavalent chromium reduction in Escherichia coli ATCC 33456. Biotech. and Bioeng, 43: 293-300.

Sherwood, T.K., Pigford, R.L., Wilke, C.R., 1975. Mass transfer, New York McGraw-Hill.

Shrivastava, A., Sharma, J., Soni, V., 2013. Various electroanalytical methods for the determination of uranium in different matrices. Bulletin of Faculty of Pharmacy, Cairo University Rev, 51: 113-129.

Singh, S., Eapen, S., Thorat, V., Kaushik, C.P., Raj, K., D'Souza, S.F., 2008. Phytoremediation of cesium-137 and strontium-90 from solutions and low-level nuclear waste by Vetiveria zizanoides. Ecotoxicology and Environmental Safety, 69: 306-311.

Sivaswamy, V., Boyanov, M.I., Peyton, B.M., Viamajala, S., Gerlach, R., Apel, W.A., Sani, R.K. Dohnalkova, A., Kemner, K.M., Borch, T., 2011. Multiple mechanisms of uranium immobilization by *Cellulomonas sp*. Strain ES6. Biotechnol. Bioeng, 108: 264-276.

Soudek, P., Valenova, S., Vavrikova, Z., Vanek, T., 2006. Study of radio-phyto-remediation on heavily polluted area in South Bohemia. J. Environ. Radio, 88: 236-250.

Sovacool, B.K., 2008. Valuing the Greenhouse Gas Emissions from nuclear Power: Acritical Survey. Energy Policy 36, Elsevier.

Spear, J.R., Figueroa, L.A., Honeyman, B.D., 2000. Modeling reduction of uranium U(VI) under variable sulfate concentrations by sulfate-reducing bacteria. Appl. Environ. Microbiol, 66: 3711–3721.

Srinath, T., Verma, T., Ramteke, P.W., Garg, S.K., 2002. Chromium (VI) biosorption and bioaccumulation by chromate resistant bacteria. Chemosphere, 48: 427–435.

Stefaniak, EA., Alsecz, A., Frost, R., Mathe, Z., Sajo, I.E., Torok, S., Worobiec, A., Grieken, R.V., 2009. Combined SEM/EDX and micro-Raman spectroscopy analysis of uranium minerals from a former uranium mine, Hazard Mater, 168: 416-423.

Suzuki, Y., Banfield, J., 2004. Resistance to, and accumulation of, uranium by bacteria from a uranium-contaminated site. J. Geomicrobiol, 21:113-121.

Suzuki, Y., Kelly, S.D., Kemner, K.M., Banfield, J.F., 2004. Enzymatic U(VI) reduction by *Desulfosporosinus* species. Radiochim. Acta, 92: 11-16.

Thijs, I., Diels, L., Maes, N., Vandenhove, H., Jacques, D., Smolders, E., Mallants, D., 2004. Laboratory testing of uranium removal efficiency of reactive media used in groundwater remediation, Geophys. Res. Abs. 6:P0259.

Tikilili, P.V., Chirwa, E.M.N., 2011. Characterization and Biodegradation of Polycyclic Aromatic Hydrocarbons in Radioactive Wastewater. J. Hazard. Mater, 192: 1589-1596.

Todorov, P.T., Ilieva, E.N., 2006. Contamination with uranium from natural and anthropological sources. Rom. J. Phys, 51:27–34.

Tudiver, S., 2009. Greenhouse Gas Emissions from Nuclear Power in 2030: Examining Emissions Estimates and Projected Growth. Yale Journal of International Affairs, 100-111.

U.S. (NAS), (1974). Geochemistry and the environment. Washington DC. U.S. Government Printing Office.

UNSCEAR (United Nations Scientific Committee on the Effects of Atomic Radiation), 1999. The report to the General Assembly with scientific annexes. New York.

Valls, M., deLorenzo, V., 2002. Exploiting the genetic and biochemical capacities of bacteria for the remediation of heavy metal pollution. FEMS Microbiol. Rev, 26(4): 327-338.

Van Lam, P., Van Ngoc, O., Thinang, N., 2000. Safe operation of existing radioactive waste management facilities at Dalat Nuclear Research Institution. In Proceedings of the International Conference on the Safety of Radioactive Waste Management, 13-17 March 2000, Córdoba, Spain, pp. 152-154.

Van Roy, S., Peys, K., Dresselaers, T., Diels, L., 1997. The use of an Alccaligenes euthropus biofilm in a membrane bioreactor for heavy metals recovery. Res. Microbiol, 148: 526-528.

Viamajala, S., Peyton, B.M., Petersen, J.N., 2003. Modeling chromate reduction in *Shewanella oneidensis* MR- 1: Development of a novel dual-enzyme kinetic model. Biotech. Bioeng, 83: 790-797.

Vehovszky, A., Szabo, H., Acs, A., Gyori J., Farkas, A., 2010. Effects of rotenone and other mitochrondrial complex I inhibitors on the brine shrimp Artemia. Acta Biol. Hung, 61(4): 401-410.

Wade Jr., R., DiChristina, T.J., 2000. Isolation of U(VI) reduction-deficient mutants of Shewanella putrefaciens. FEMS Microbiol. Lett, 184: 143-248.

Wall, J.D., Krumholz, L.R., 2006. Uranium reduction. Ann. Rev. Microbiol, 60:149-166.

Wang, Y.T., Shen, H., 1997. Modelling Cr(VI) reduction by pure bacterial cultures. Water Research, 41(4): 727-732.

Wanner, O., Cunningham, A.B., Lundman, R., 1995. “Modeling biofilm accumulation and mass transport in a porous medium under high substrate loading.” Biotech. and Bioeng, 47(6): 703-712.

WHO 2001. Depleted Uranium, Sources, Exposure and Health Effects. WHO, Geneva.

Wilke, C.R., Cheng, P.I.N., 1955. Correlation of diffusion coefficients in dilute solutions. A.I.Ch.E Journal, 264-270.

Winde, F., 2010. Uranium pollution of the Wonderfonteinspruit 1997- 2008 Part 1: Uranium toxicity, regional background and mining - related sources of uranium pollution. Water SA, 36(3): 239-256.

Woolfolk, C.A., Whiteley, H.R., 1962. Reduction of inorganic compouds with molecular hydrogen by Micrococcus lactilyticus. I. Stoichiometry with compounds of arsenic, selium, tellurium, transitions and other elements. J. Bacteriol, 84: 647-658.

World Nuclear Association (WNA), 2008. http://www.world-nuclear.org/info/inf88.html (accessed 7 January 2015).

Wu, Q., Sanford, R.A., Löffler, F.E., 2006. Uranium reduction by Anaeromyxobacter dehalogenans strain 2CP-C. Appl. Environ. Microbiol, 72(5): 3608-3614.

Xie, S., Yang, J., Chen, C., Zhang, X., Wang, Q, Zhang, C., 2008. Study on biosorption kinetics and thermodynamic of uranium by Citrobacter freudii. J. Environ. Radioactivity, 99: 126-133

Zaganiaris, E.J., 2009. Ion Exchange Resins in Uranium Hydrometallurgy, Books on Demand GmbH, Paris, France.

Zeller, T., Klug, G., 2006. Thioredoxins in bacteria: functions in oxidative stress response and regulation of thioredoxin genes. Naturwissenschaften Rev, 93: 259-266.

Zhou, P., Gu, P., 2005. Extraction of oxidized and reduced forms of uranium from contaminated soils: effects of carbonate concentration and pH. Environ. Sci. Technol, 39(12): 4435-4440.

APPENDIX A

PROTEIN ANALYSIS STANDARD CURVE

****

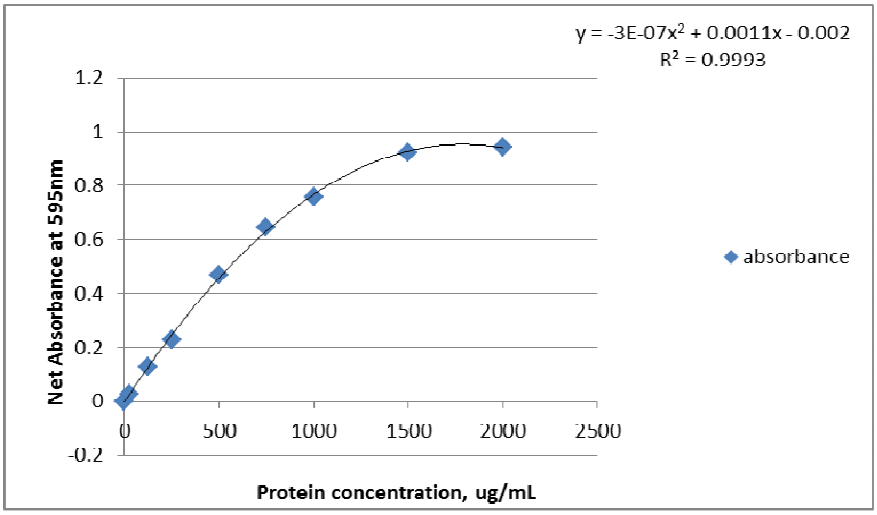

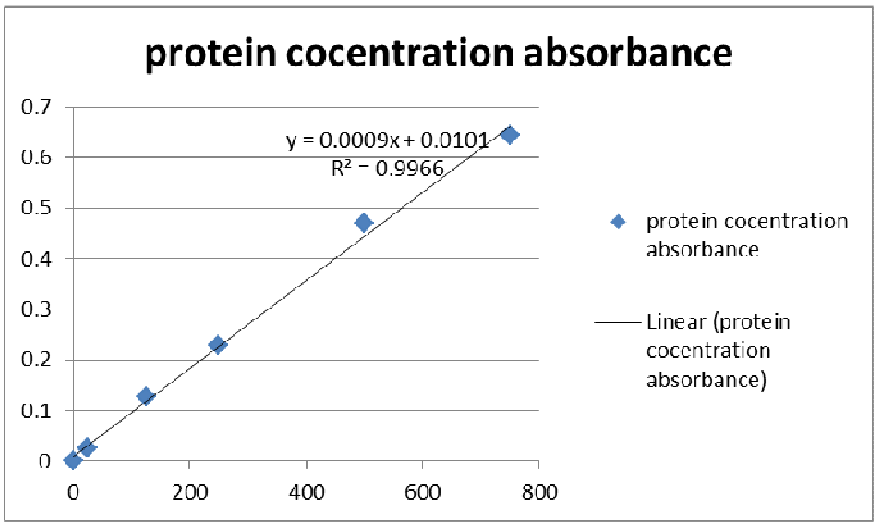

APPENDIX B

Octave Version 3.0

****

In[49]:= Quit[]

In[1]:= $$eq = Ub'[t] == \frac{Q}{Vb}(Uin[t] - Ub[t]) - \frac{ku\,Ub[t]}{(Ku + Ub[t])\,\frac{1}{2}\left(1 - \frac{Ub[t]}{100}\right)}\left(Xb0 - \left(\frac{Uin[t] - Ub[t]}{Xb0\,Tu}\right) - (Kad\,(Bx\,Ub[t]))\right) - \frac{Duw}{Lw}Ub[t]\,\frac{Af}{Vb}$$

Out[1]= $$Ub'[t] == -\frac{Af\,Duw\,Ub[t]}{Lw\,Vb} + \frac{Q\,(-Ub[t] + Uin[t])}{Vb} - \frac{2^{1 - \frac{Ub[t]}{100}}\,ku\,Ub[t]\left(Xb0 - Bx\,Kad\,Ub[t] - \frac{-Ub[t] + Uin[t]}{Tu\,Xb0}\right)}{Ku + Ub[t]}$$

In[3]:=
```
Q = 0.00792;
Vb = 0.00785;
Uin[t_] = Piecewise[{{75, 0 ≤ t < 29}, {85, 29 ≤ t < 42}, {100, 42 ≤ t < 100}}];
Ku = 2.5;
ku = 0.5;
Xb0 = 80;
Tu = 2.5;
Kad = 0.05;
Bx = 0.05;
Duw = 6 x 10^-6;
Lw = 1.108 x 10^-3;
Af = 0.00785;
```

In[15]:=
```
eq;
```

In[32]:=
```
Ubsol[t_] = Ub[t] /. NDSolve[{eq, Ub[0] == 71.58}, Ub, {t, 0, 100}][[1]]
Plot[%, {t, 0, 100}, PlotRange → {0, 80}]
```

Out[32]= InterpolatingFunction[{{0., 100.}}, <>][t]

APPENDIX C

Octave Version 3.0

RUNGE_KUTTA METHOD

****

```
% Author Ido Schwartz
clc;                                % Clears the screen
clear all;
#_____________________________________________________________________________
Q = 0.00792;
V = 0.00785;
Uin =[75 85 100];
Du = 5.976×10^-6;
Lw =  1.108×10^-3;
A = 0.00785;
rho_s =2300000;
a= 0.3298;
kg =Du/Lw;
Xf= 60;
b=0.0005;
kd=0.006;
porosity = 0.95;
u= 1.0627;
#_____________________________________________________________________________
#Simulation parameters
initial_time = 0;
final_time = 120;
h=2;                                % step size
```

```
x = initial_time:h:final_time;                    % Calculates up to final_time

y = zeros (1, length(x));

#_____________________________________________________________________________


F_xy = @(Lf,t)(((1/(1-ε))*(1/rho_s))*(Xf*Lf))-1/rho*(kd*A*(u^2/2)*Xf*A/V*Lf));

#_____________________________________________________________________________

#RK  algorithm

for i=1:(length(x)-1)                    % calculation loop

   k_1 = F_xy(x(i),y(i));

   k_2 = F_xy(x(i)+0.5*h,y(i)+0.5*h*k_1);

   k_3 = F_xy((x(i)+0.5*h),(y(i)+0.5*h*k_2));

   k_4 = F_xy((x(i)+h),(y(i)+k_3*h));

   y(i+1) = y(i) + (1/6)*(k_1+2*k_2+2*k_3+k_4)*h;  % main equation

end

vv = [y' x']

plot(x,y,'--')

xlabel 'time (d)'

ylabel 'Lf (m)'
```